AHEAD 2020

eROSITA - Science and Data Analysis School

2024 November 18 – 22, MPE

eROSITA Calibration

Konrad Dennerl
MPE

From photons to bits: the fate of X-rays grabbed by eROSITA

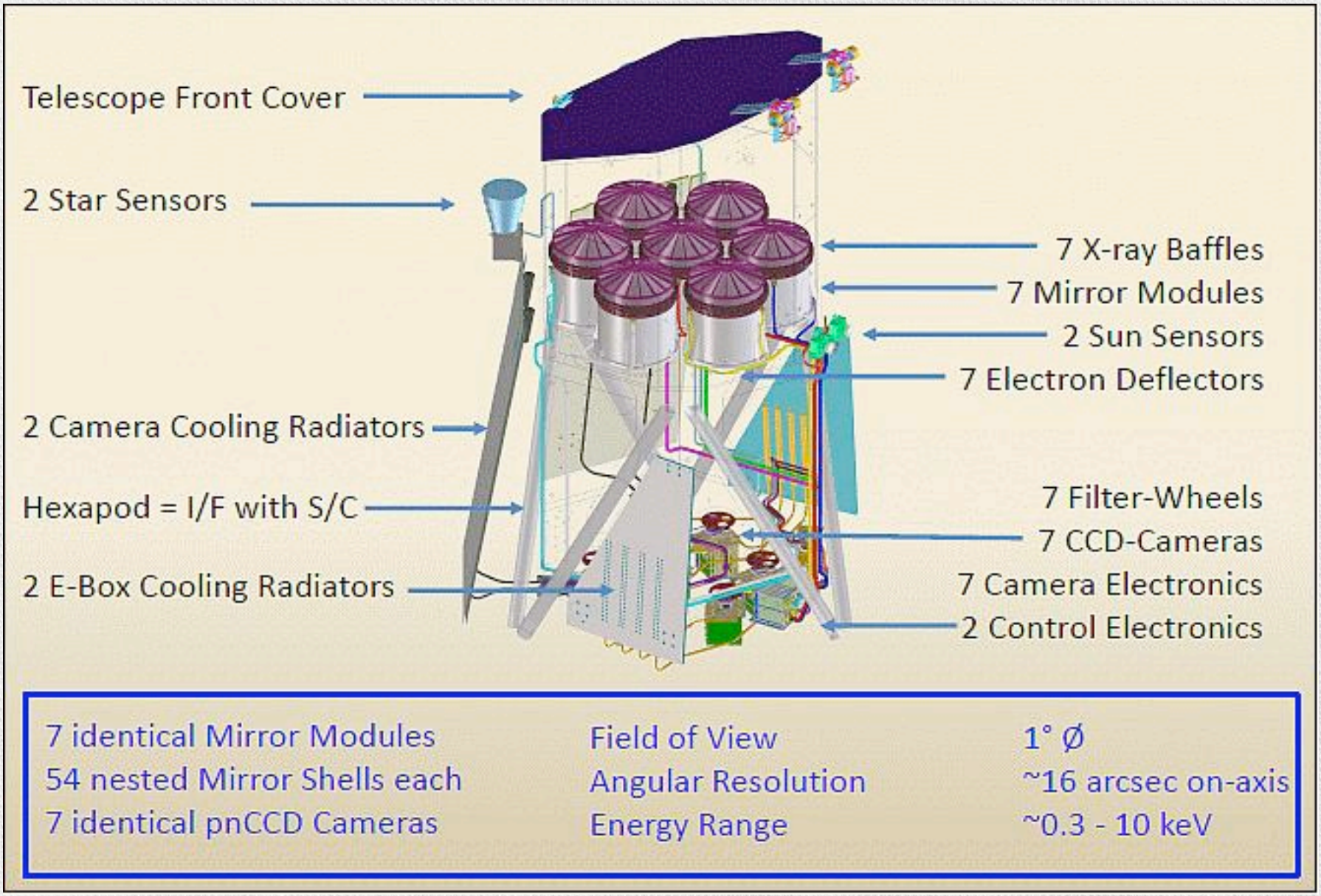

7 identical Mirror Modules	Field of View	1° Ø
54 nested Mirror Shells each	Angular Resolution	~16 arcsec on-axis
7 identical pnCCD Cameras	Energy Range	~0.3 - 10 keV

From photons to bits: the fate of X-rays grabbed by eROSITA

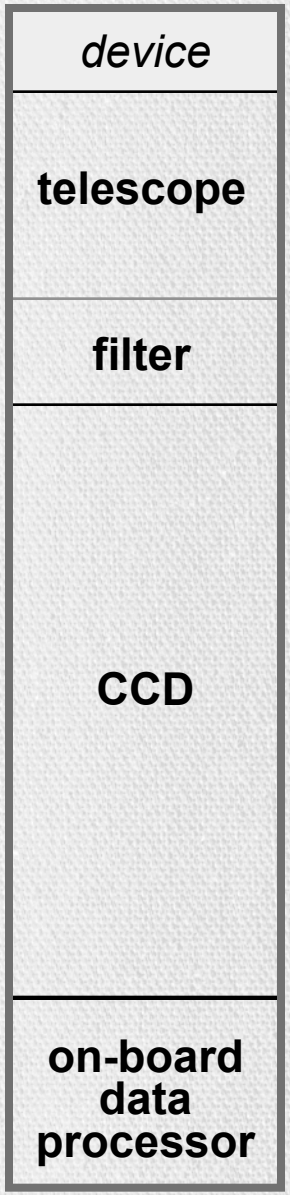

From photons to bits: the fate of X-rays grabbed by eROSITA

device	*process*
telescope	reflection (scattering)
filter	absorption
CCD	charge release
	charge transfer
	charge readout
on-board data processor	signal processing

From photons to bits: the fate of X-rays grabbed by eROSITA

device	*process*	*signal*
telescope	reflection (scattering)	*photon [eV]*
filter	absorption	
CCD	charge release	*charge [e^-]*
	charge transfer	
	charge readout	*pulse height amplitude [adu]*
on-board data processor	signal processing	*event [bit]*

From photons to bits: the fate of X-rays grabbed by eROSITA

device	*process*	*signal*	*characteristic properties*	
telescope	reflection (scattering)	*photon [eV]*	effective area (E,θ,φ) point spread function (E,θ,φ) field of view (FOV) boresight	collecting area, reflectivity, vignetting mirror quality, encircled energy fraction focal length, detector geometry, plate scale alignment
filter	absorption			
CCD	charge release	*charge [e^-]*		
	charge transfer			
	charge readout	*pulse height amplitude [adu]*		
on-board data processor	signal processing	*event [bit]*		

From photons to bits: the fate of X-rays grabbed by eROSITA

device	*process*	*signal*	*characteristic properties*	
telescope	reflection (scattering)	*photon [eV]*	effective area (E,θ,φ) point spread function (E,θ,φ) field of view (FOV) boresight	collecting area, reflectivity, vignetting mirror quality, encircled energy fraction focal length, detector geometry, plate scale alignment
filter	absorption			
CCD	charge release	*charge [e^-]*		
	charge transfer			
	charge readout	*pulse height amplitude [adu]*		
on-board data processor	signal processing	*event [bit]*		

Imaging Analysis of X-ray data

While the imaging analysis of X-ray data is generally similar to imaging analysis in other energies/wavelengths, it has some specific properties which must be considered:

- strong dependence of the image quality on the off-axis angle
- generally low photon statistics

Telescope Calibration: Point Spread Function (PSF)

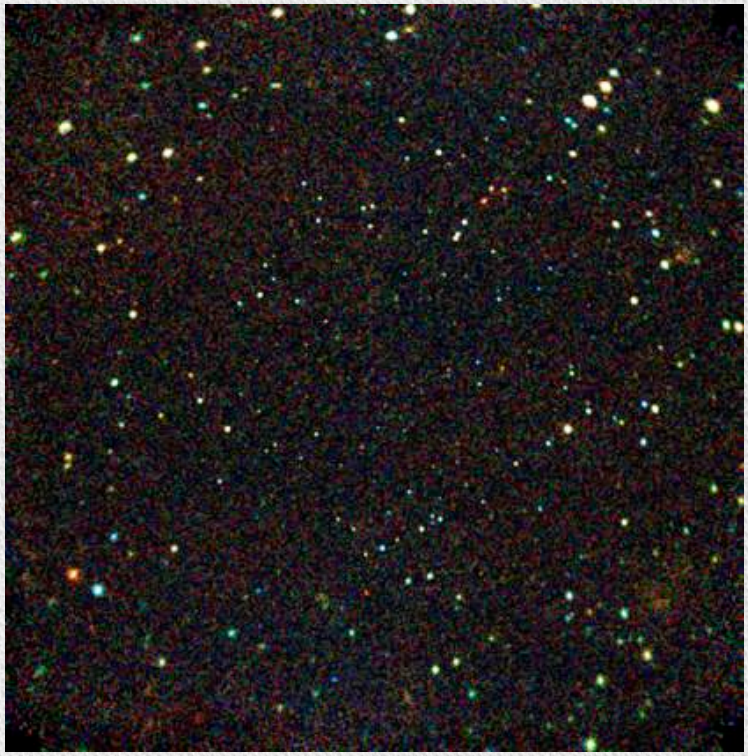

This one-million-second image ("Chandra Deep Field-South“) is an extremely deep X-ray exposure.
The darker area at center is caused by a sharper PSF.

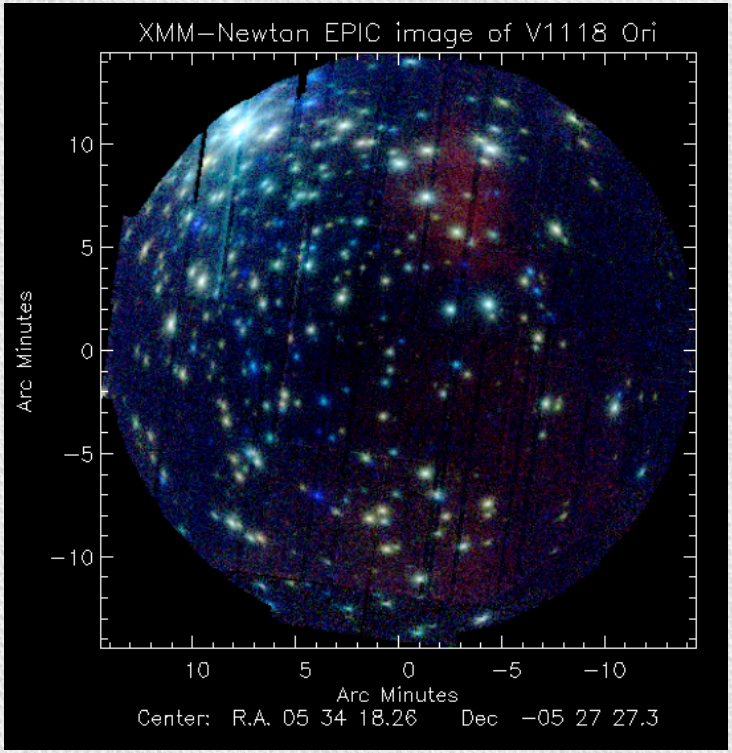

XMM-Newton image of the V1118 Ori field

Telescope Calibration: eROSITA Point Spread Function (PSF)

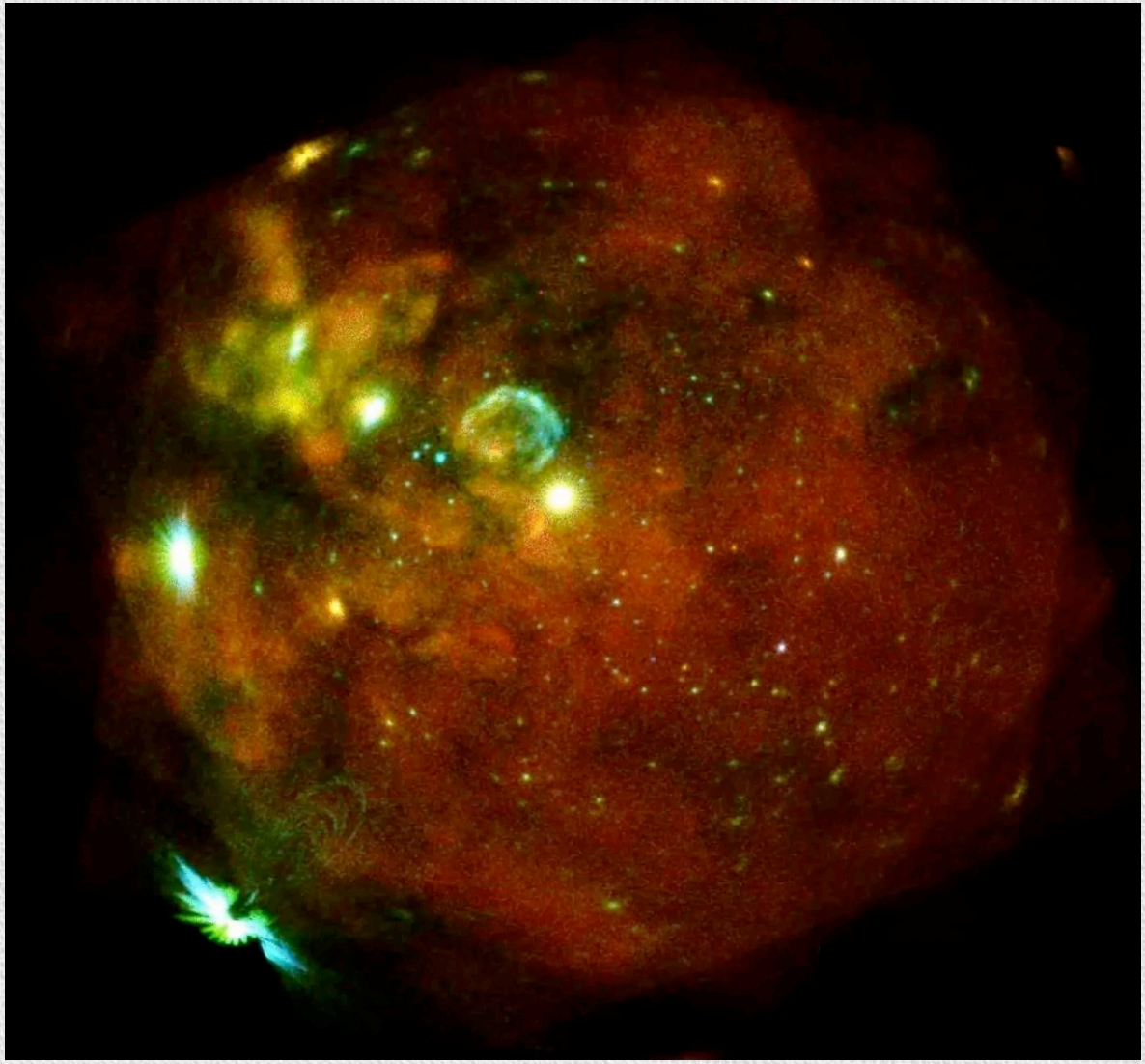

eROSITA first light image of the LMC

MPE X-ray test facility PANTER

PSF Focal Plane Mapping

PANTER Geometry (overview)

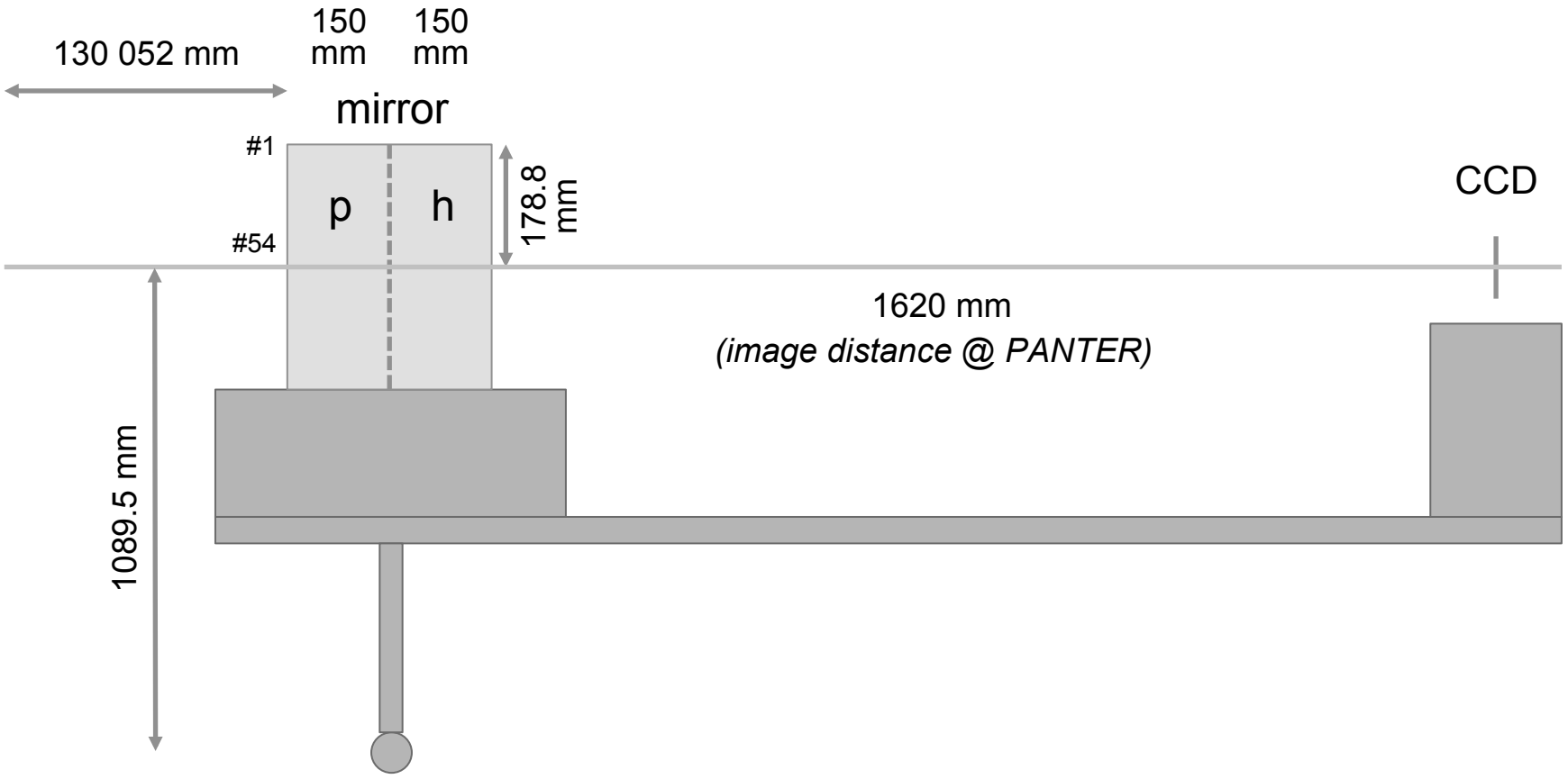

PSF Focal Plane Mapping

PANTER Geometry (overview)

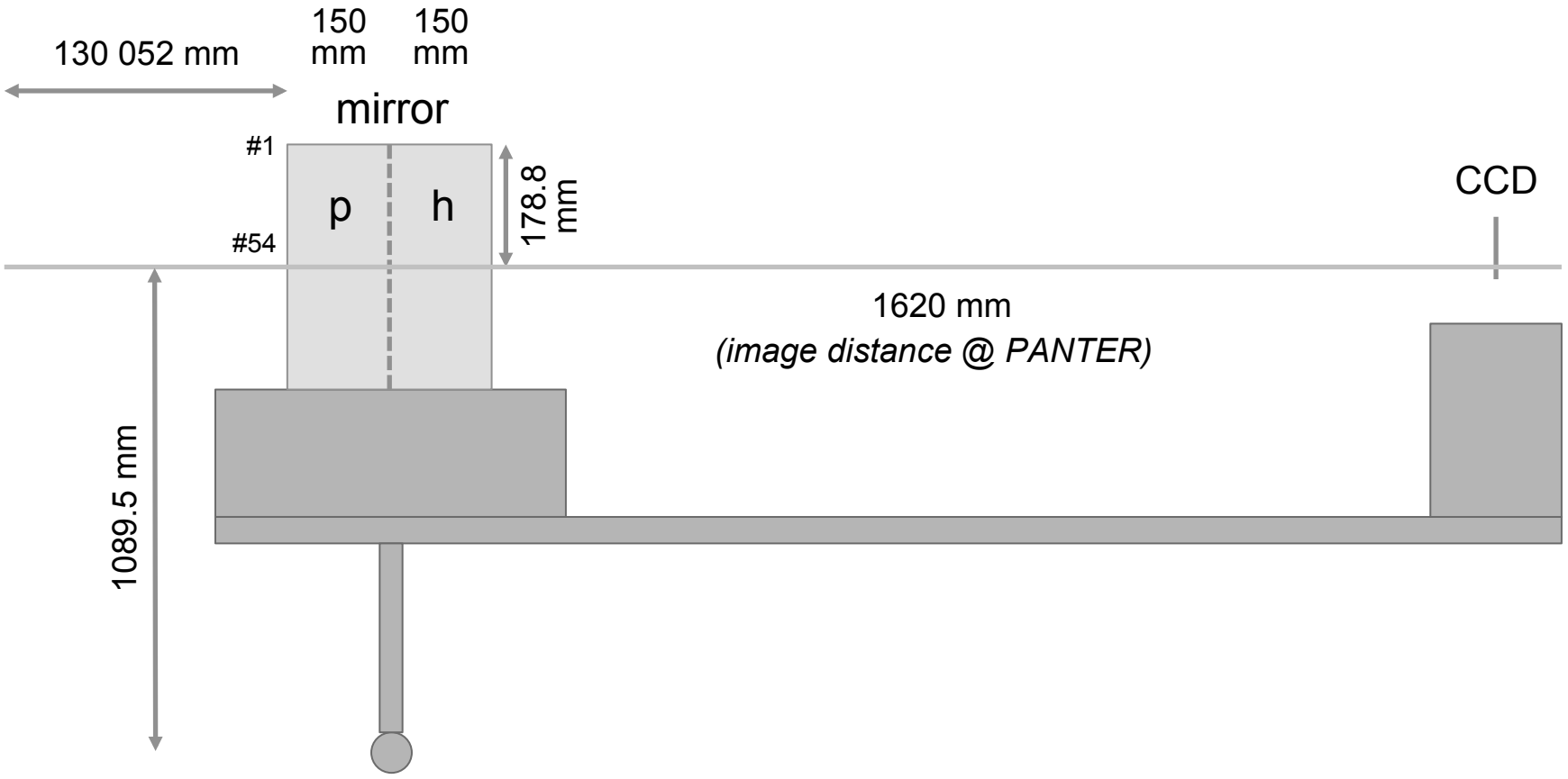

PSF Focal Plane Mapping

PANTER Geometry (overview)

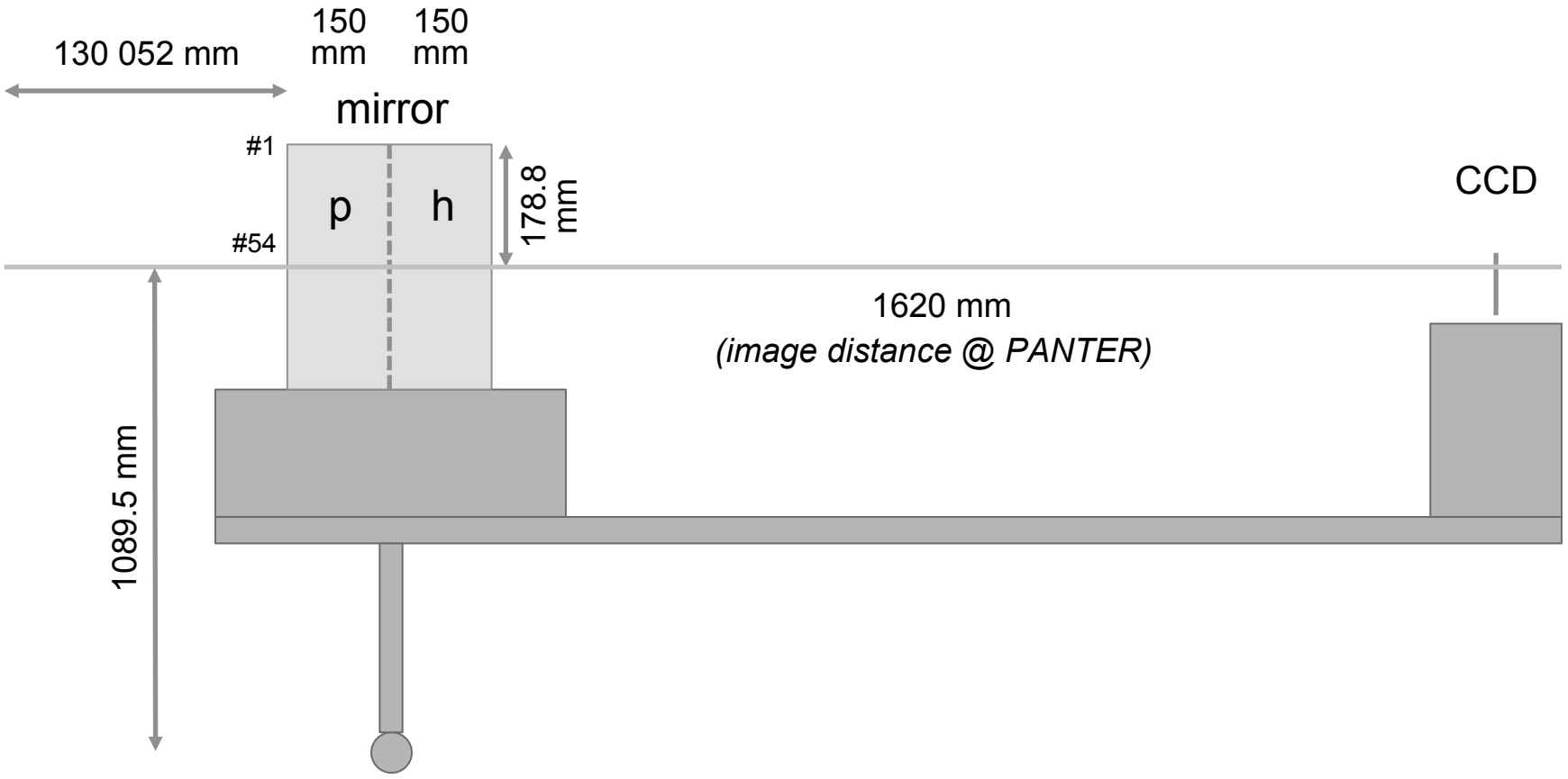

PSF Focal Plane Mapping

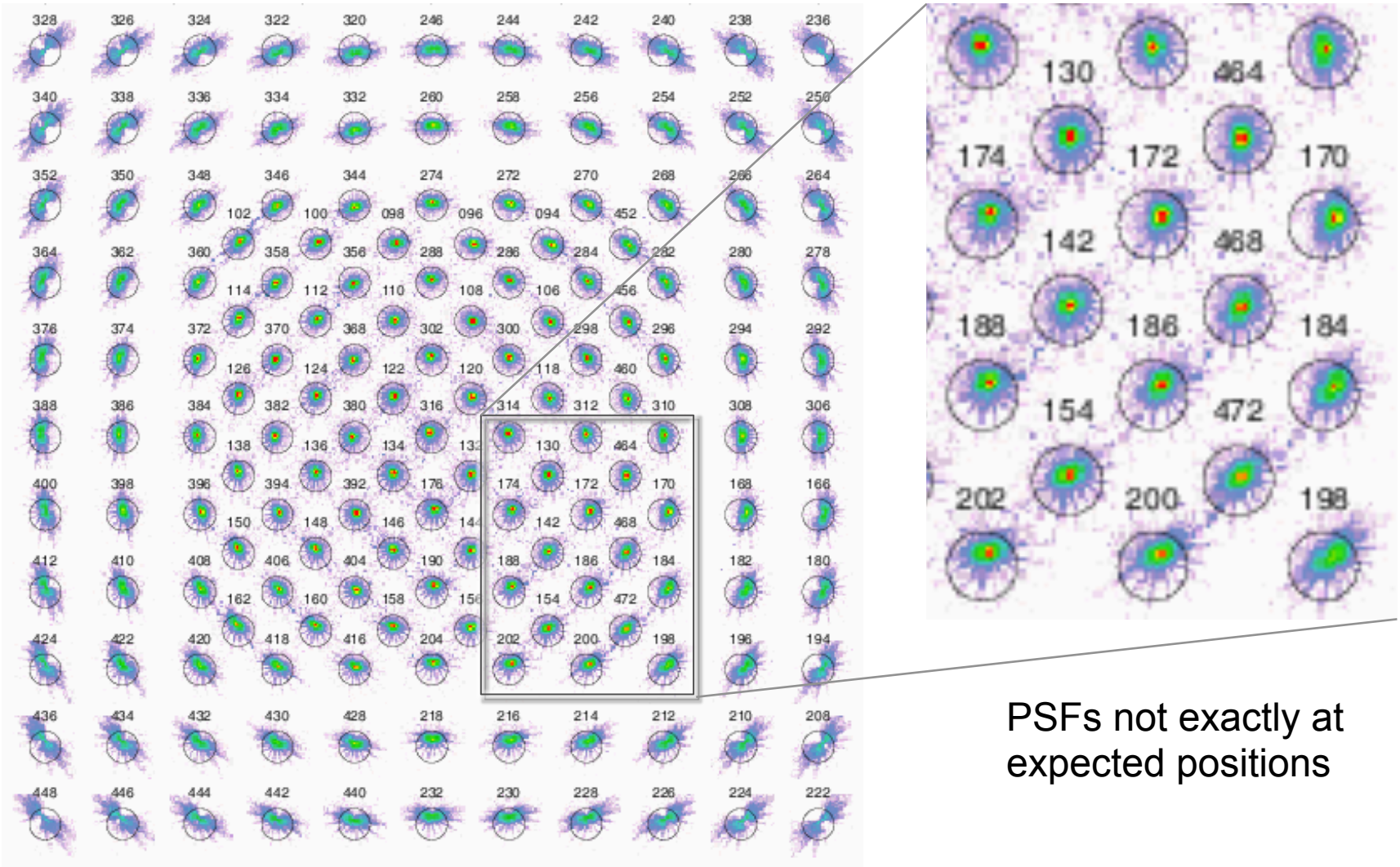

PSFs not exactly at expected positions

PSF Focal Plane Mapping

PANTER Geometry (details)

(axis 03: mirror translation, axis 10: detector focus)

X-ray source distance to mirror center: S = 123 822 mm

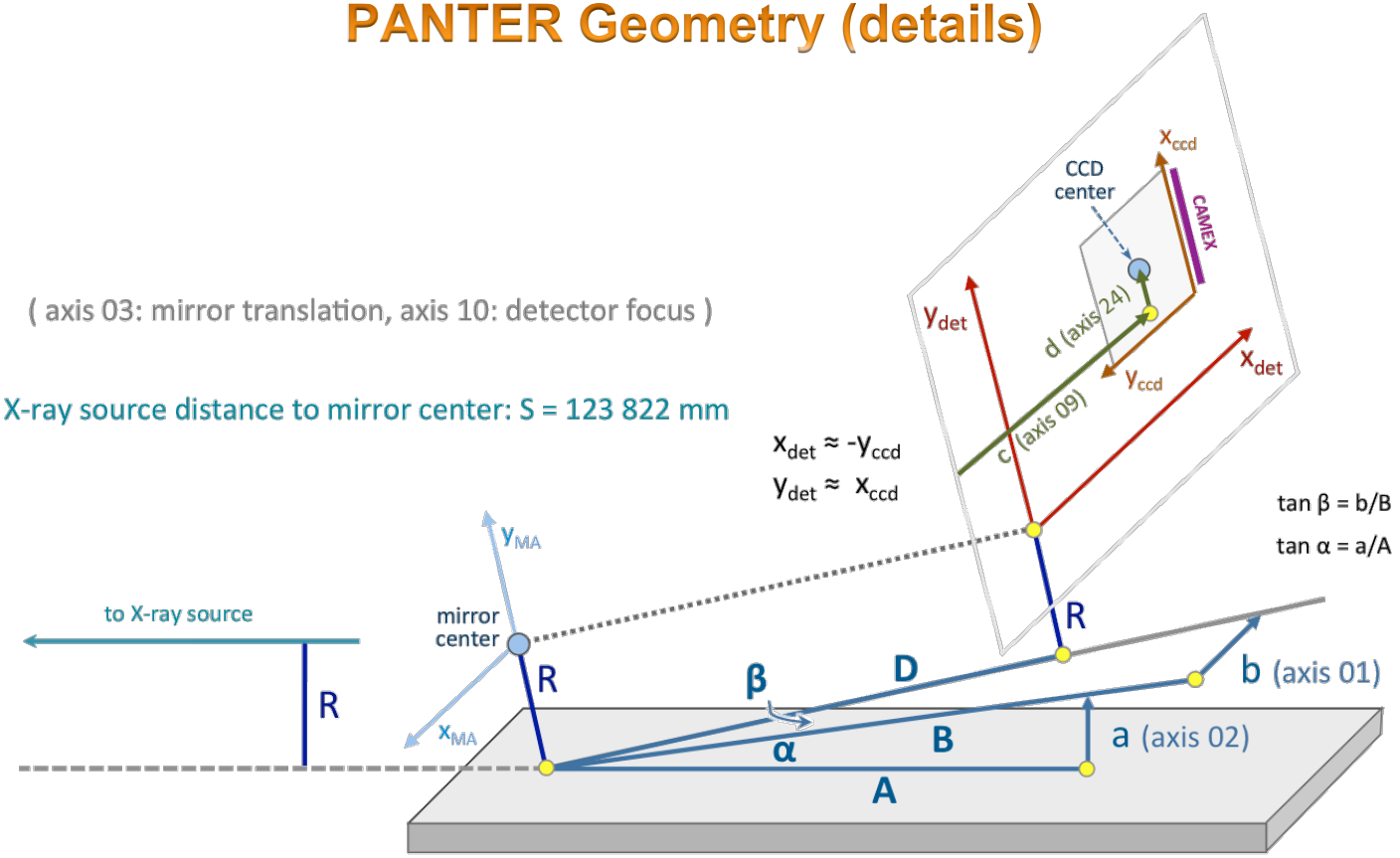

D = 1622.2 mm
A = 3060.4 mm (62.5 nm/step)
B = 3270.0 mm (1.25 µm/step) (+/- 10mm)
R = 1089.5 mm

1 step = 62.5 nm
4610017 steps → α = 5.37835 deg
→ a = 288.126 mm
→ A = a / tan α = 3060.4 mm

PSF Focal Plane Mapping

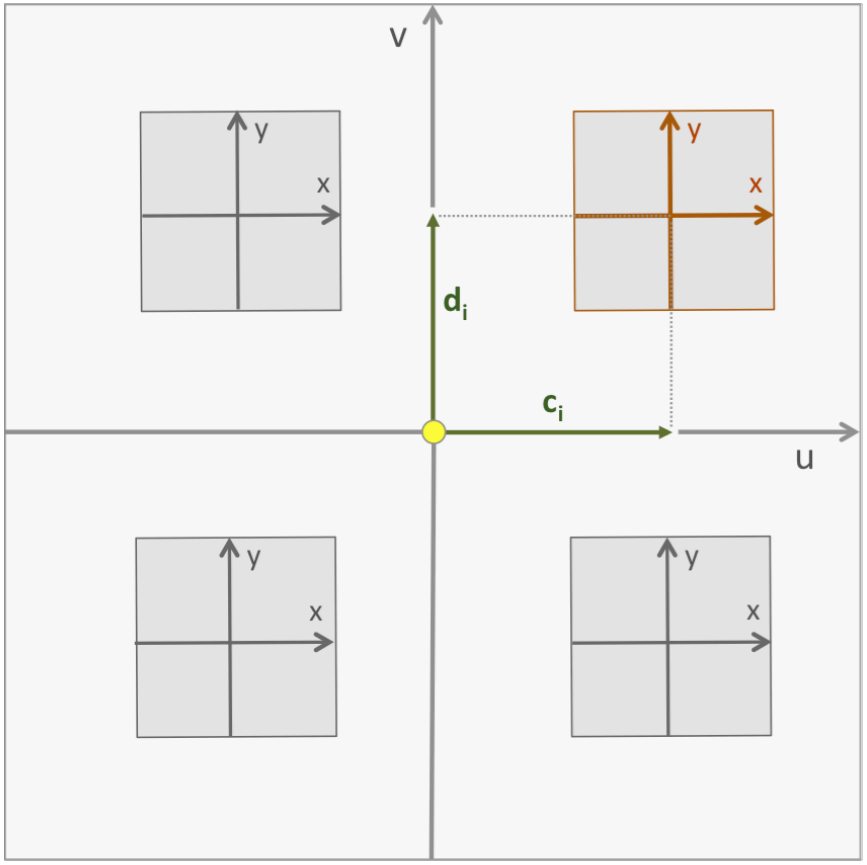

$u_i = c_i + x$

$v_i = d_i + y$

PSF Focal Plane Mapping

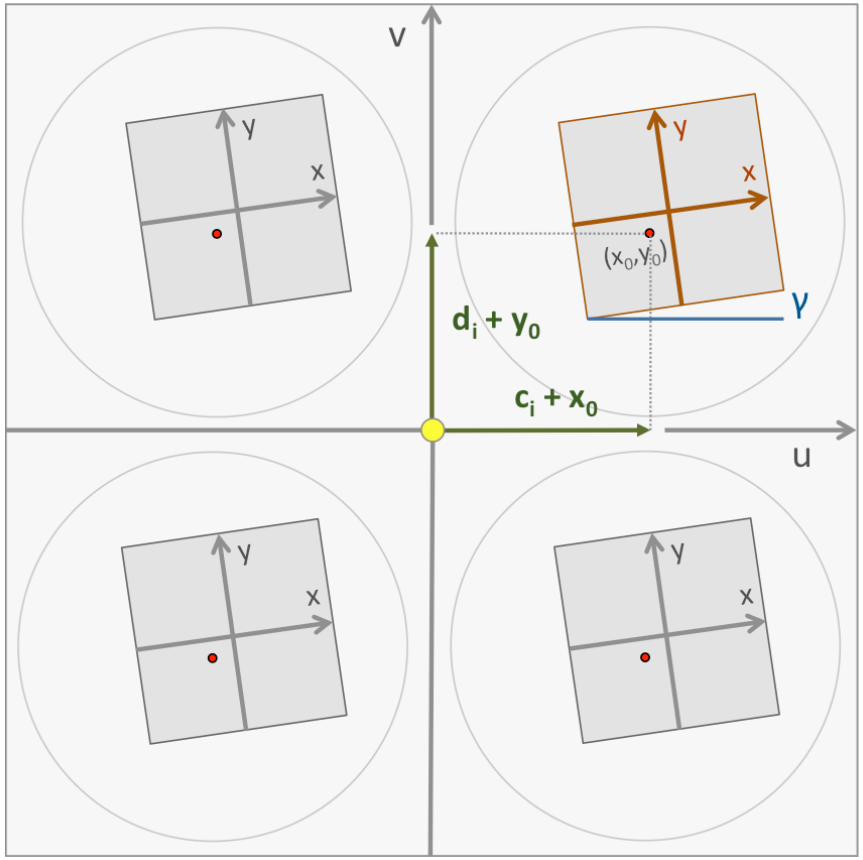

$$u_i = c_i + x_0 + (x-x_0)\cos\gamma - (y-y_0)\sin\gamma$$
$$v_i = d_i + y_0 + (x-x_0)\sin\gamma + (y-y_0)\cos\gamma$$

PSF Focal Plane Mapping

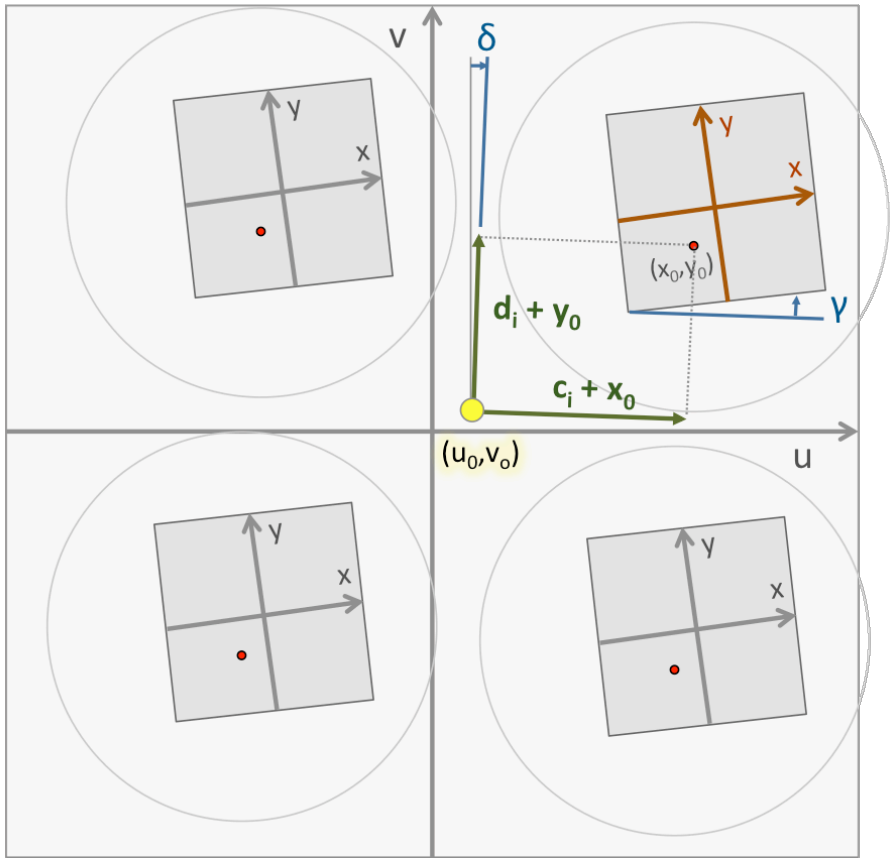

$$u_i = c_i + x_0 + (x-x_0)\cos\gamma - (y-y_0)\sin\gamma$$
$$v_i = d_i + y_0 + (x-x_0)\sin\gamma + (y-y_0)\cos\gamma$$

$$u_i' = u_0 + (u_i-u_0)\cos\delta - (v_i-v_0)\sin\delta$$
$$v_i' = v_0 + (u_i-u_0)\sin\delta + (v_i-v_0)\cos\delta$$

PSF Focal Plane Mapping

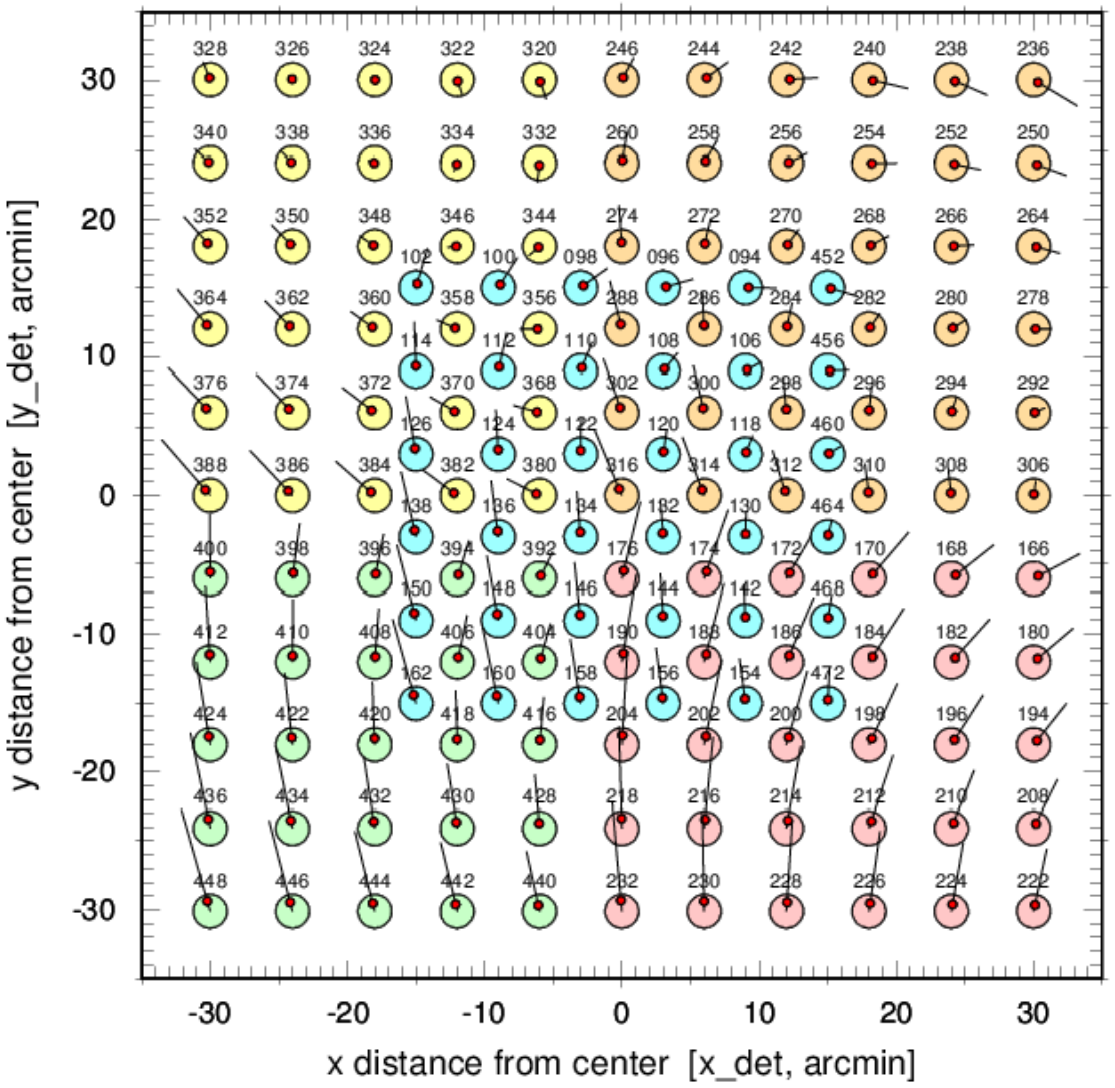

large circles: predicted PSF centers
small circles: corr. measured PSF centers
displacement lines enlarged by factor 10.0

A = 3060.4 mm, B = 3270.0 mm, C = 1621.0 mm
gamma = 0.0 arcmin, delta = 0.0 arcmin
x = (128.0 - y_ccd) , y = (x_ccd - 128.0)

mean positional 1σ deviation: 20.6“

PSF Focal Plane Mapping

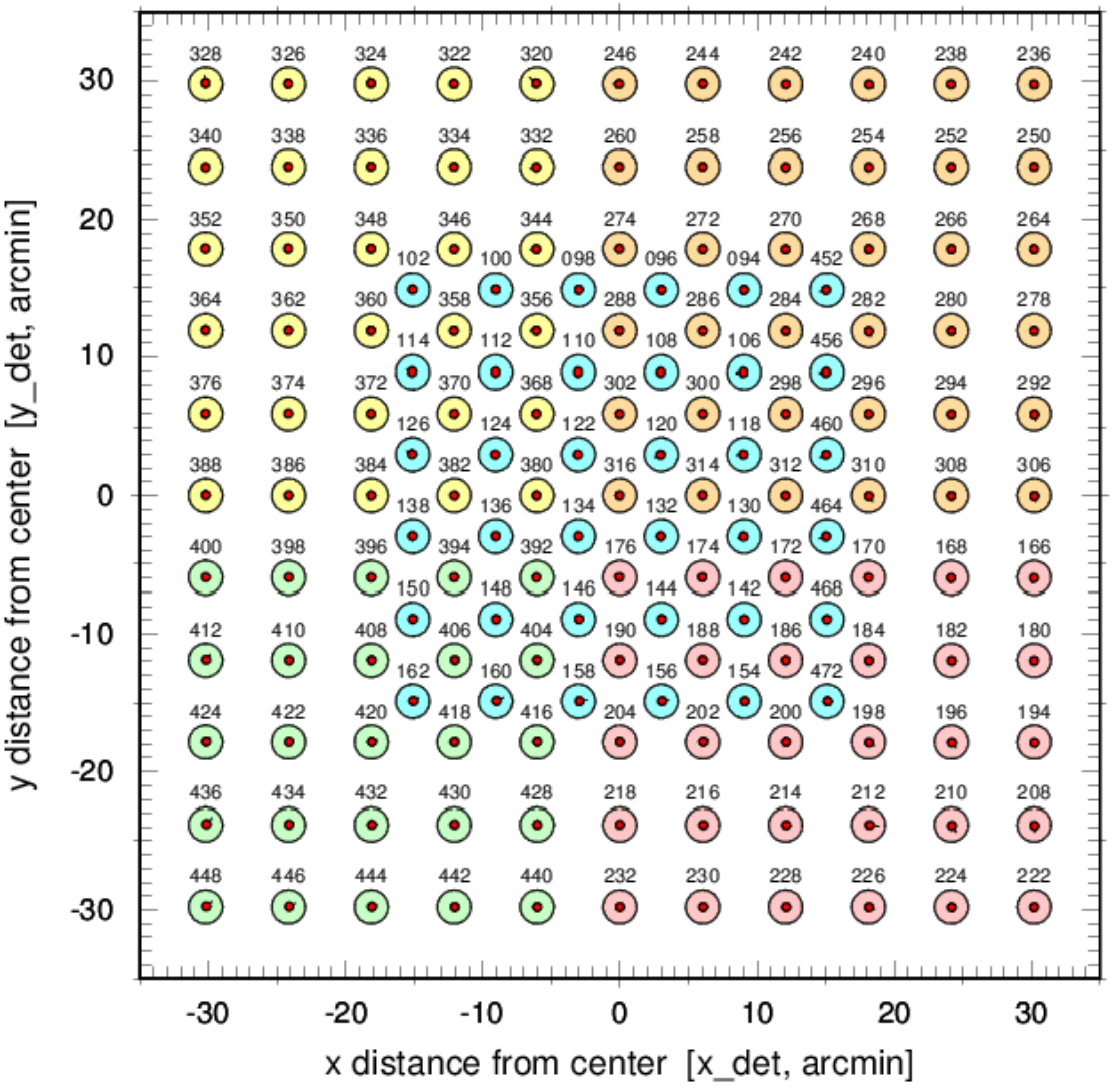

Result of geometrical fit with 7 parameters:

A, B, D, γ, δ, x_0, y_0

large circles: predicted PSF centers
small circles: corr. measured PSF centers
displacement lines enlarged by factor 10.0

A = 3095.3 mm, B = 3252.7 mm, D = 1622.2 mm
gamma = 46.4 arcmin, delta = -9.9 arcmin
x = (127.8 - y_ccd) , y = (x_ccd - 129.7)

mean positional 1σ deviation: 2.1“

PSF Focal Plane Mapping

FM2, Al-K

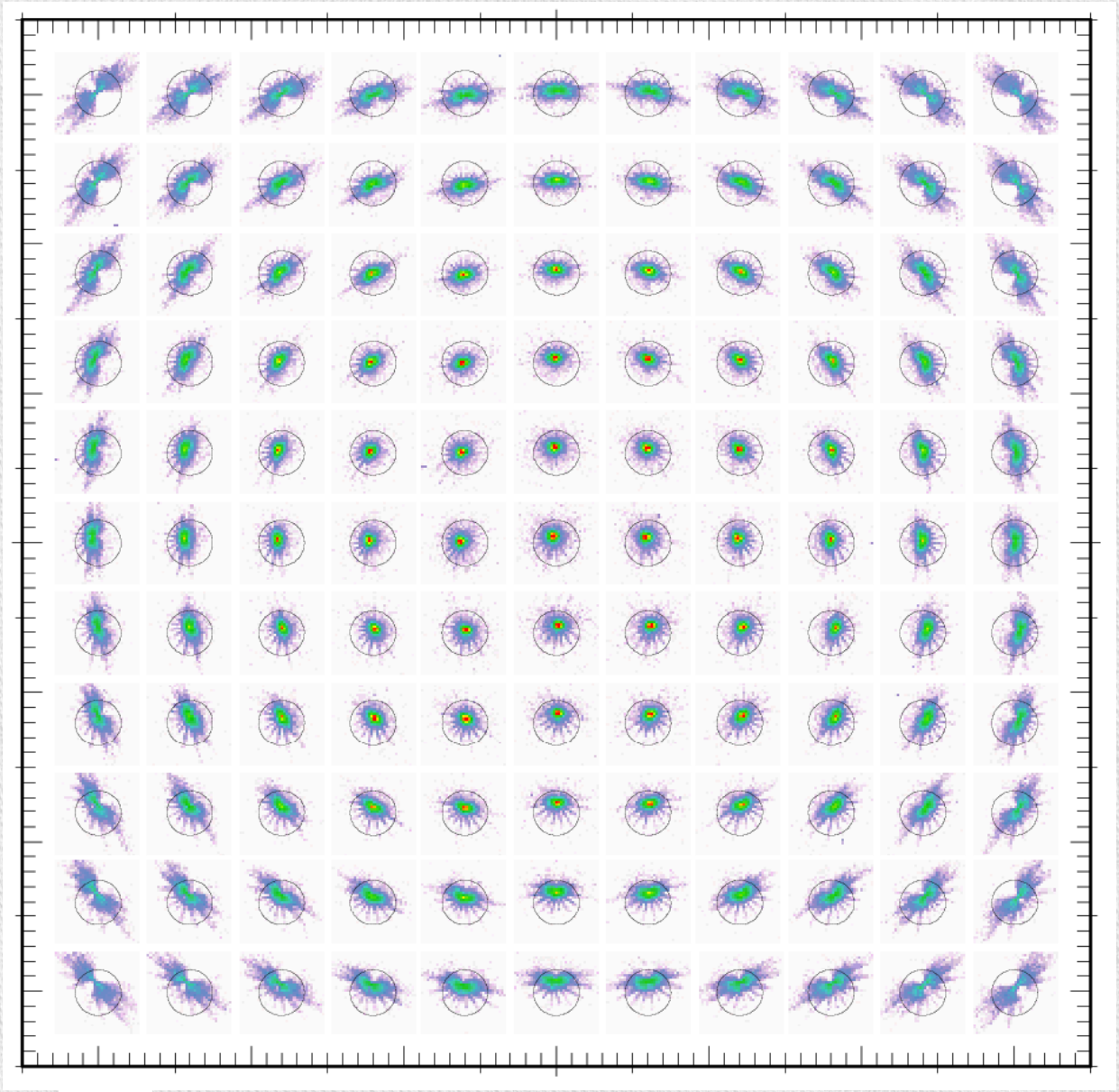

before geometry correction

PSF Focal Plane Mapping

FM2, Al-K

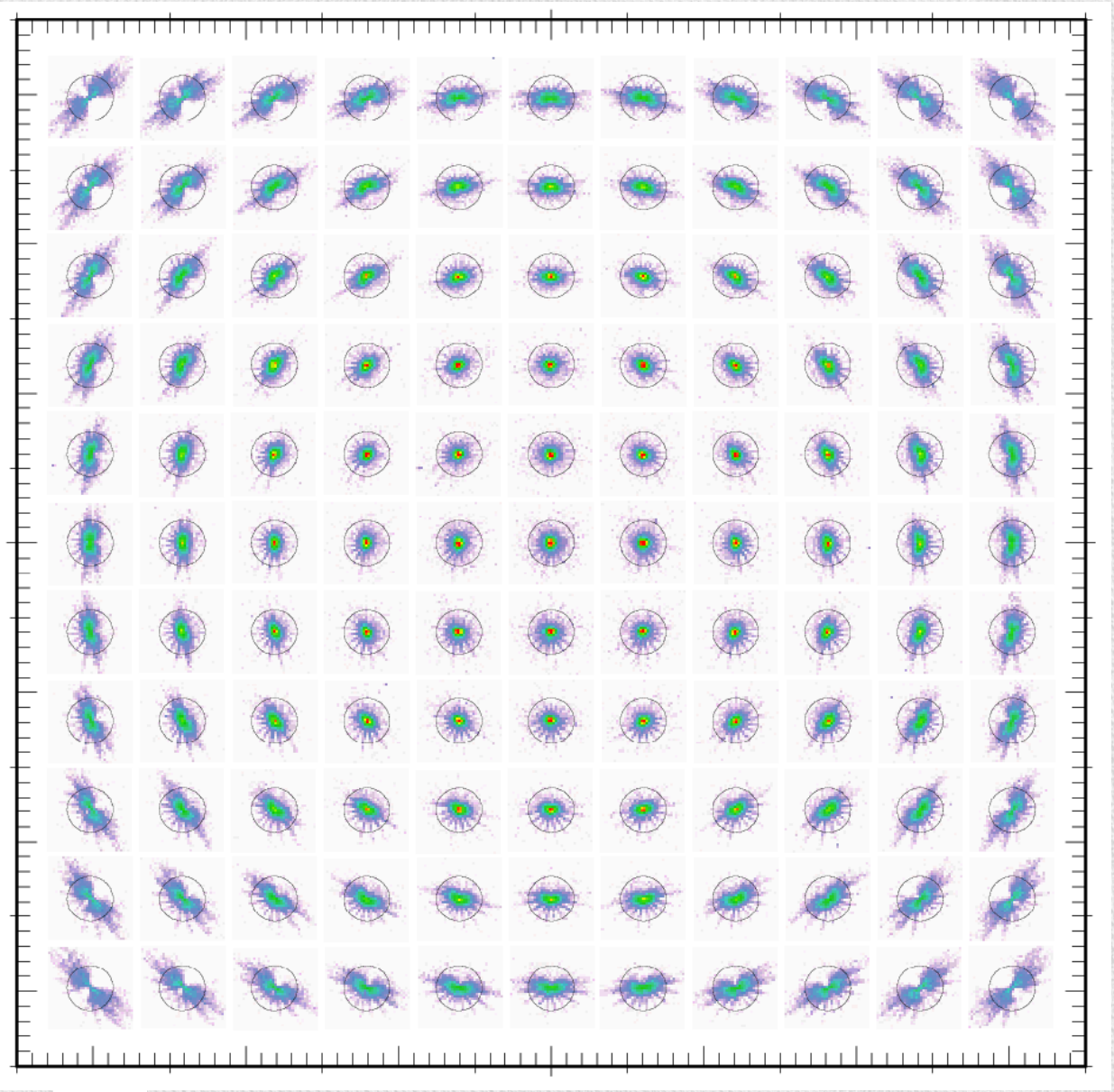

after
geometry
correction

PSF Focal Plane Mapping

FM2, Al-K

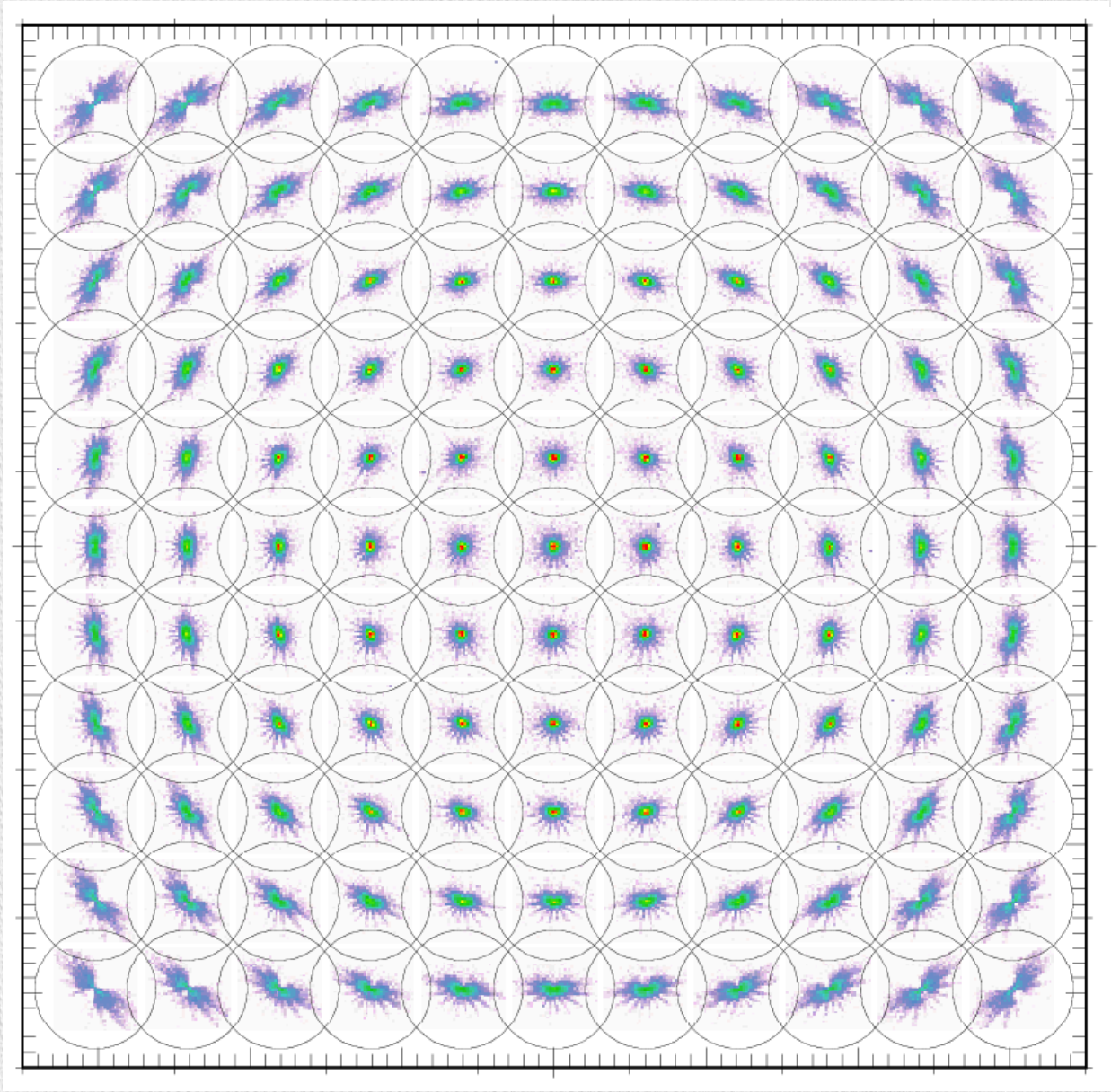

after
geometry
correction

extraction radius:
4 arcmin

→ vignetting

PSF Focal Plane Mapping

FM2, Al-K

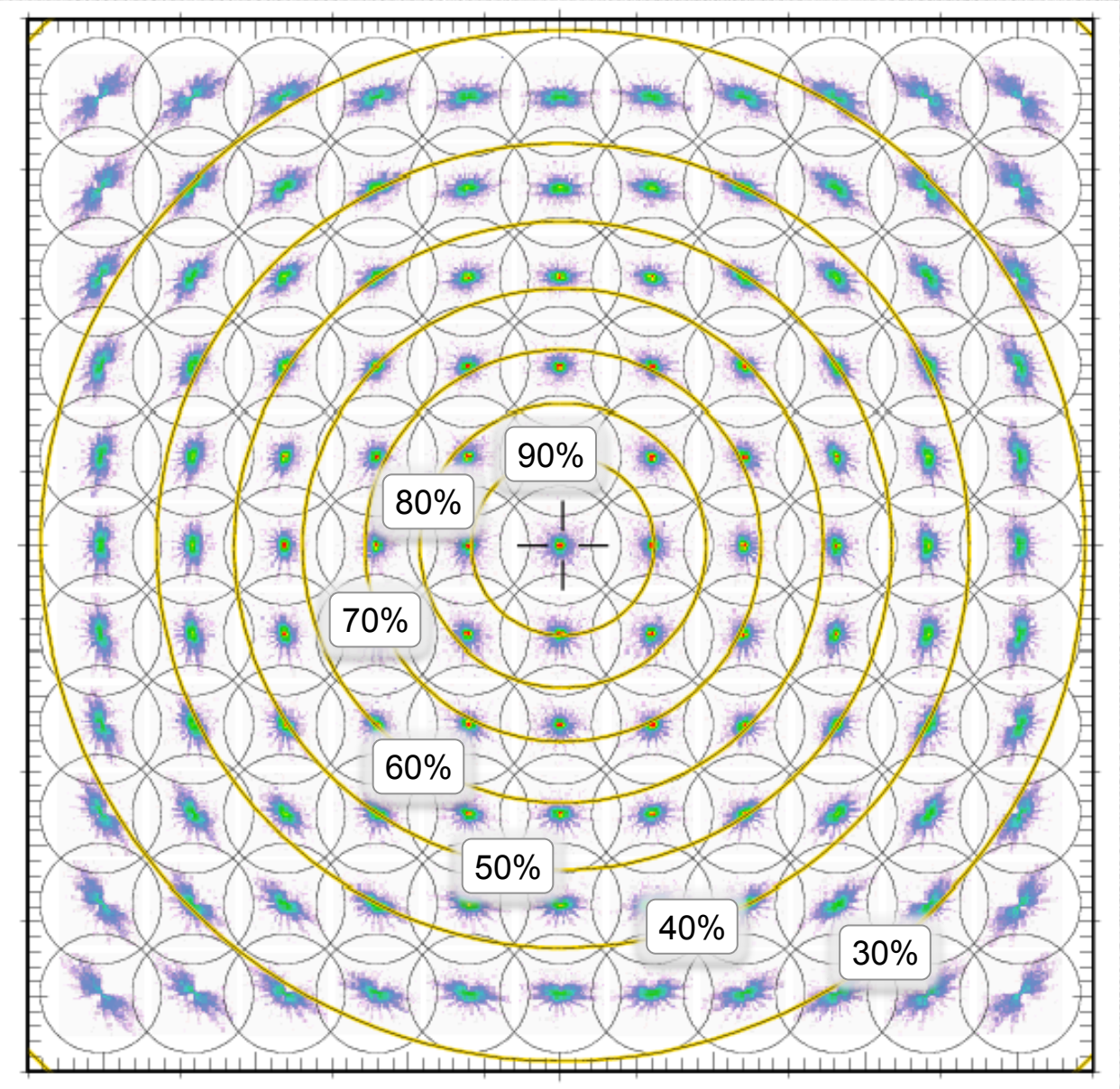

after
geometry
correction

extraction radius:
4 arcmin

→ vignetting

PSF Focal Plane Mapping: Vignetting

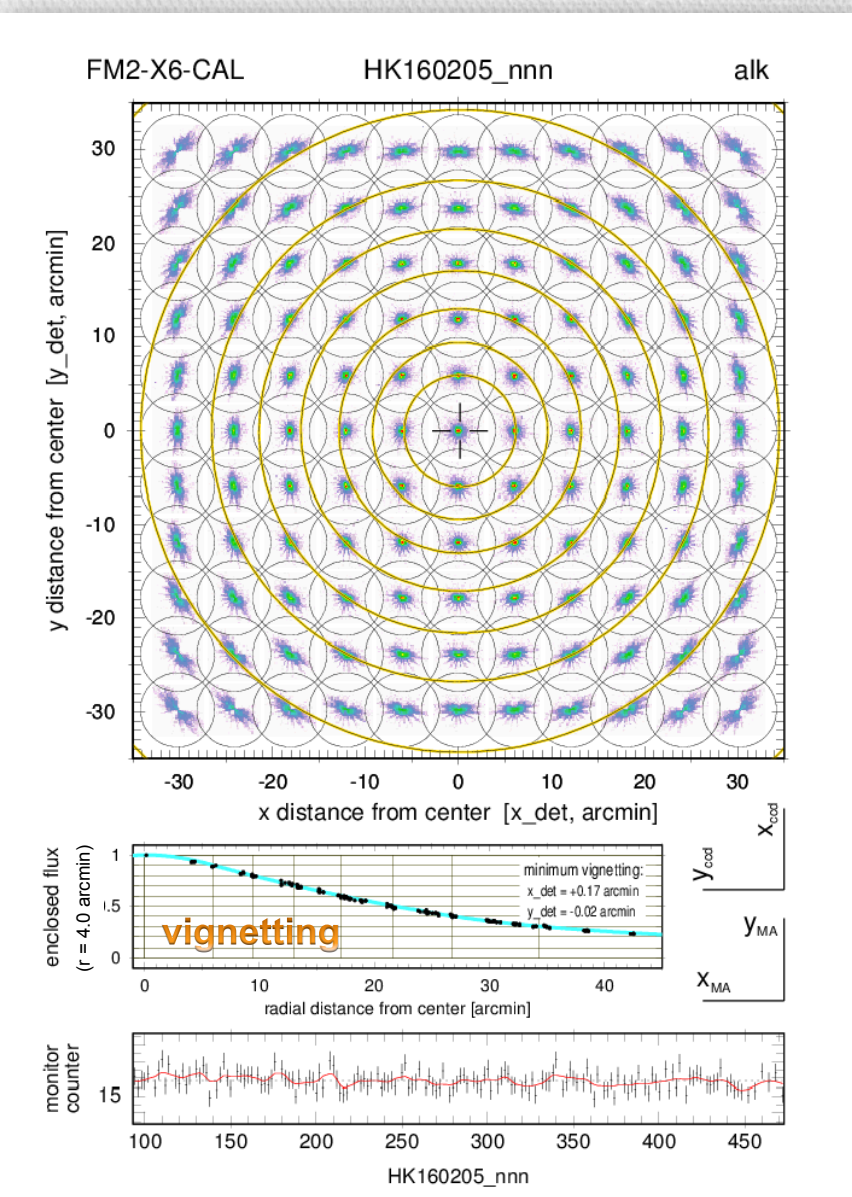

PSF Focal Plane Mapping: Vignetting and HEW

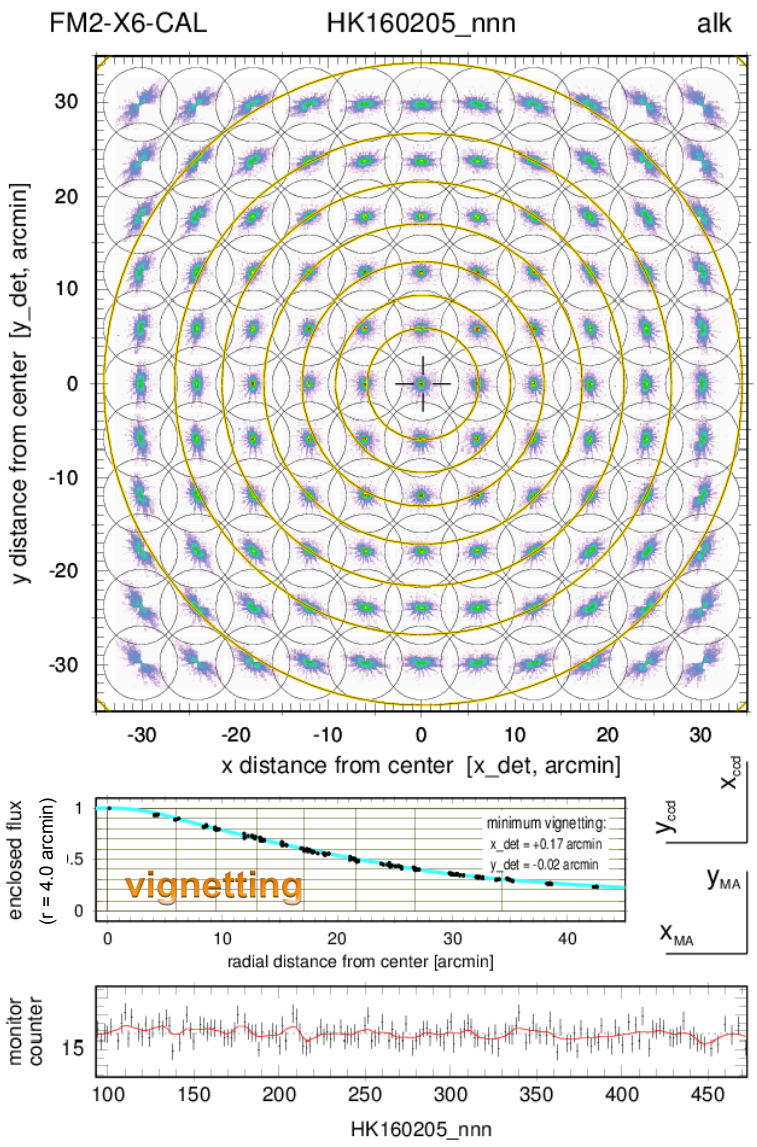

Al-K

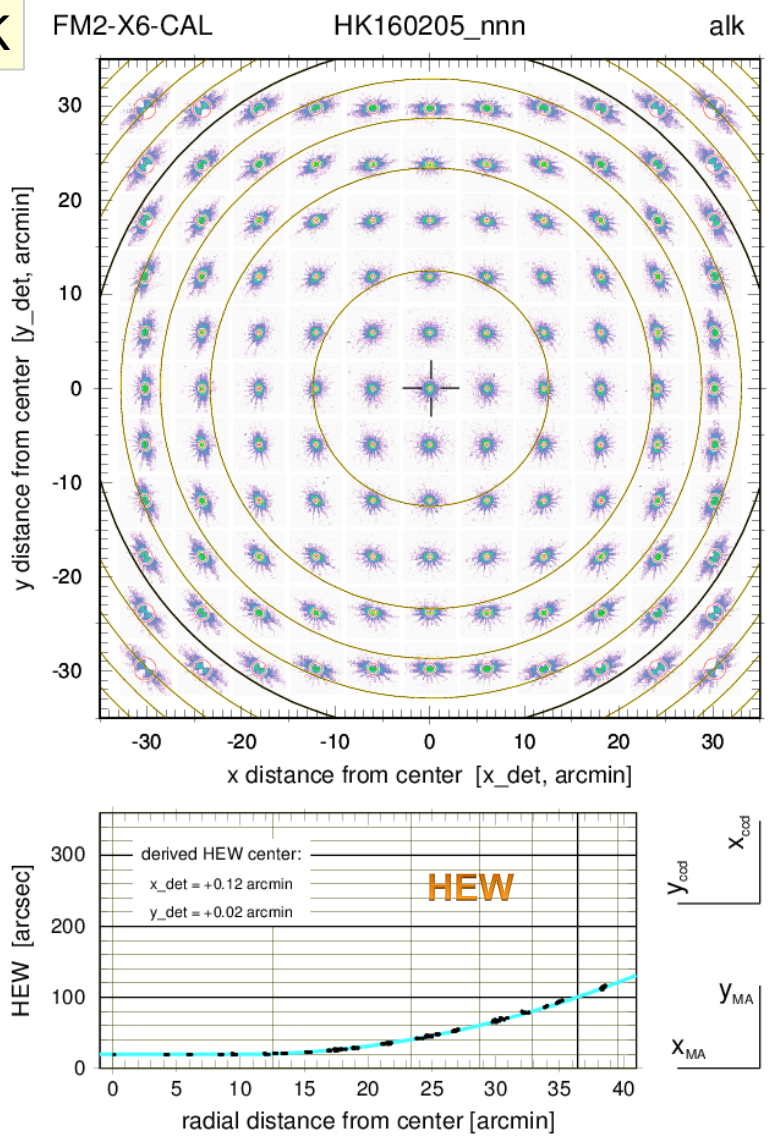

PSF Focal Plane Mapping: Vignetting and HEW

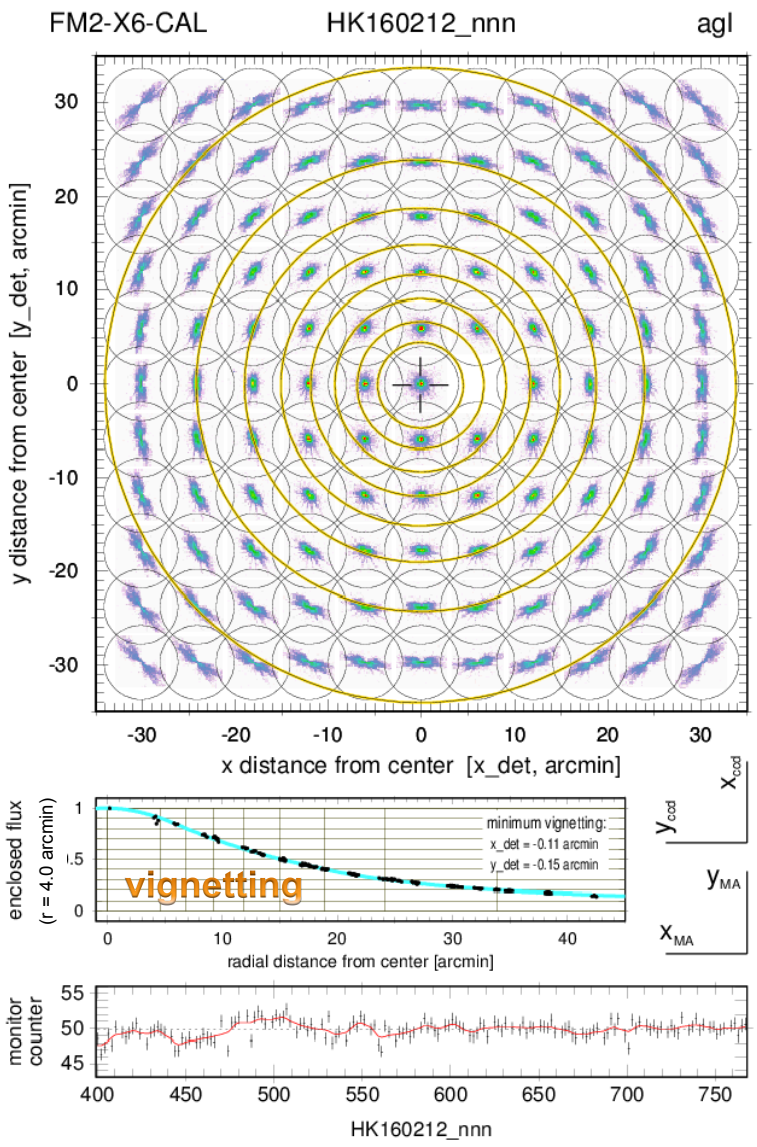

Ag-L

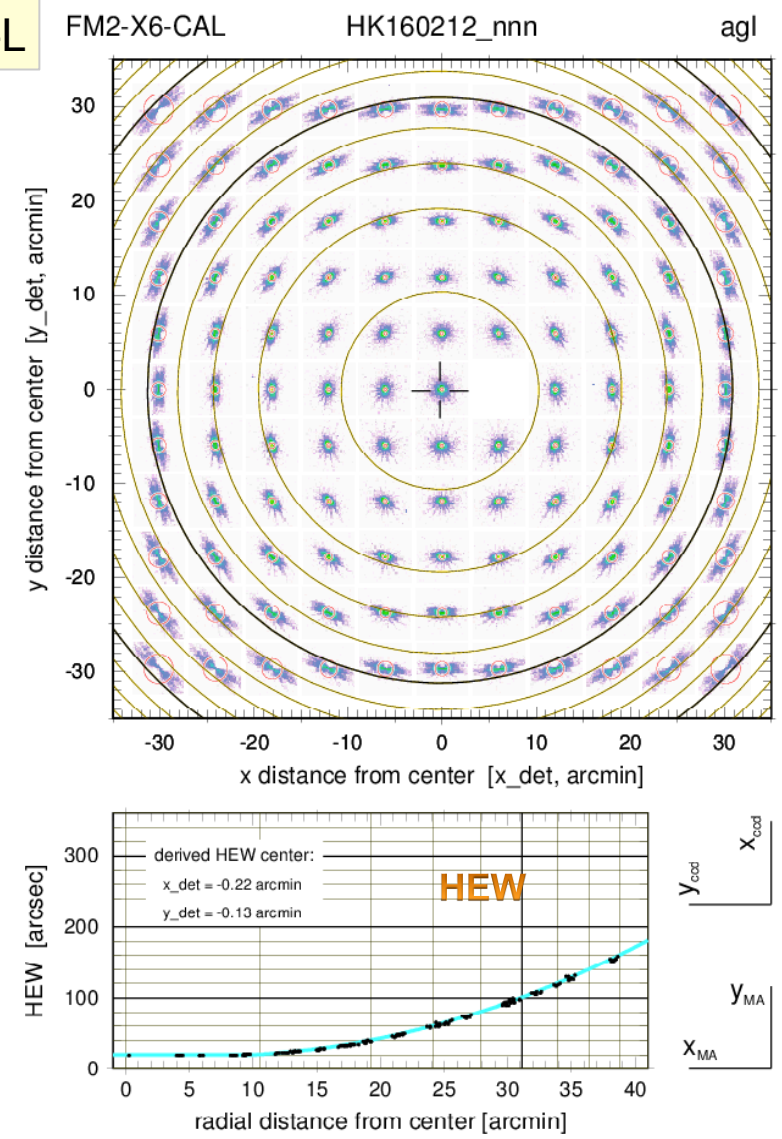

PSF Focal Plane Mapping: Vignetting and HEW

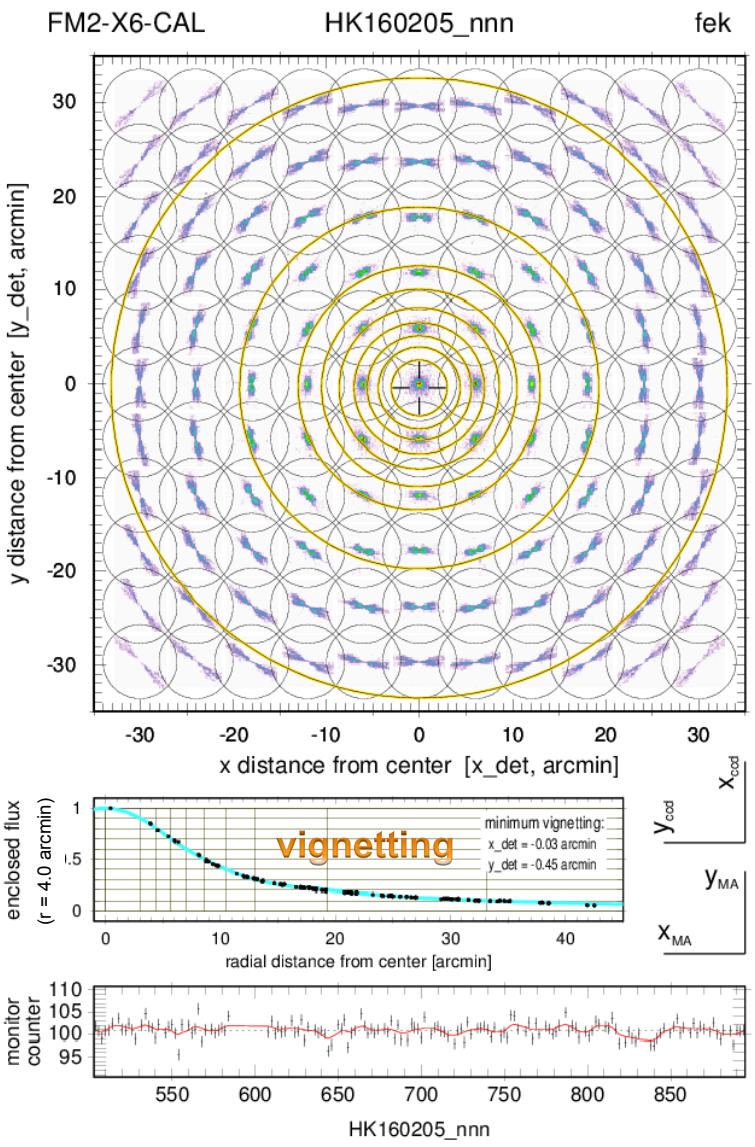

Fe-K

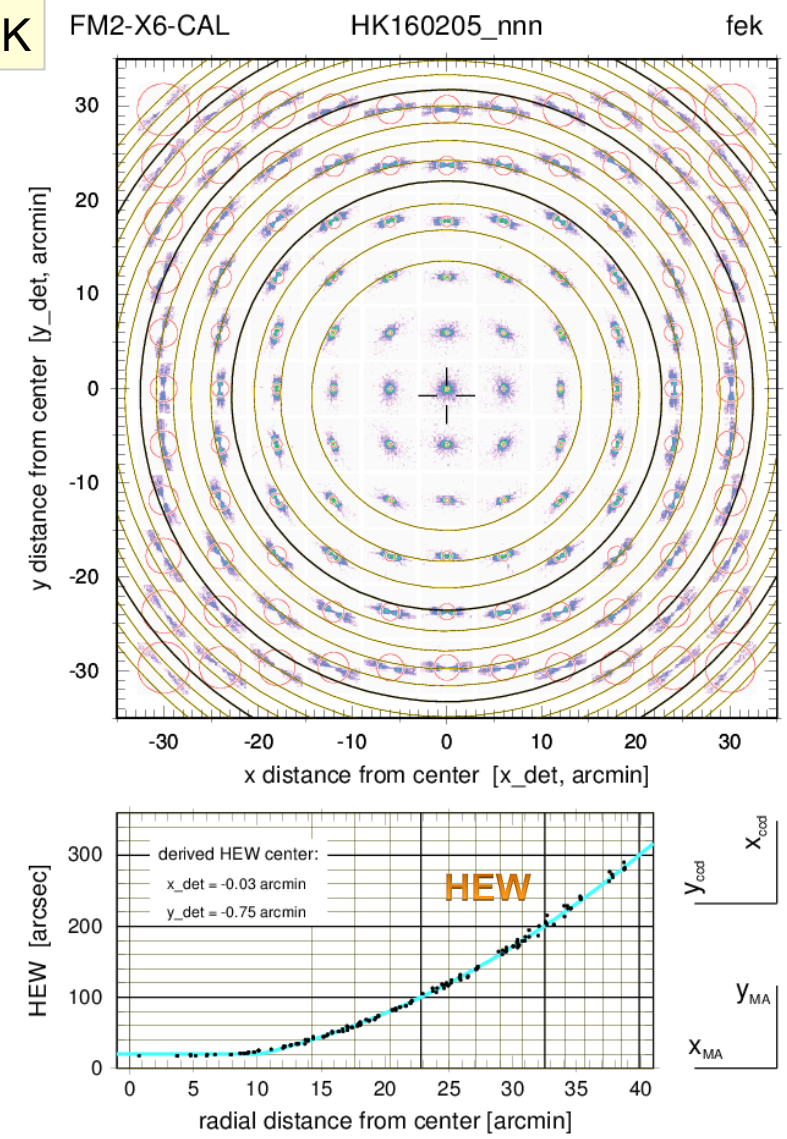

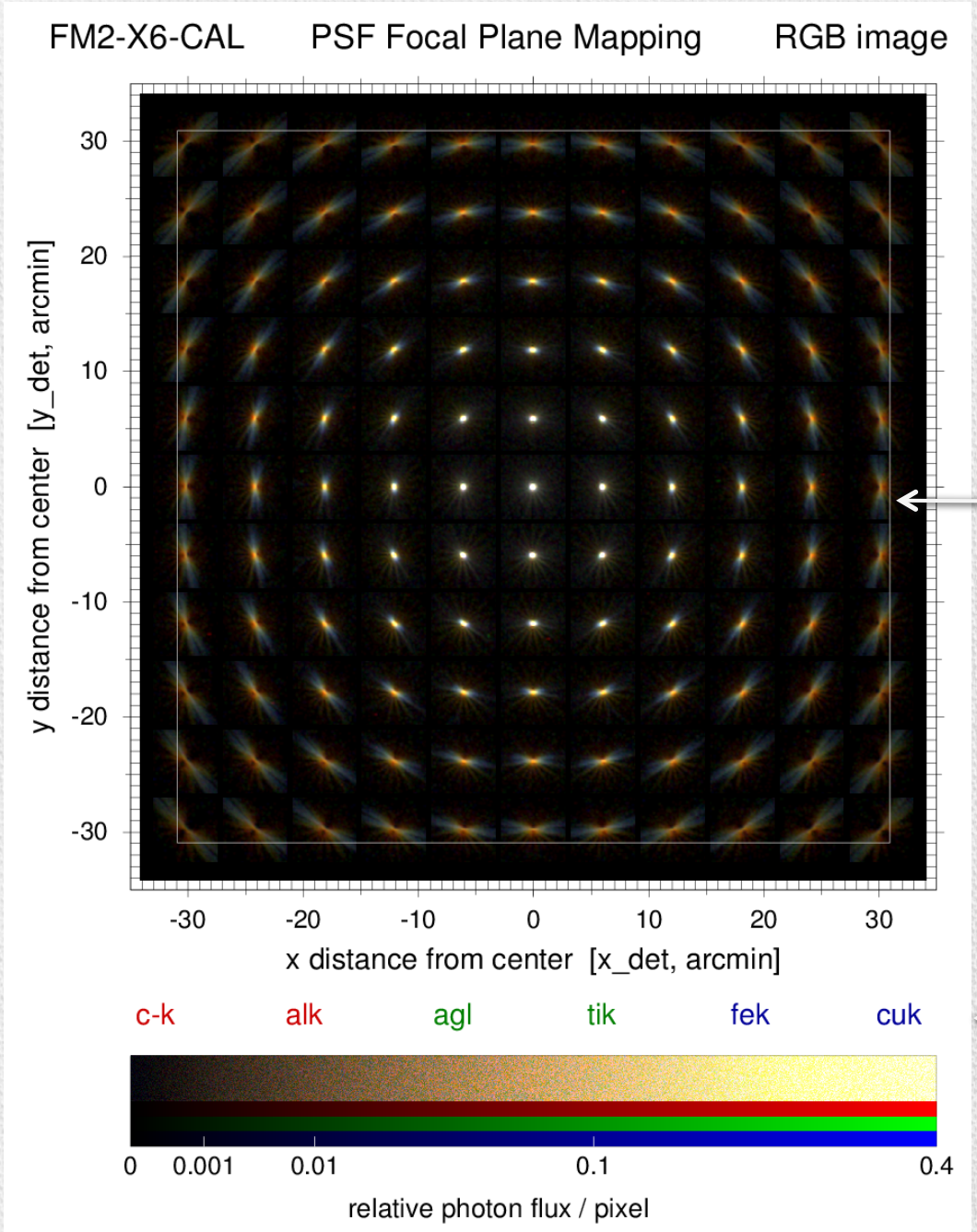

PSF Focal Plane Mapping: RGB images

eROSITA FoV

121 PSFs from scans 1 – 4, each composed of 6 energies

brightest pixel of all PSFs at each energy normalized to 1.0

transfer function: $f(z) = z^{0.4}$, zoomed to [0.0, 0.4]

selected RGB energies

image contains 6 x 121 = 726 PSFs !

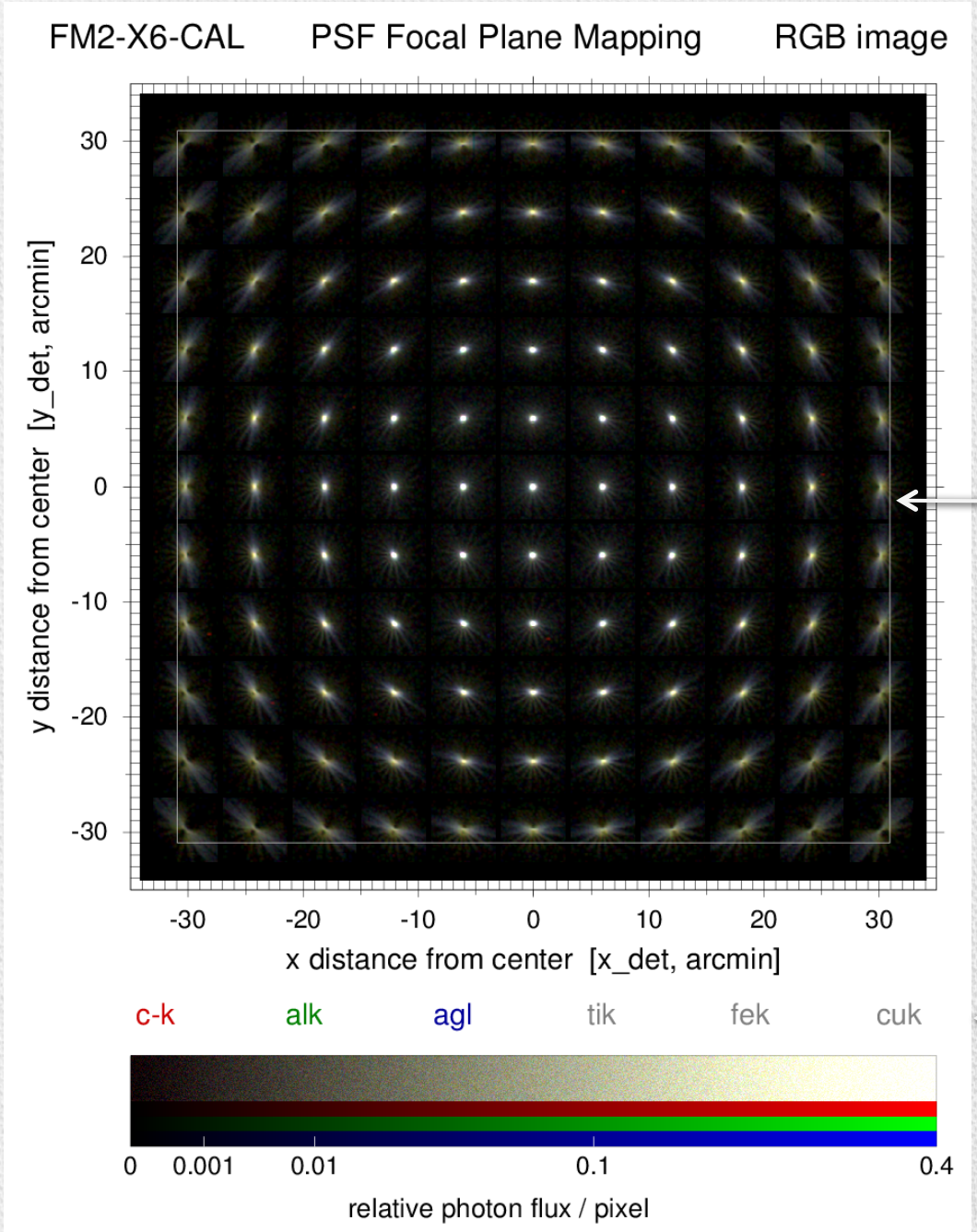

PSF Focal Plane Mapping: RGB images

eROSITA FoV

121 PSFs from scans 1 – 4, each composed of 3 energies

brightest pixel of all PSFs at each energy normalized to 1.0

transfer function: $f(z) = z^{0.4}$, zoomed to [0.0, 0.4]

selected RGB energies

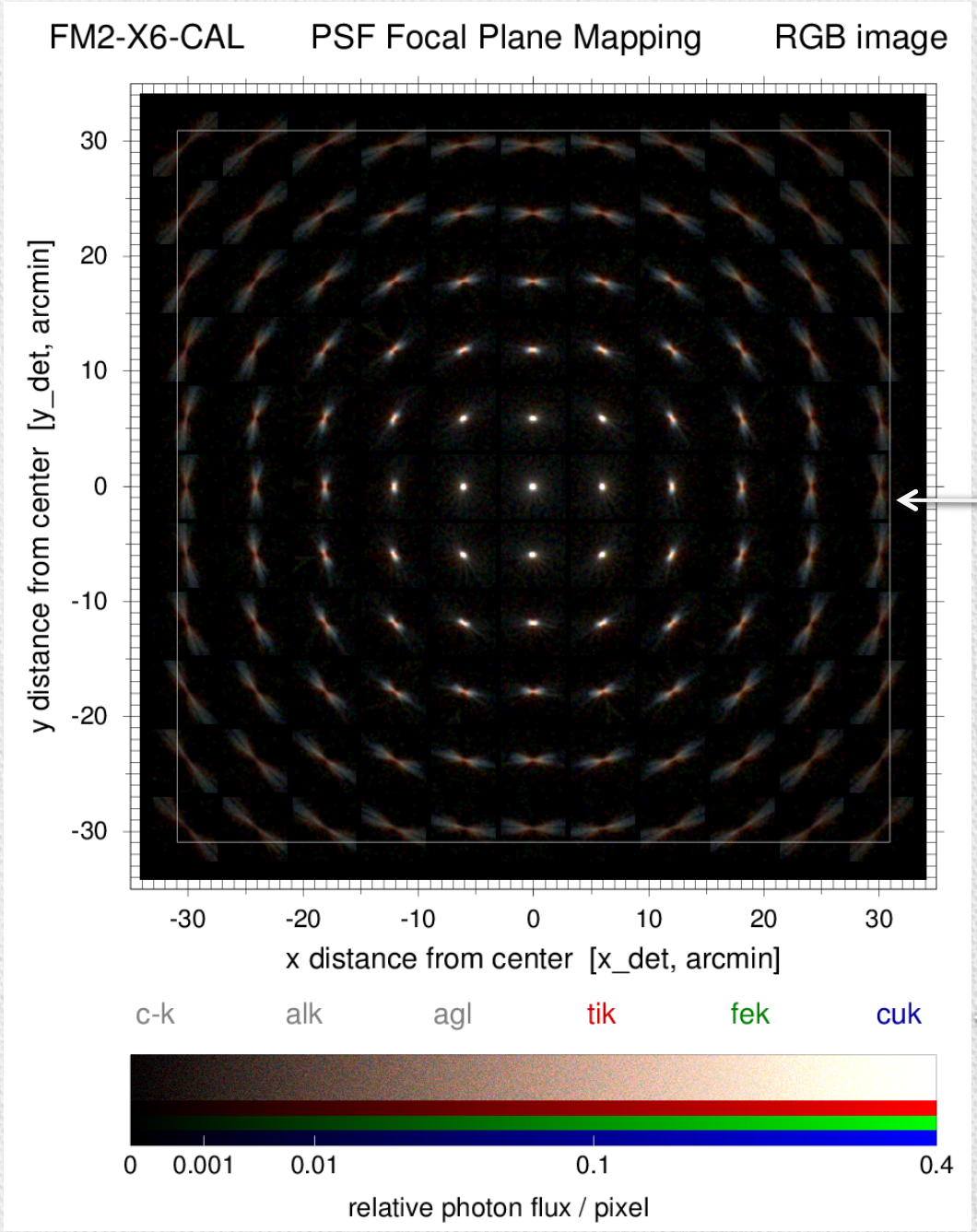

PSF Focal Plane Mapping: RGB images

eROSITA FoV

121 PSFs from scans 1 – 4, each composed of 3 energies

brightest pixel of all PSFs at each energy normalized to 1.0

transfer function: $f(z) = z^{0.4}$, zoomed to [0.0, 0.4]

selected RGB energies

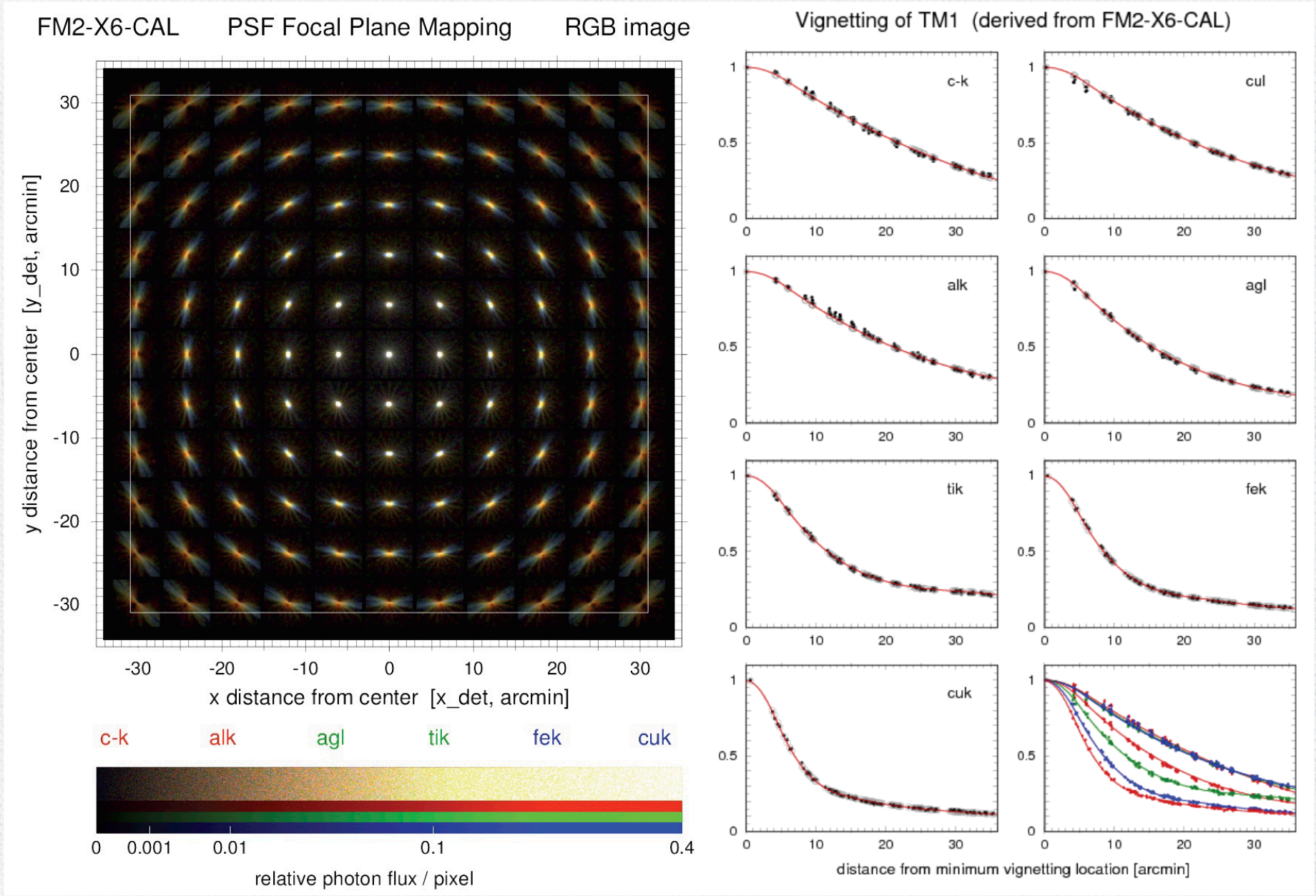
FM2-X6-CAL PSF Focal Plane Mapping RGB image
y distance from center [y_det, arcmin]
x distance from center [x_det, arcmin]
c-k alk agl tik fek cuk
0 0.001 0.01 0.1 0.4
relative photon flux / pixel
Vignetting of TM1 (derived from FM2-X6-CAL)
c-k
cul
alk
agl
tik
fek
cuk
distance from minimum vignetting location [arcmin]

Effective Area, Vignetting

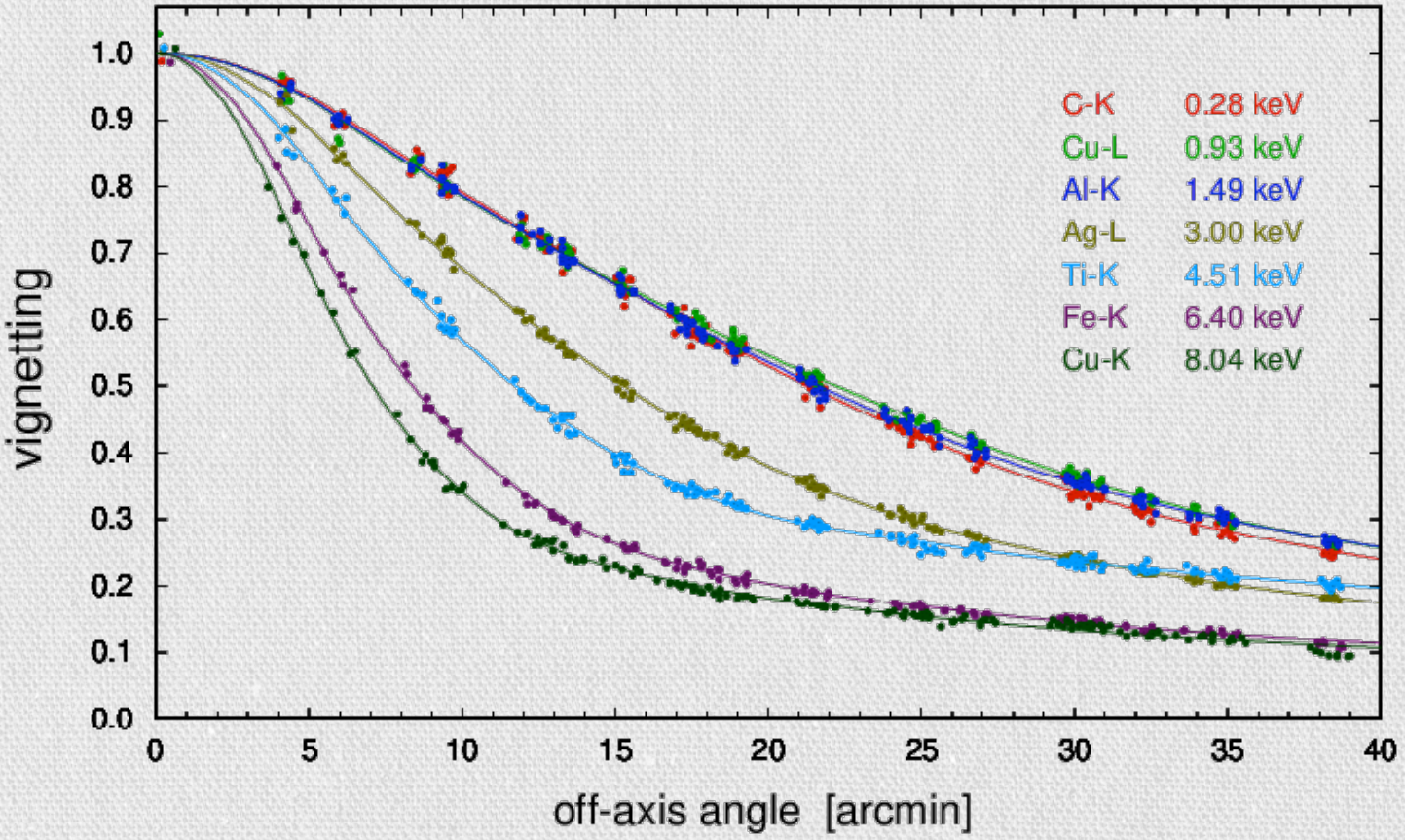

Vignetting derived from PSF focal plane mapping at PANTER

From photons to bits: the fate of X-rays grabbed by eROSITA

device	*process*	*signal*	*characteristic properties*	
telescope	reflection (scattering)	*photon [eV]*	effective area (E,θ,φ) point spread function (E,θ,φ) field of view (FOV) boresight	collecting area, reflectivity, vignetting mirror quality, encircled energy fraction focal length, detector geometry, plate scale alignment
filter	absorption		transmission (E,x,y) contamination (E,x,y,t)	
CCD	charge release	*charge [e^-]*		
	charge transfer			
	charge readout	*pulse height amplitude [adu]*		
on-board data processor	signal processing	*event [bit]*		

Filter Calibration

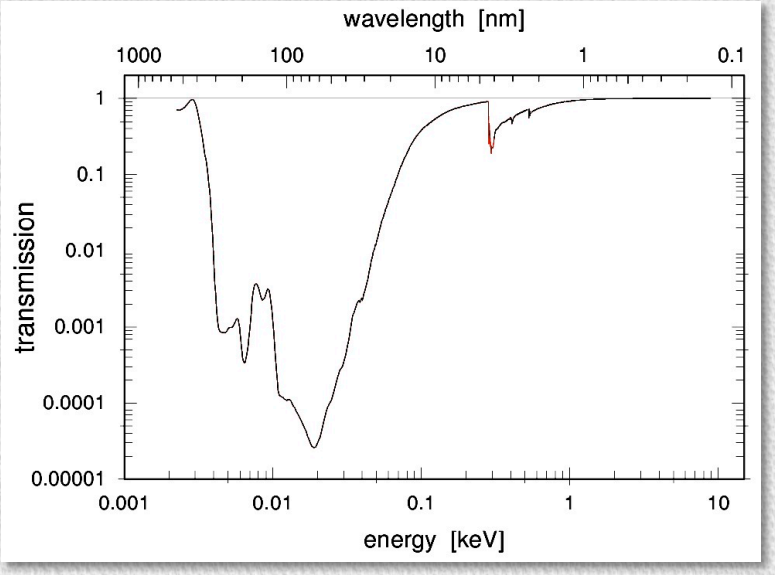

eROSITA
207.4 nm Polyimide filter

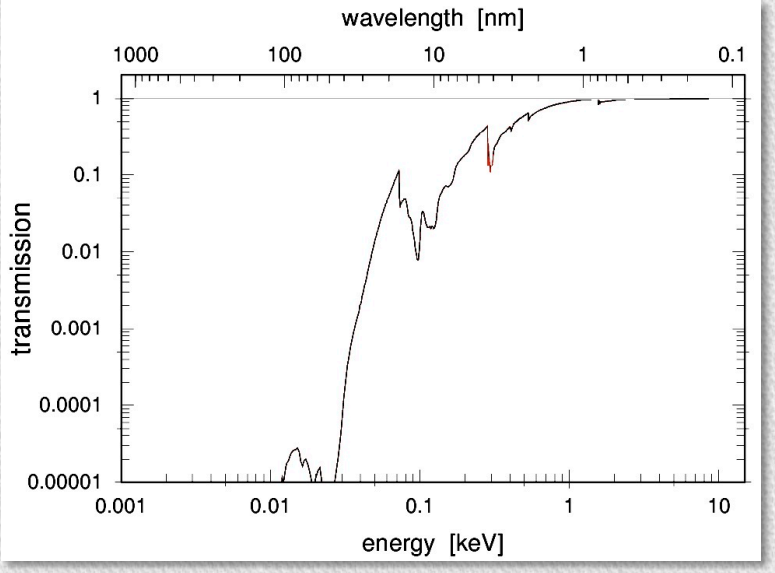

eROSITA
193.8 nm Polyimide filter +
101.2 nm Aluminium filter

From photons to bits: the fate of X-rays grabbed by eROSITA

device	*process*	*signal*	*characteristic properties*	
telescope	reflection (scattering)	*photon [eV]*	effective area (E,θ,φ) point spread function (E,θ,φ) field of view (FOV) boresight	collecting area, reflectivity, vignetting mirror quality, encircled energy fraction focal length, detector geometry, plate scale alignment
filter	absorption		transmission (E,x,y) contamination (E,x,y,t)	
CCD	charge release	*charge [e^-]*	charge splitting	**patterns** (singles, doubles, triples, quadruples, invalid..)
	charge transfer			
	charge readout	*pulse height amplitude [adu]*		
on-board data processor	signal processing	*event [bit]*		

Charge splitting → Pixel patterns

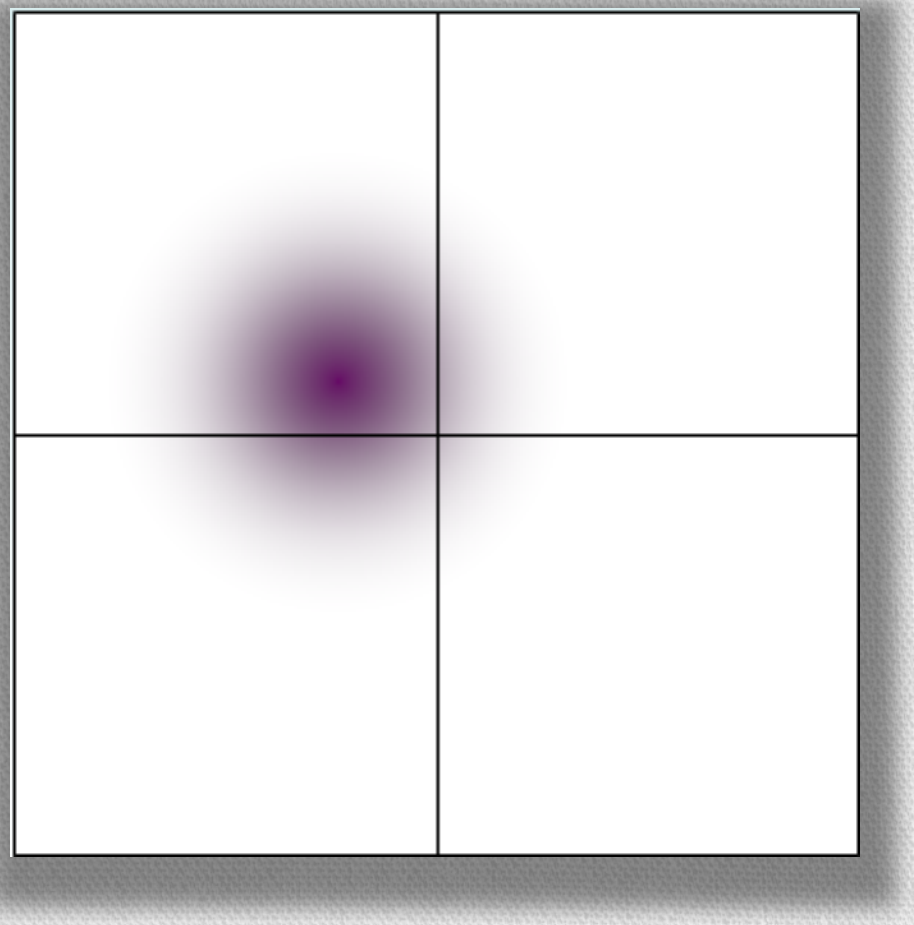

From photons to bits: the fate of X-rays grabbed by eROSITA

device	*process*	*signal*	*characteristic properties*	
telescope	reflection (scattering)	*photon [eV]*	effective area (E,θ,φ) point spread function (E,θ,φ) field of view (FOV) boresight	collecting area, reflectivity, vignetting mirror quality, encircled energy fraction focal length, detector geometry, plate scale alignment
filter	absorption		transmission (E,x,y) contamination (E,x,y,t)	
CCD	charge release	*charge [e^-]*	charge splitting low energy threshold	**patterns** (singles, doubles, triples, quadruples, invalid..)
	charge transfer			
	charge readout	*pulse height amplitude [adu]*		
on-board data processor	signal processing	*event [bit]*		

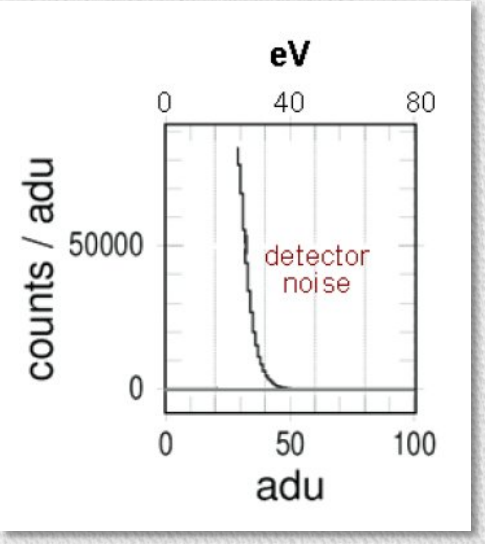

Charge splitting and the low energy threshold

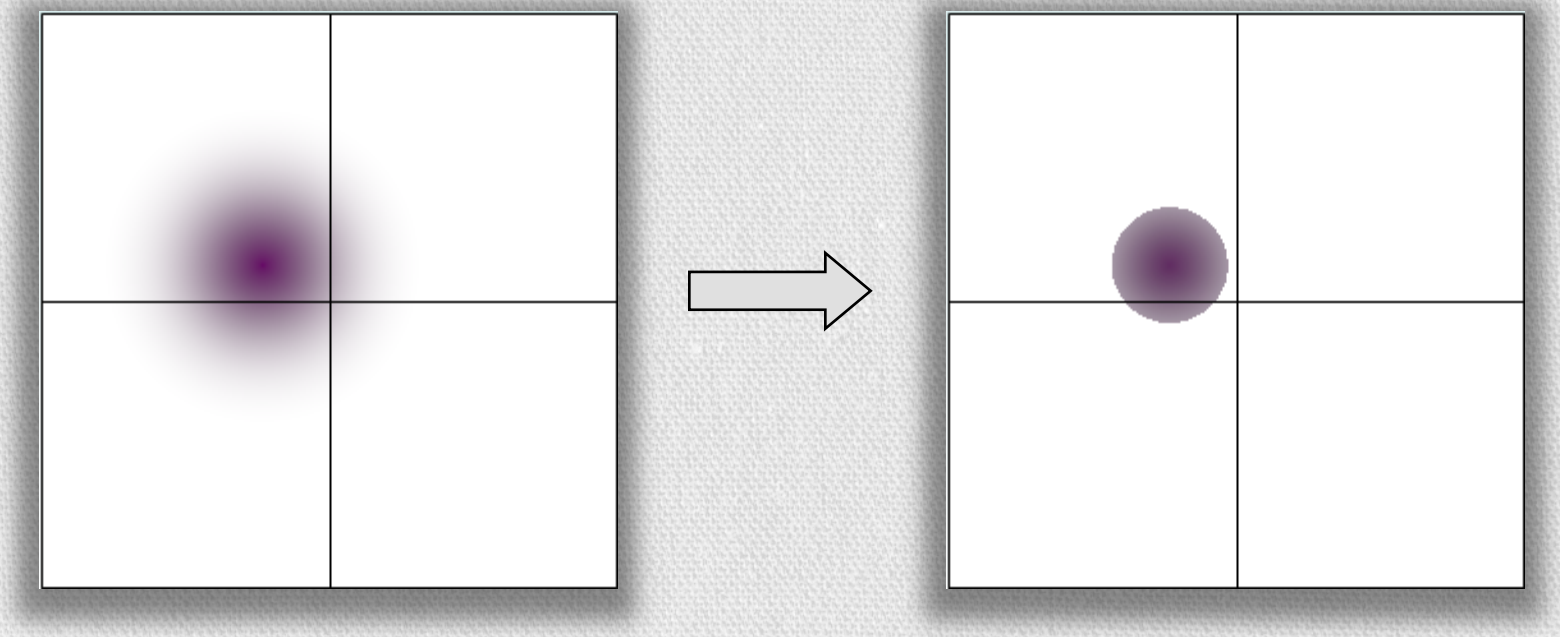

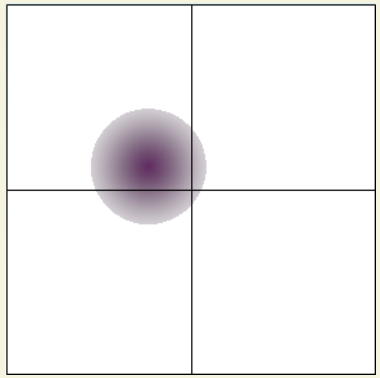

very low threshold

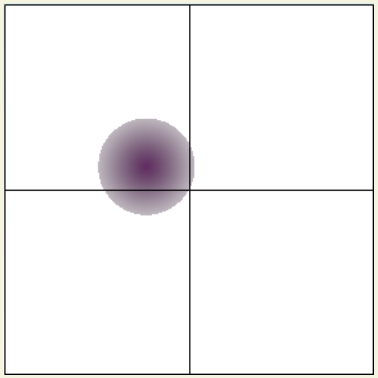

low threshold

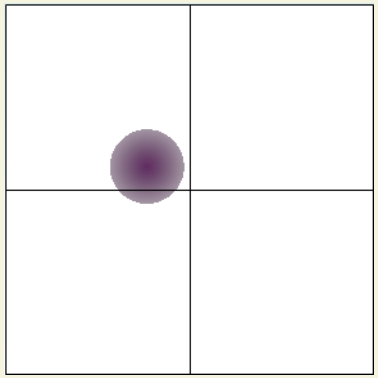

high threshold

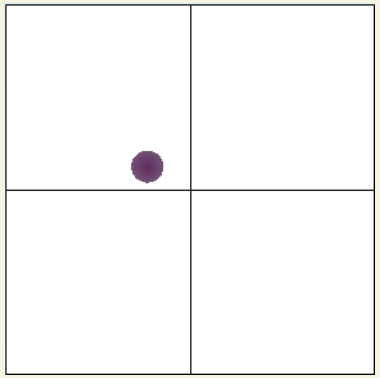

very high threshold

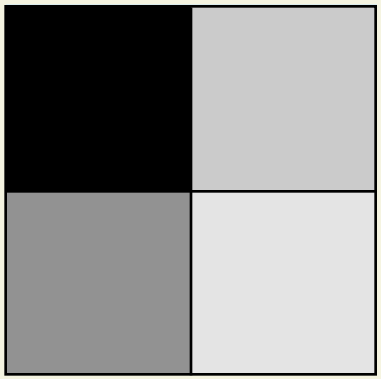

quadruple

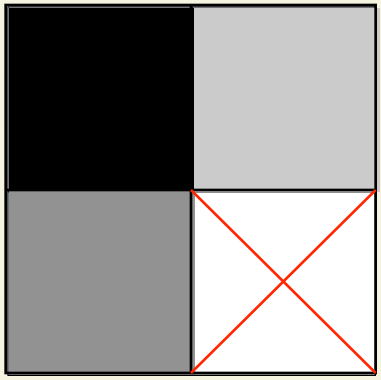

triple

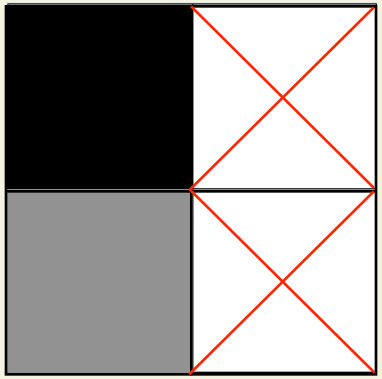

double

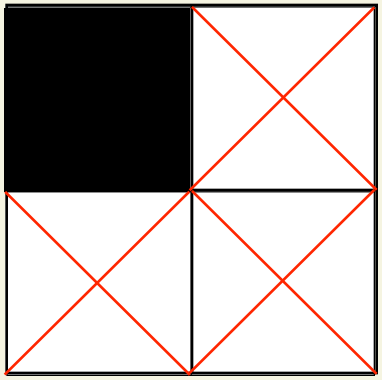

single

→ *observed* pattern depends on the low energy threshold

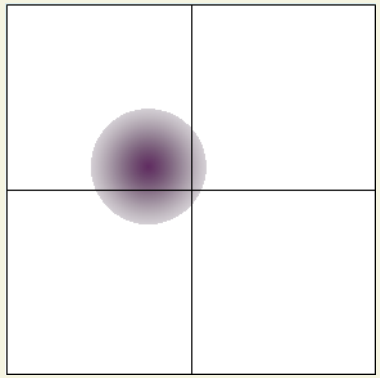

very low threshold

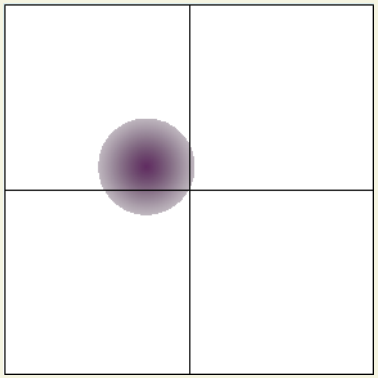

low threshold

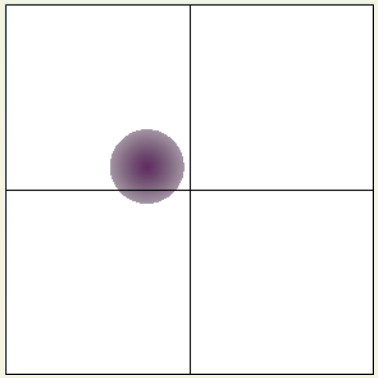

high threshold

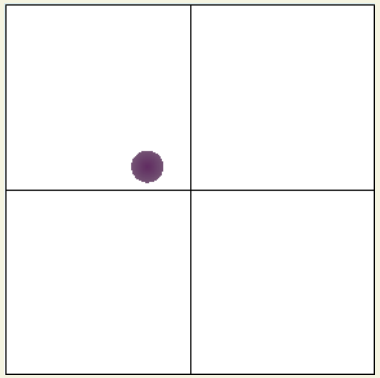

very high threshold

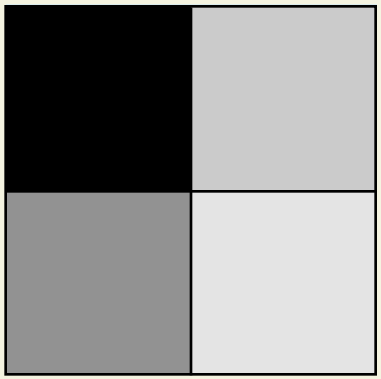

quadruple

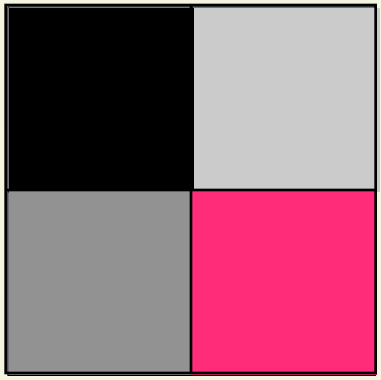

triple

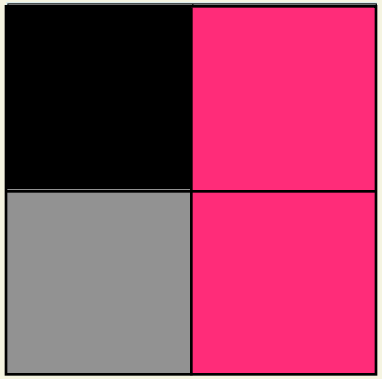

double

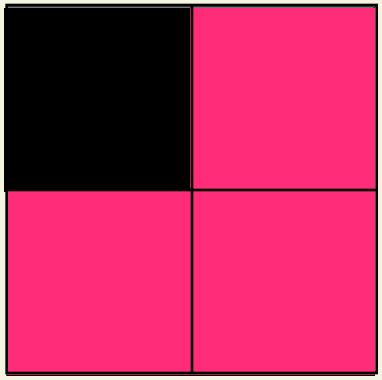

single

charge lost → degradation of the energy resolution

Impact of the low energy threshold on the *spectral resolution*

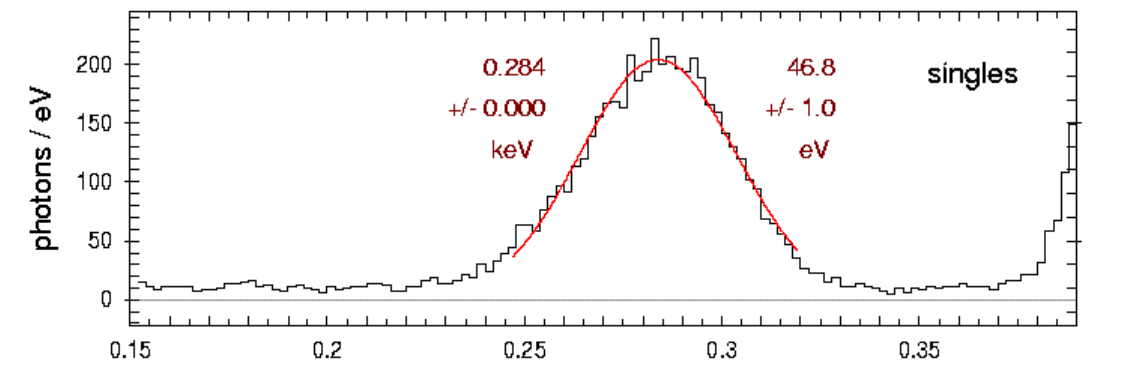

low energy threshold: **~40 eV**

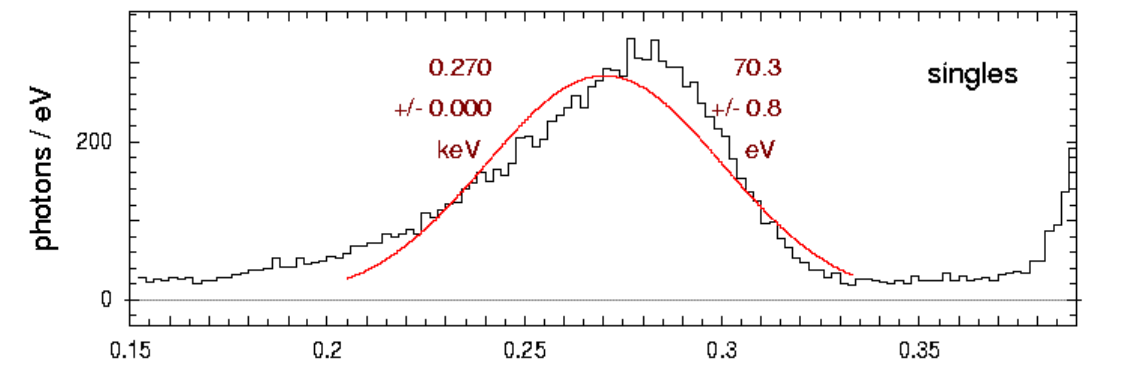

low energy threshold: **~100 eV**

→ the spectral resolution of X-ray CCDs depends on the low energy threshold

PSF Focal Plane Mapping: HEW

The effect of charge splitting can be utilized for improving the spatial resolution

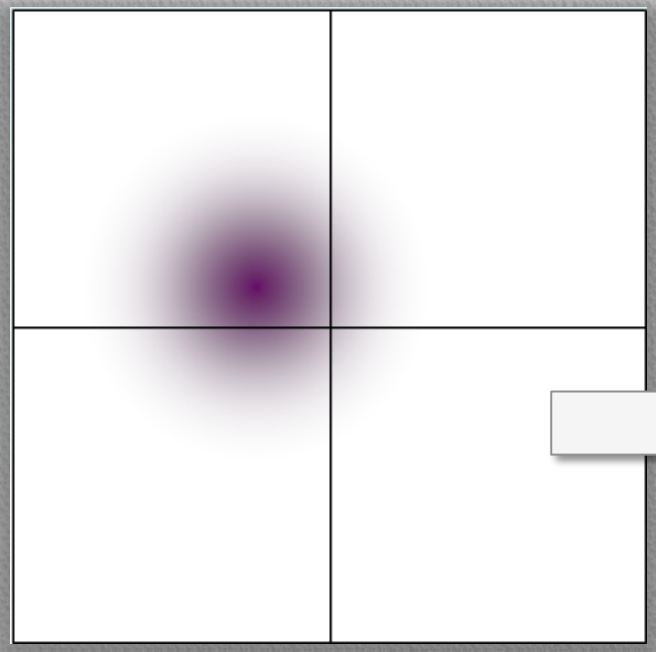

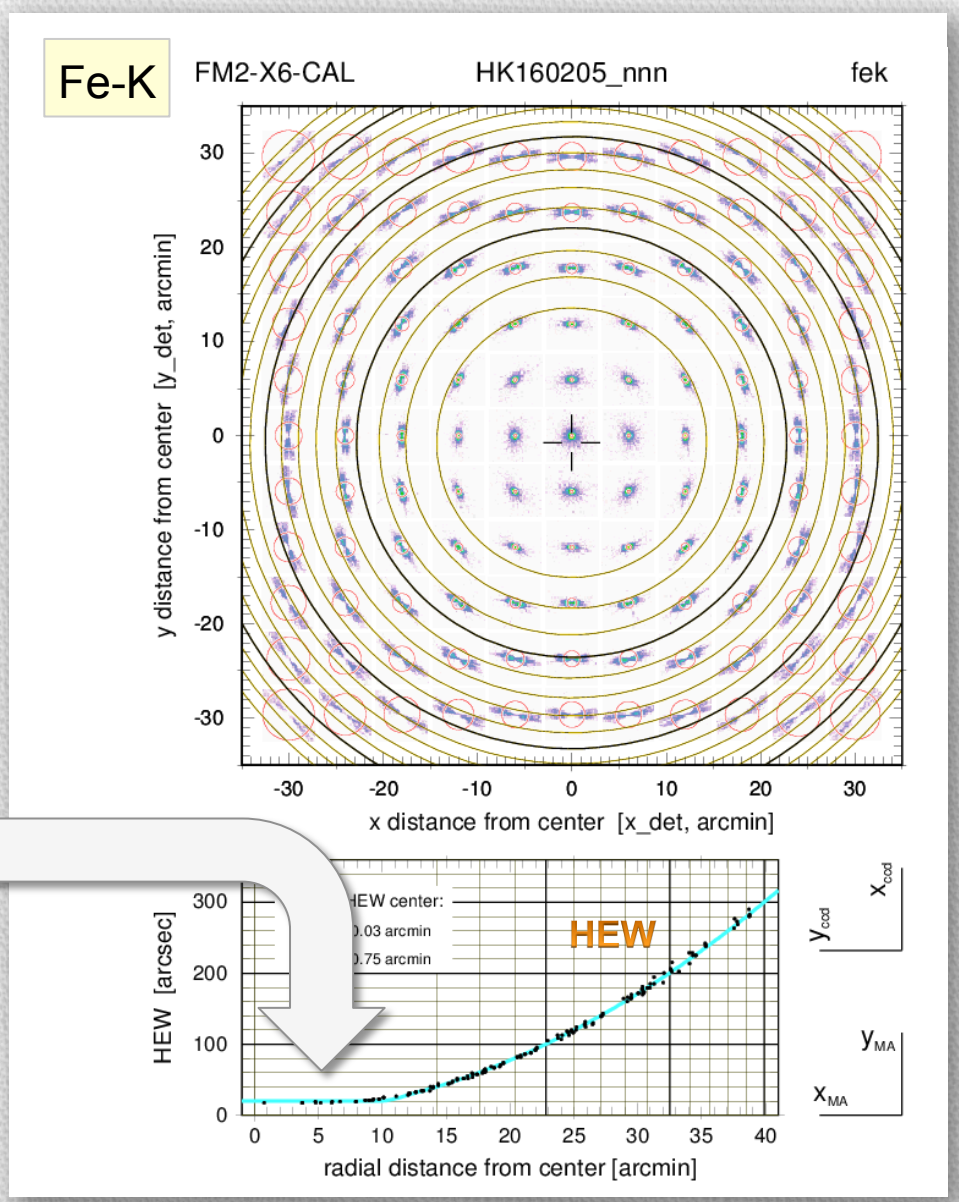

Determination of the eROSITA PSF

On-axis PSF

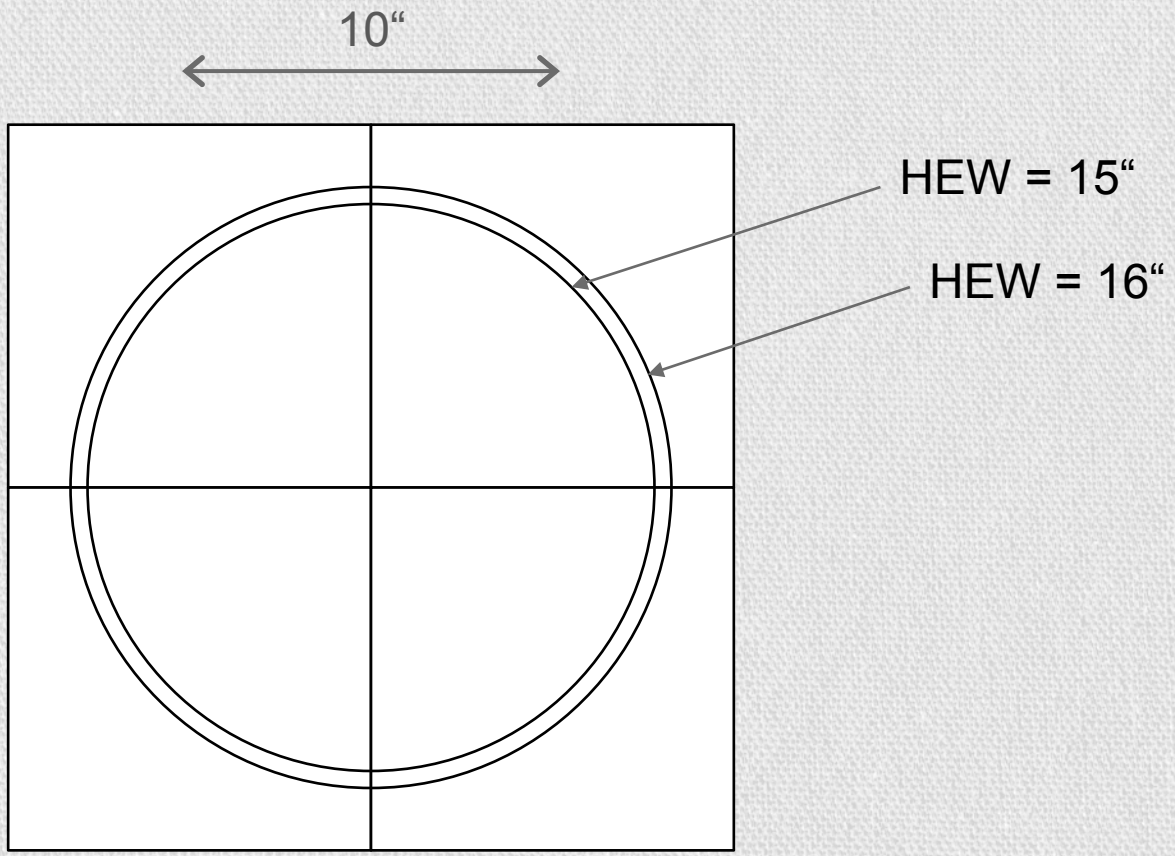

1 px = 9.6“ x 9.6“
= 75 µm x 75 µm

Distribution of reconstructed photon positions

single pixel events

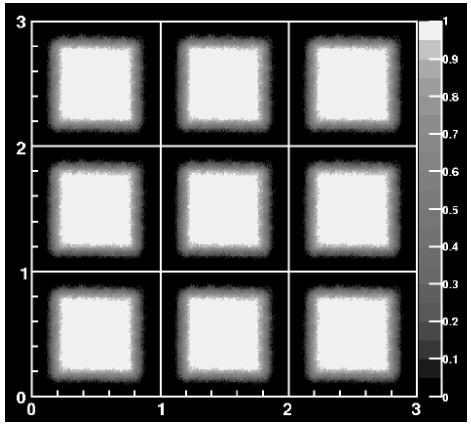

Kimmel et al., SPIE 6276, 2006

Distribution of reconstructed photon positions

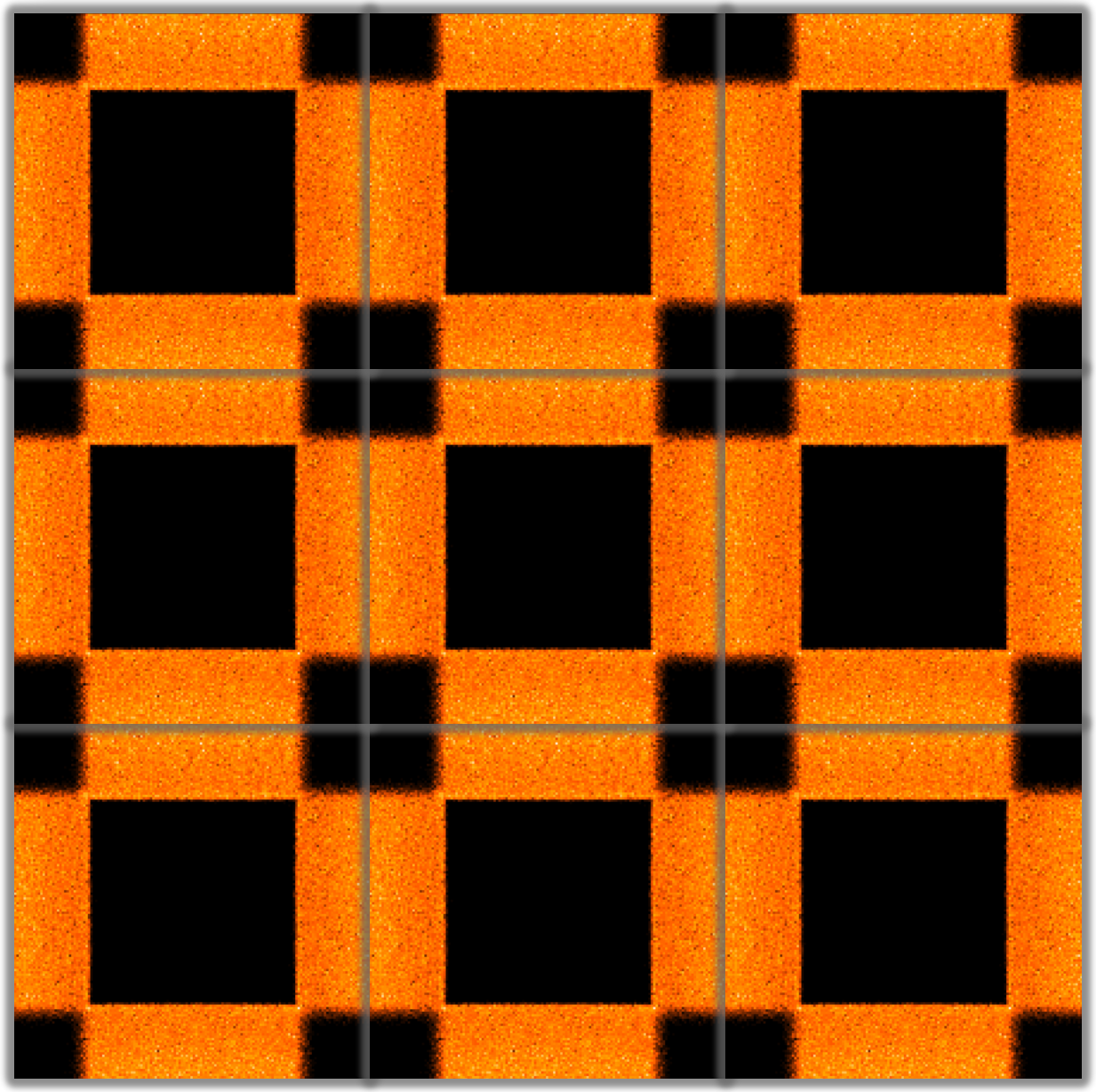

double events

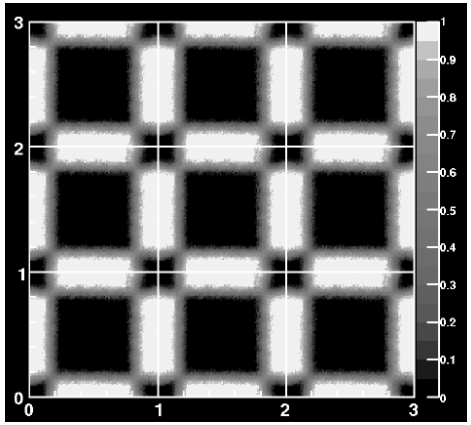

Kimmel et al., SPIE 6276, 2006

Distribution of reconstructed photon positions

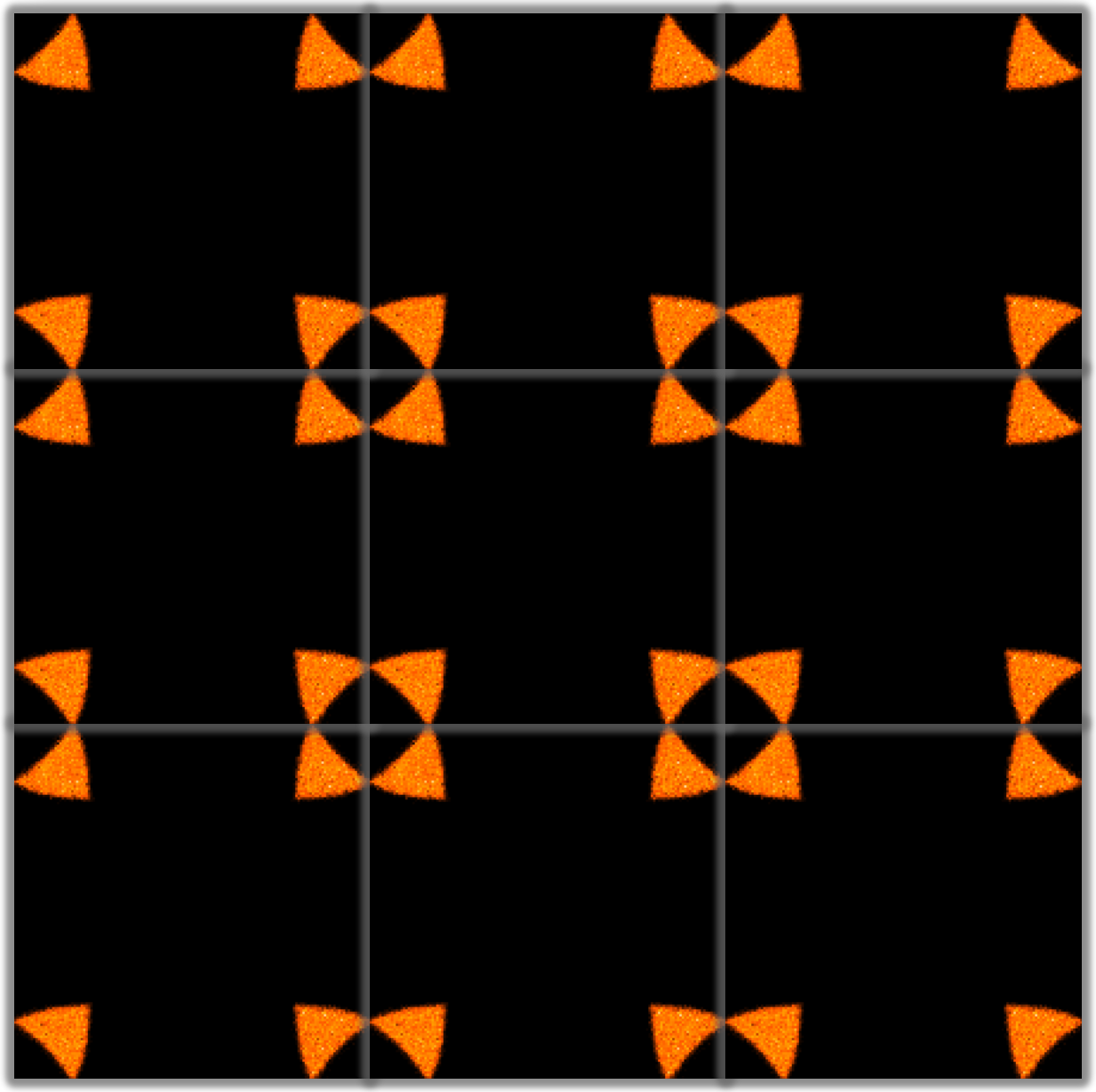

triple events

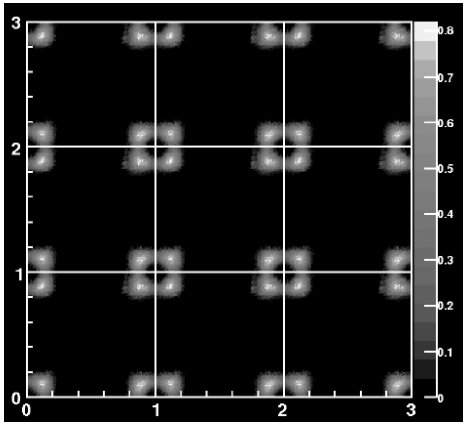

Kimmel et al., SPIE 6276, 2006

Distribution of reconstructed photon positions

quadruple events

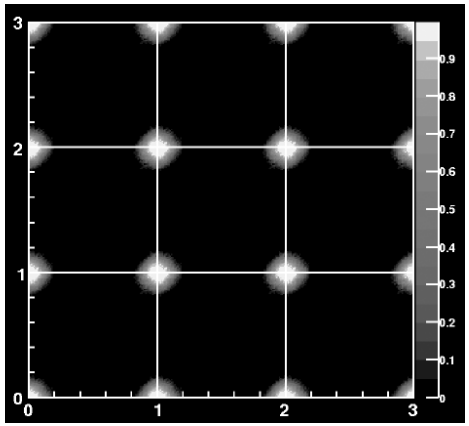

Kimmel et al., SPIE 6276, 2006

Comparison of X-ray CCD images without subpixel resolution

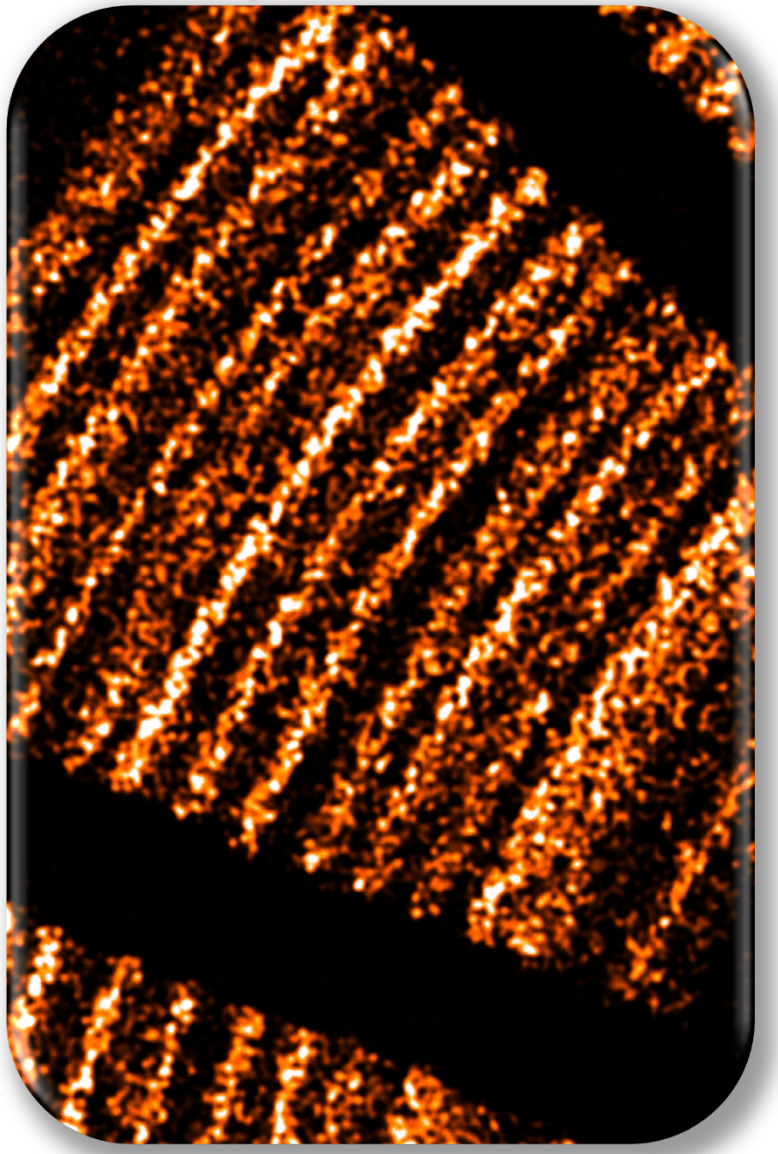

Pattern resolved subpixel anatomy of an X-ray CCD image

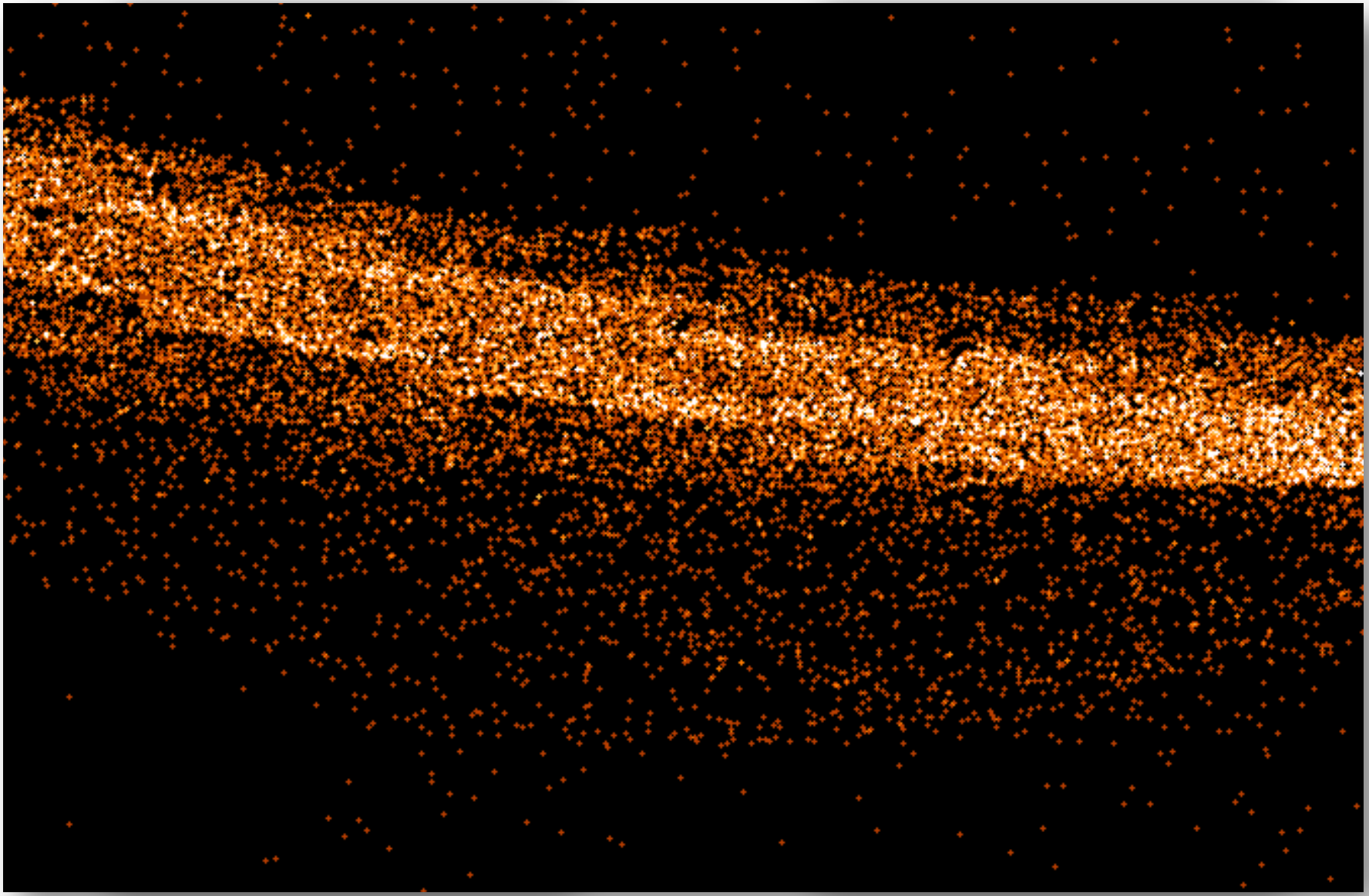

Pattern resolved subpixel anatomy of an X-ray CCD image

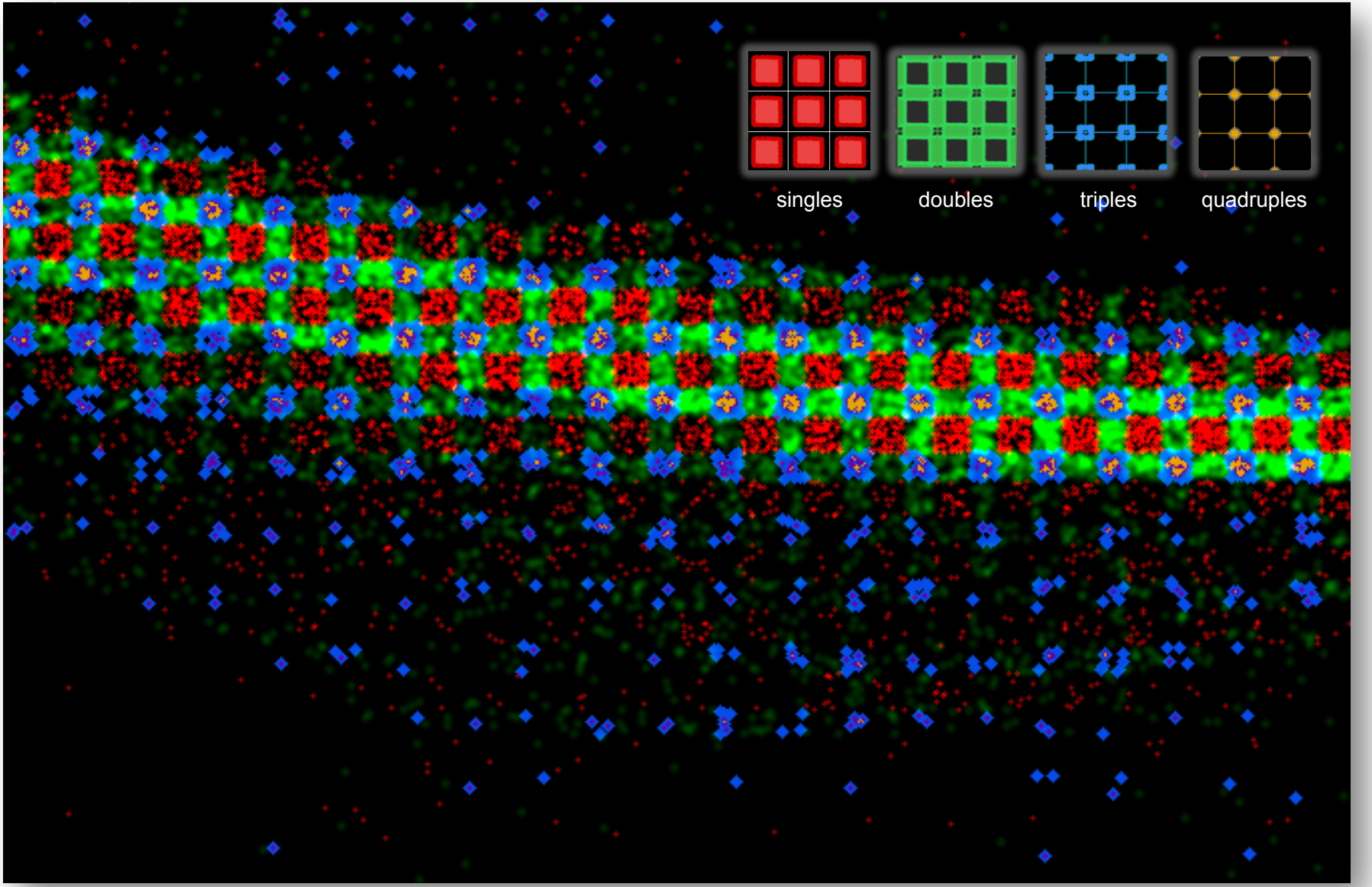

Pattern resolved subpixel anatomy of an X-ray CCD image

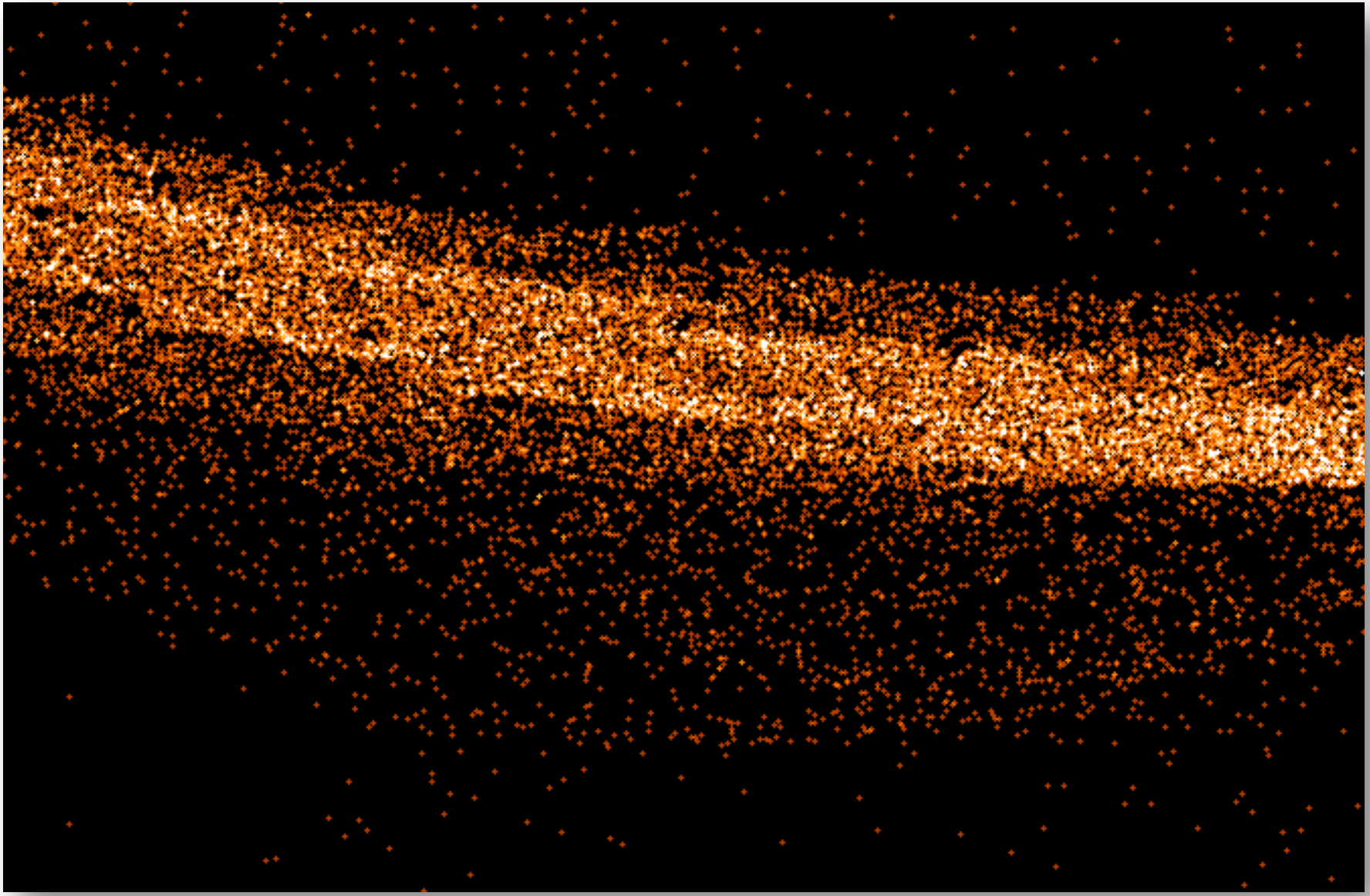

Determination of the eROSITA PSF

On-axis PSF

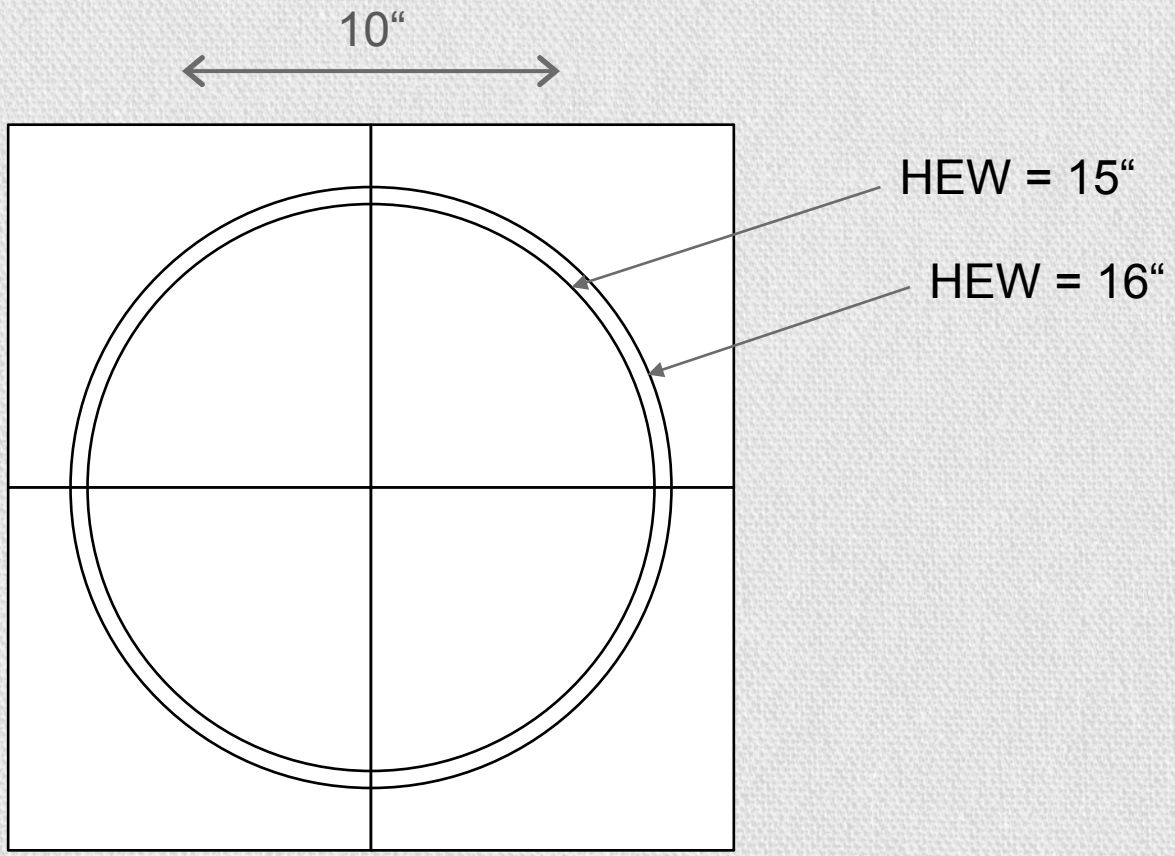

1 px = 9.6“ x 9.6“
= 75 µm x 75 µm

Determination of the eROSITA PSF

On-axis PSF

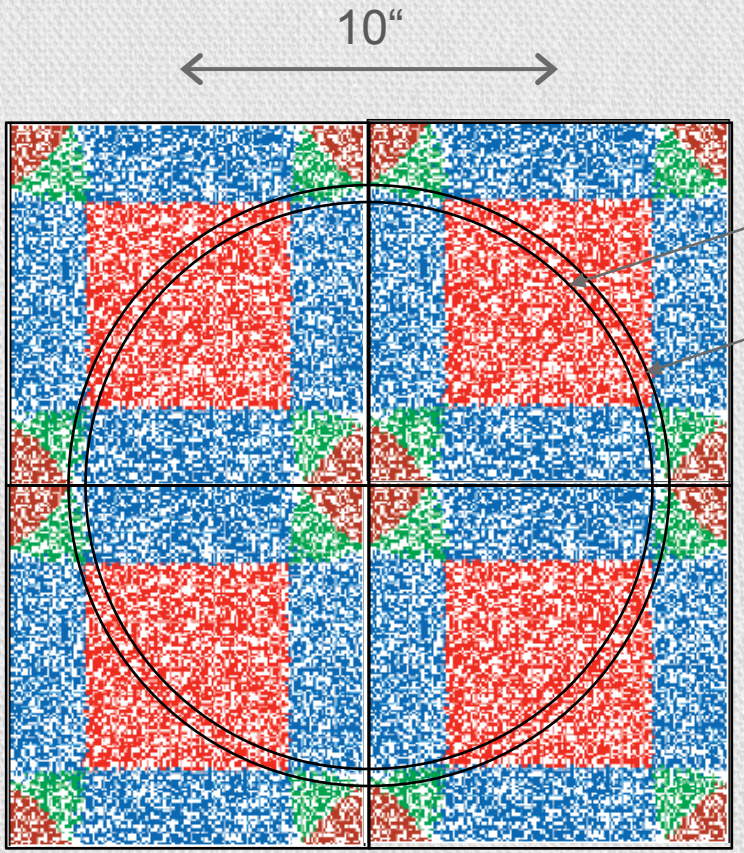

1 px = 9.6“ x
9.6“ = 75 µm x
75 µm

Impact of the low energy threshold on the *spatial resolution*

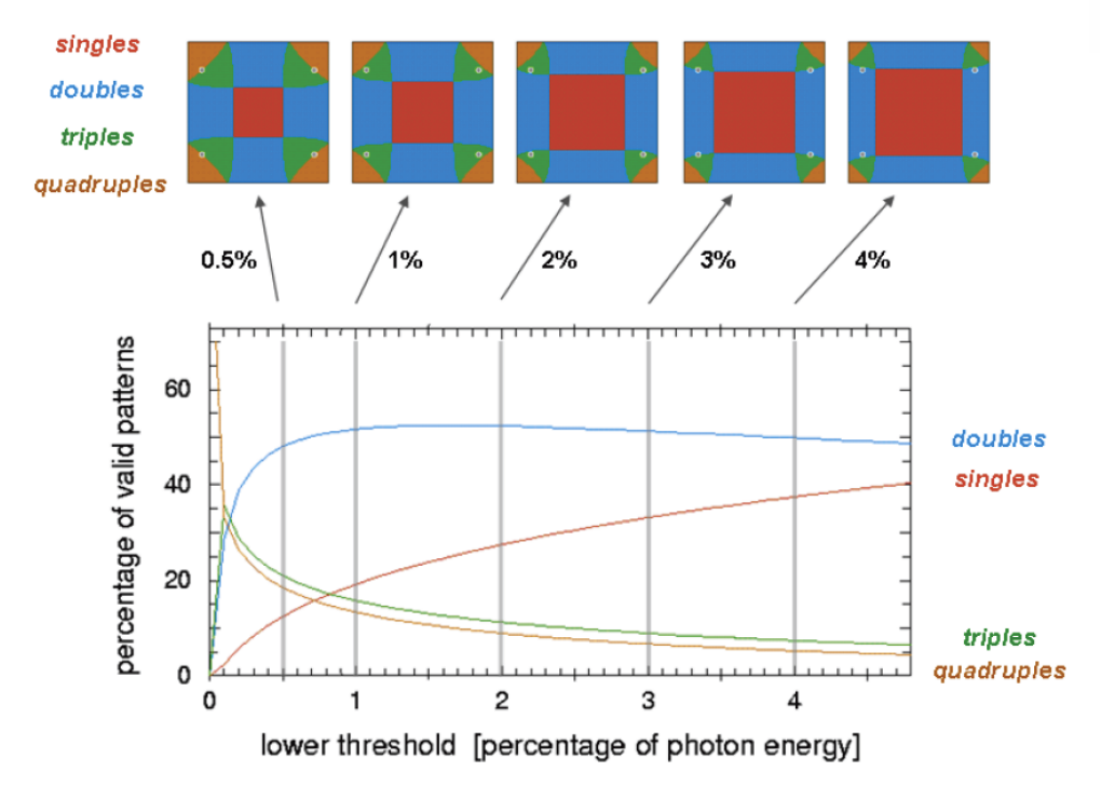

→ **the spatial resolution of X-ray CCDs depends on the low energy threshold**

12x12 pixel scans at Al-K, without subpixel resolution

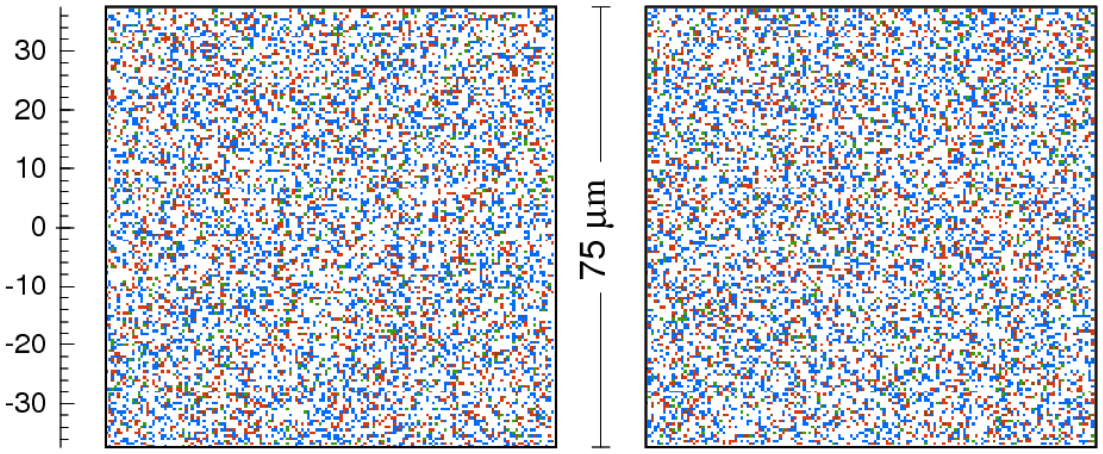

subpixel position in CCD frame

subpixel position in telescope frame

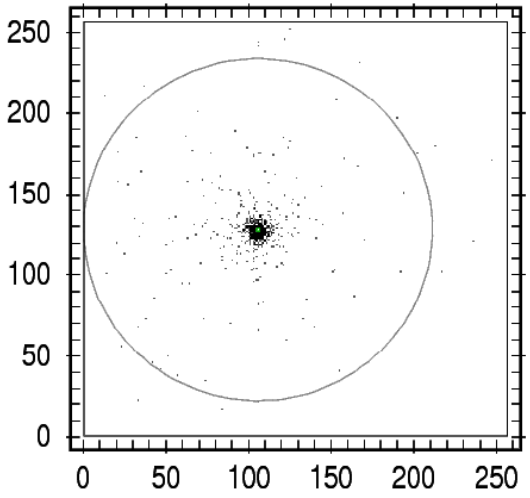

full CCD image (telescope frame)

reference frame: HK110509_294.fits

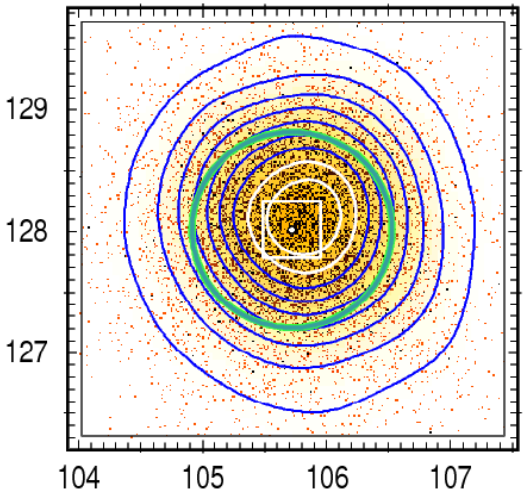

zoomed region (telescope frame)

HEW center: 105.72 128.01

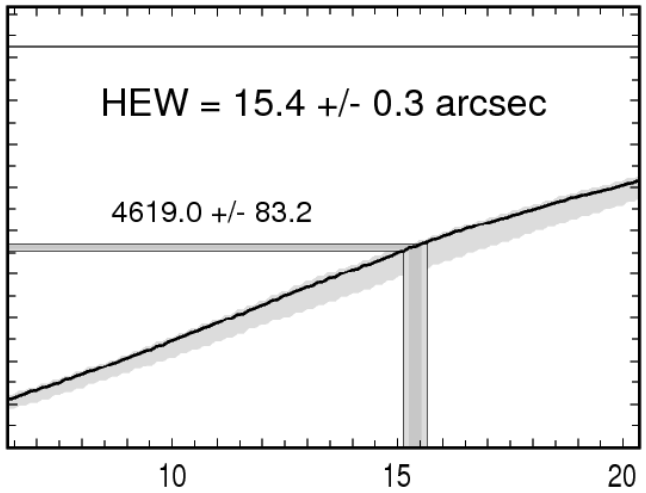

HEW [arcsec]

12x12 pixel scans at Al-K, with subpixel resolution

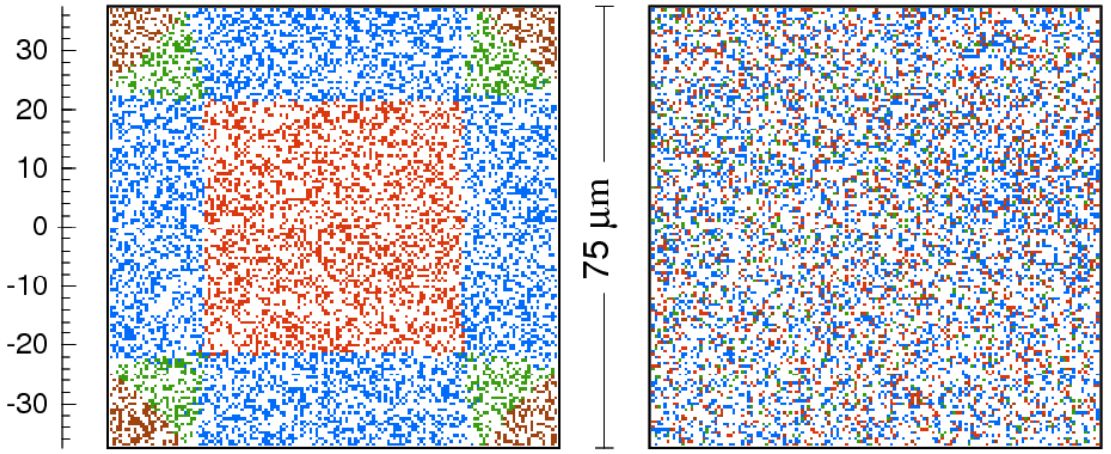

subpixel position in CCD frame

subpixel position in telescope frame

using all valid patterns

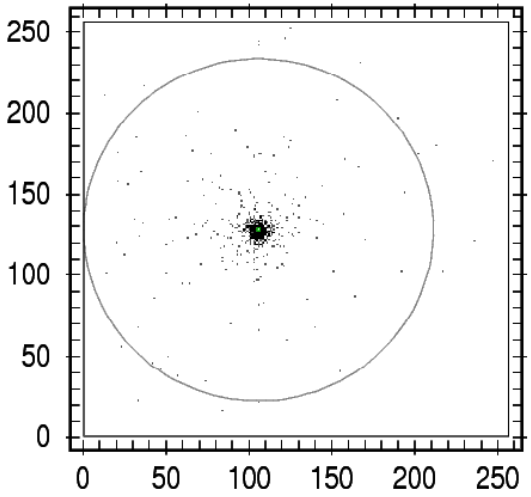

full CCD image (telescope frame)

reference frame: HK110509_294.fits

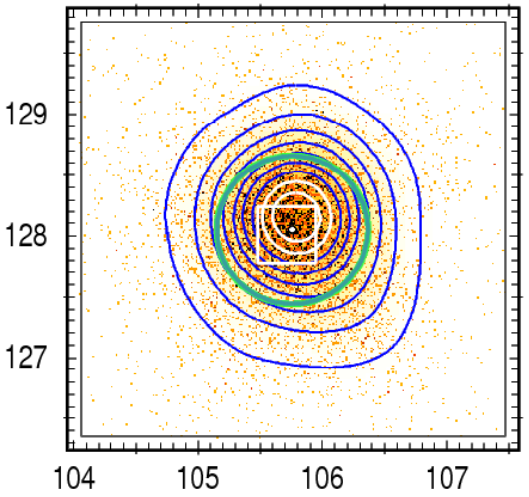

zoomed region (telescope frame)

HEW center: 105.76 128.05

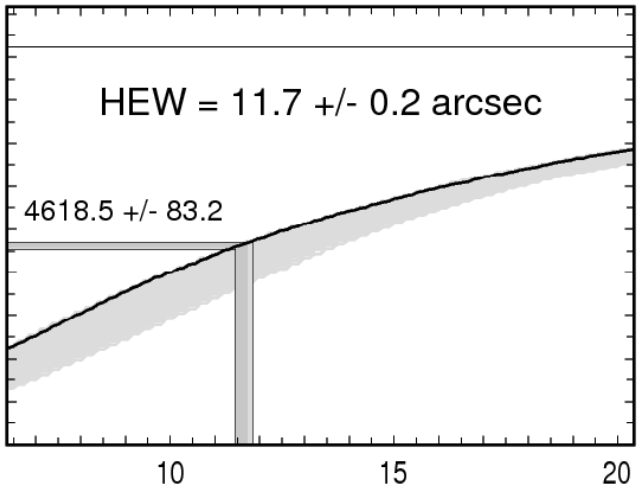

From photons to bits: the fate of X-rays grabbed by eROSITA

device	*process*	*signal*	*characteristic properties*	
telescope	reflection (scattering)	*photon [eV]*	effective area (E,θ,φ) point spread function (E,θ,φ) field of view (FOV) boresight	collecting area, reflectivity, vignetting mirror quality, encircled energy fraction focal length, detector geometry, plate scale alignment
filter	absorption		transmission (E,x,y) contamination (E,x,y,t)	
CCD	charge release	*charge [e^-]*	charge splitting low energy threshold	**patterns** (singles, doubles, triples, quadruples, invalid..)
			contaminating effects	**pile-up** (single pixel, pattern) **photon background** (fluorescence, optical loading) **particle induced background** (soft protons, MIPs) **detector induced background** (noise, bright pixels)
	charge transfer			
	charge readout	*pulse height amplitude [adu]*		
on-board data processor	signal processing	*event [bit]*		

Contaminating effects: pile-up

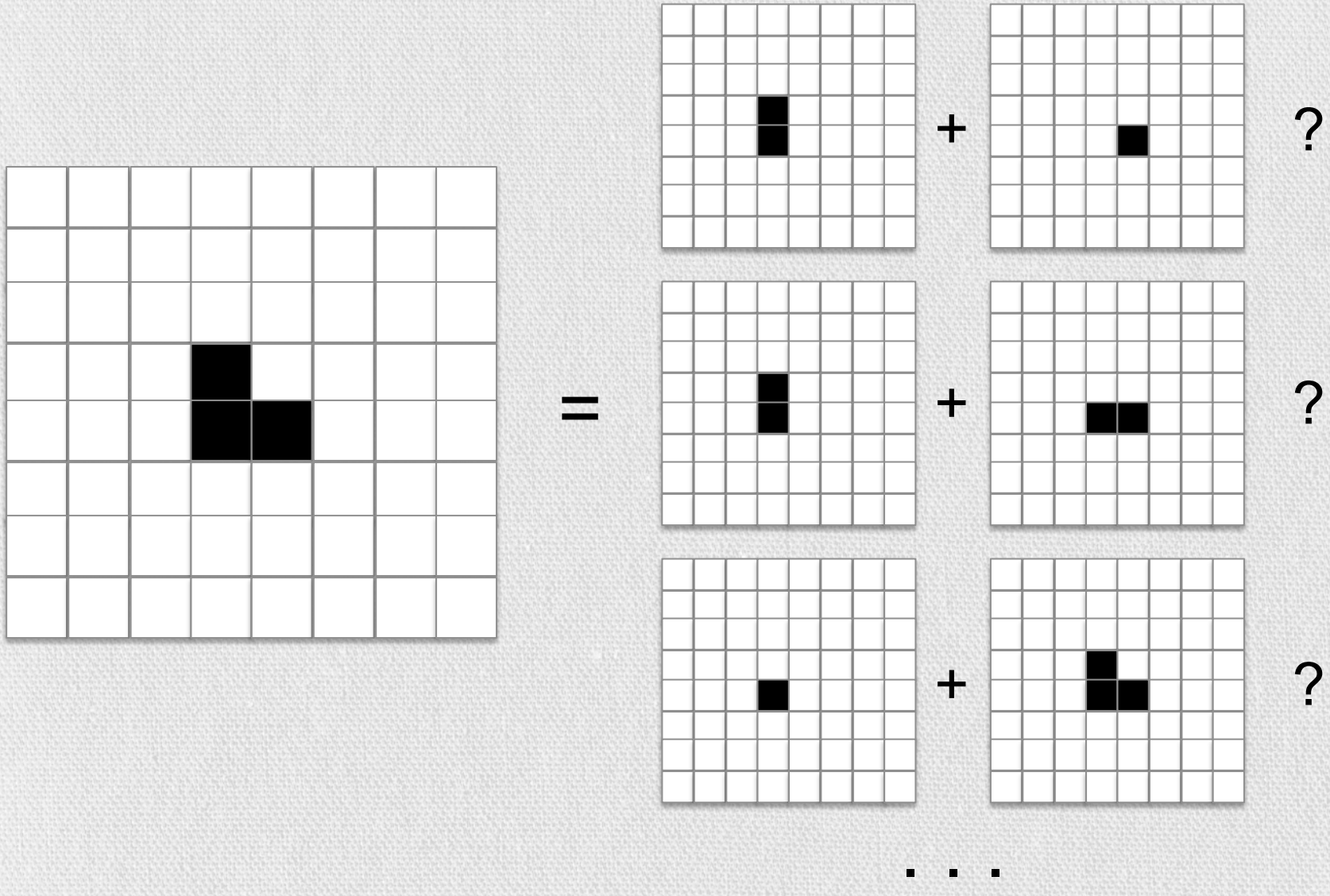

Contaminating effects: pile-up of X-ray photons

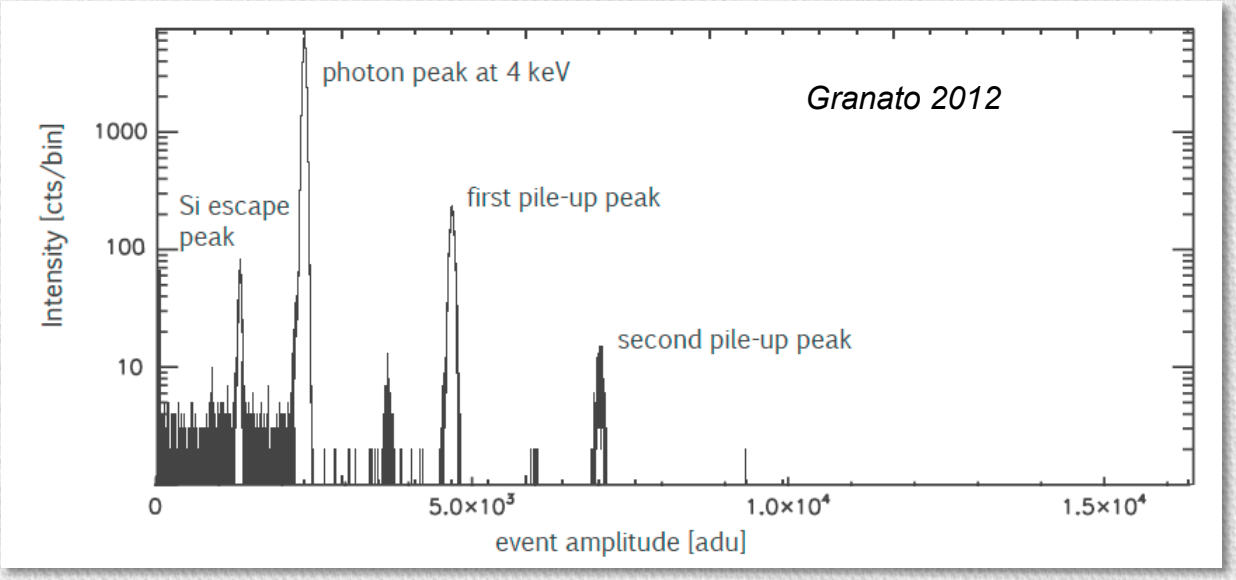

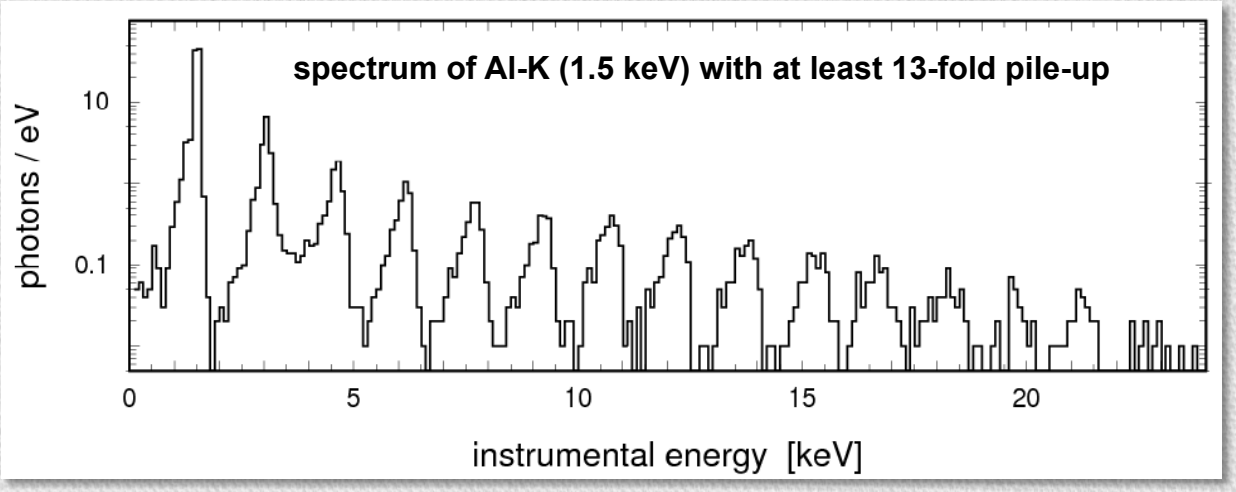

Contaminating effects: pile-up of X-ray and optical photons

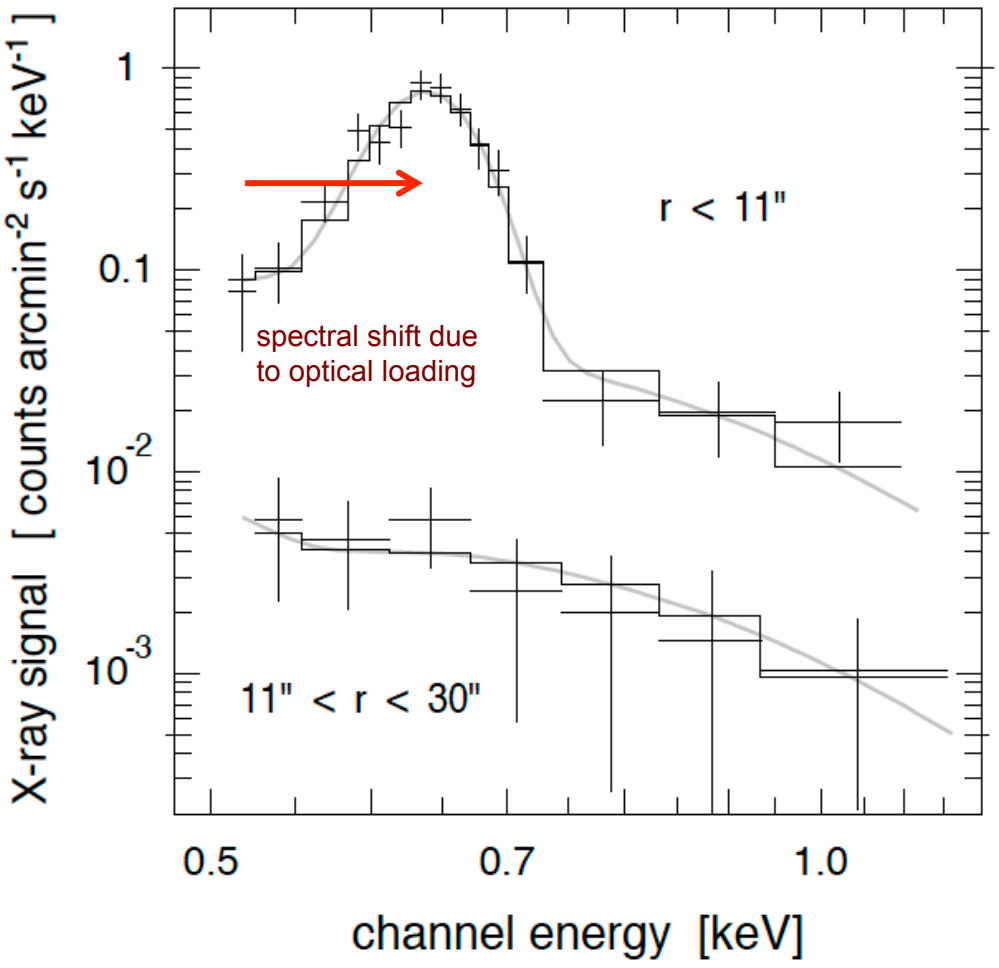

Chandra X-ray spectrum of Mars (Dennerl 2002)

Contaminating effects: optical photon background

SRG/eROSITA-TM5 Optical light leak 10 min time bins

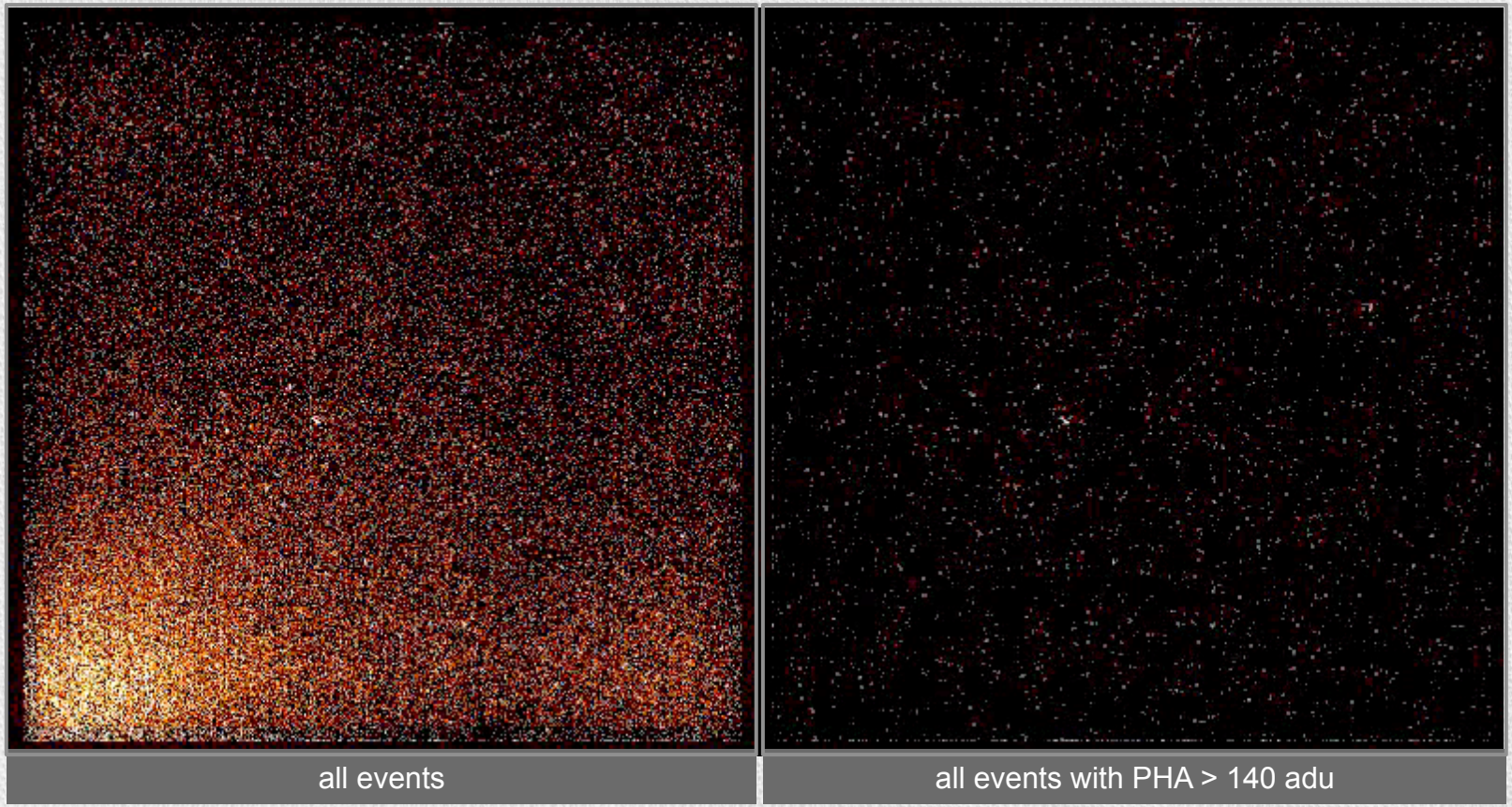

all events | all events with PHA > 140 adu

```
begin: Sa, 2019-08-31T19:37:15.00, eROday: 43098 (+0.66)
end:   Su, 2019-09-01T18:49:05.00, eROday: 43104 (+0.45)
elapsed time: 83.5 ks, net exposure time: 77.5 ks (92.8%)
linear intensity scale from 0 to 4 events/10 min
```

Contaminating effects: particle induced background

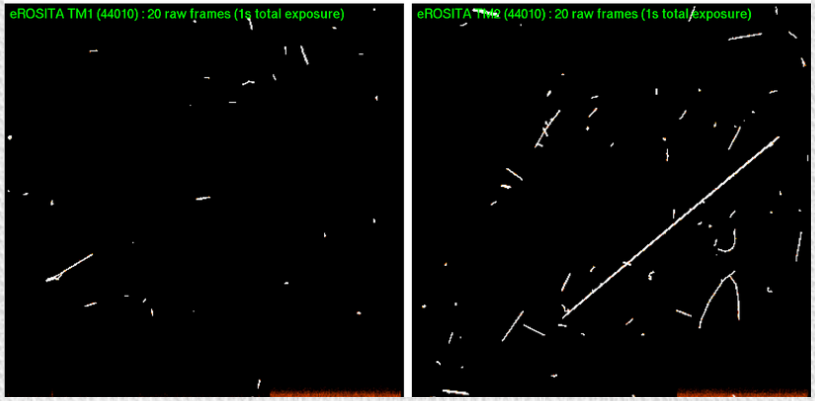

tracks of minimum ionizing particles (Freyberg et al. 2020)

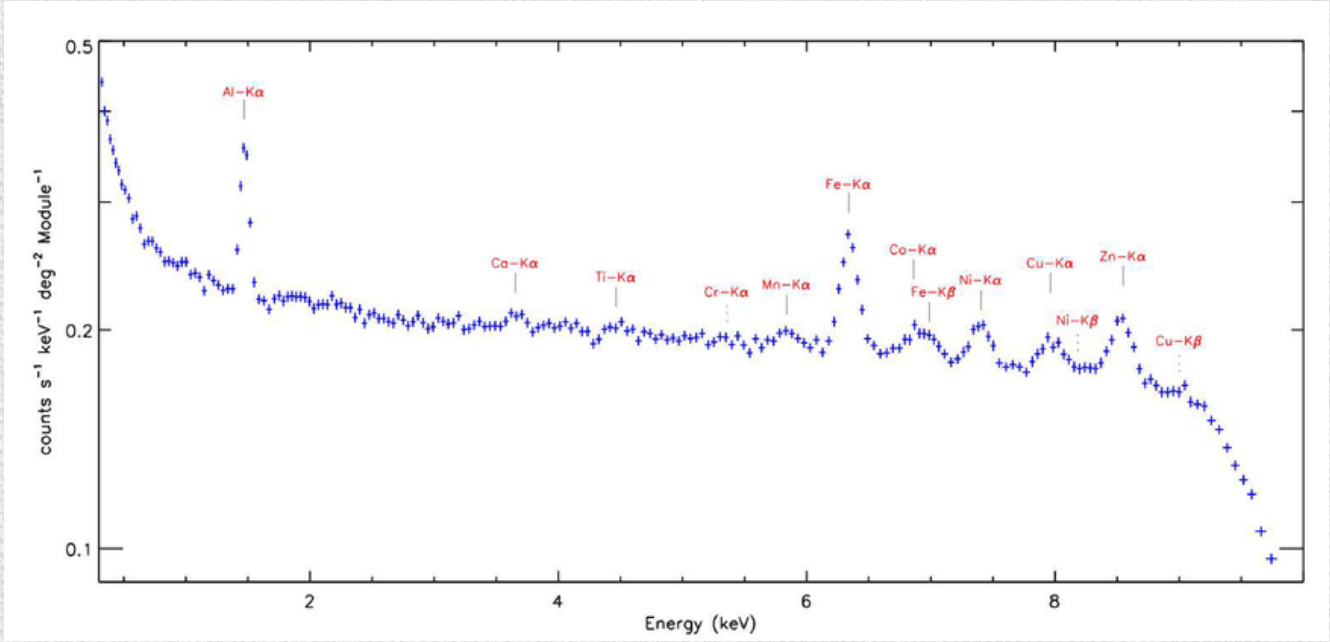

average eROSITA spectrum in closed filter position (Freyberg et al. 2020)

Contaminating effects: detector noise

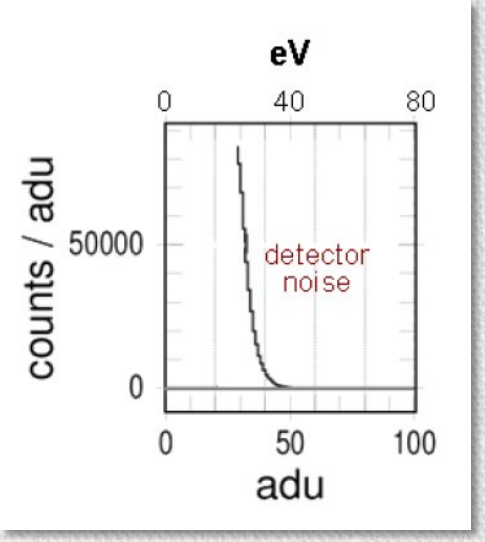

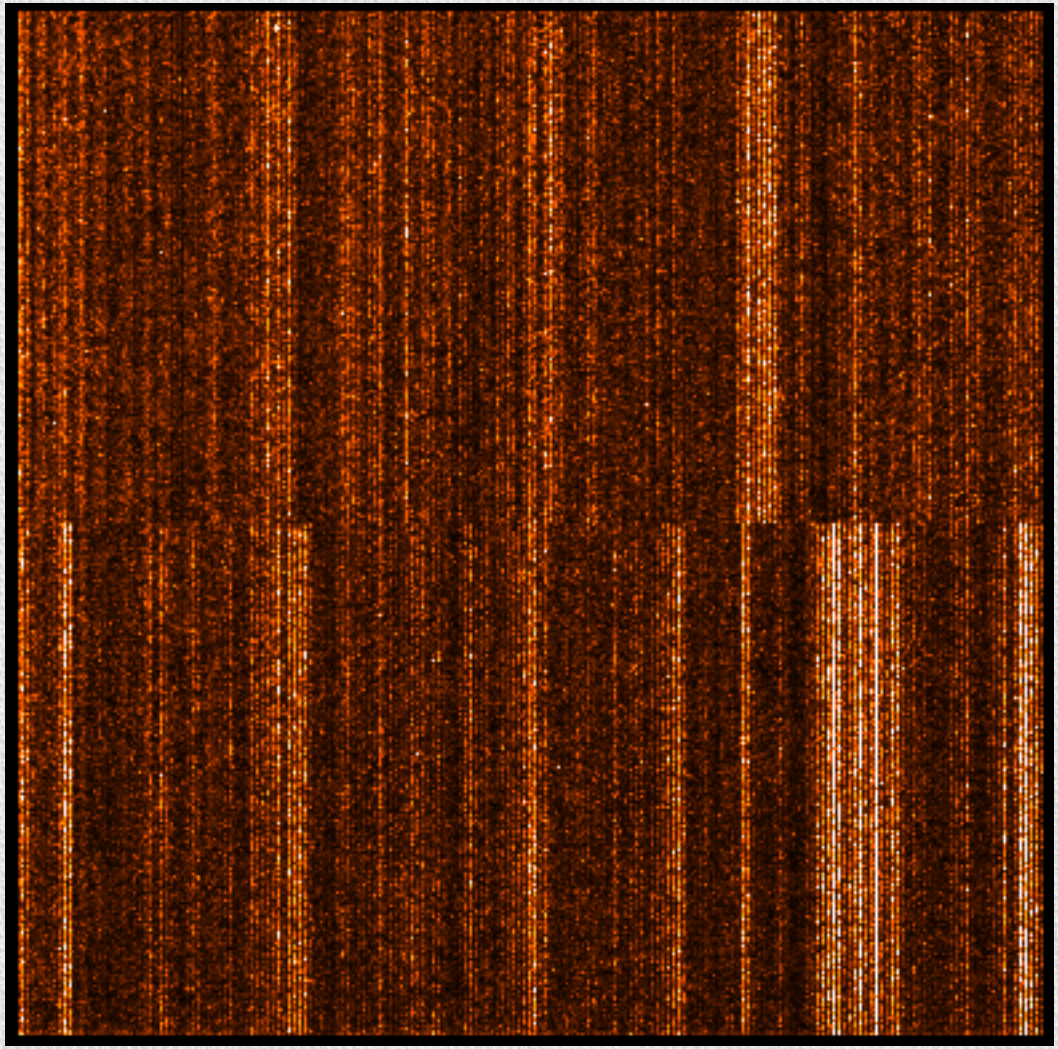

Contaminating effects: electronic artefacts

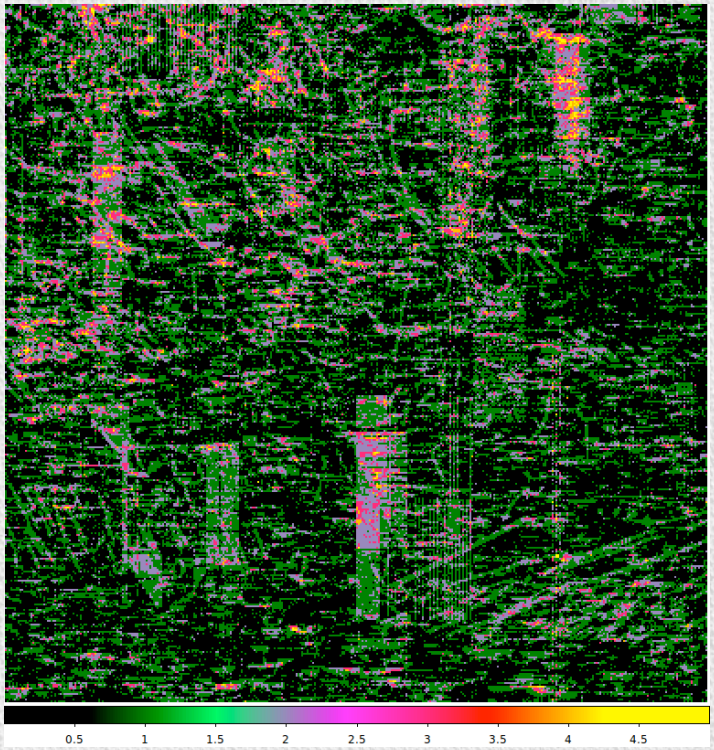

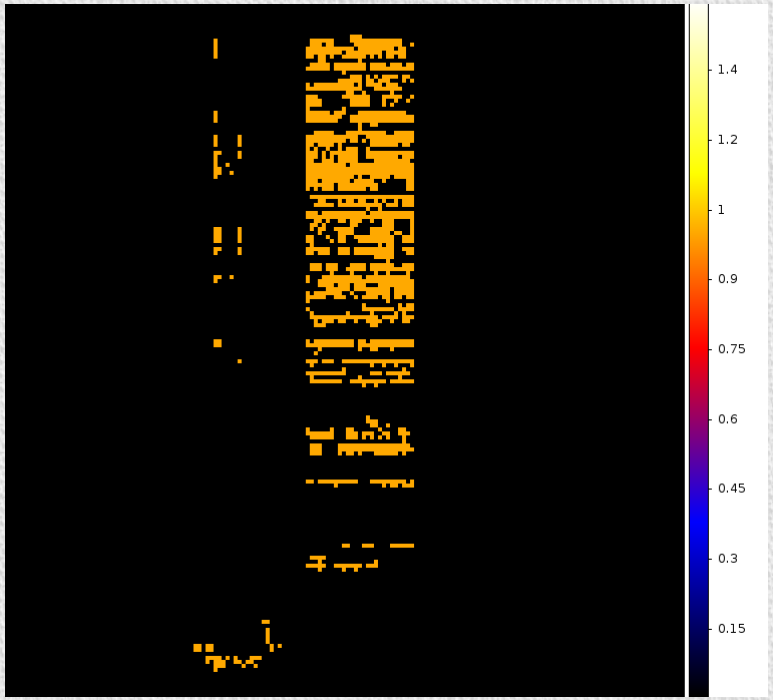

From photons to bits: the fate of X-rays grabbed by eROSITA

device	*process*	*signal*	*characteristic properties*	
telescope	reflection (scattering)	*photon [eV]*	effective area (E,θ,φ) point spread function (E,θ,φ) field of view (FOV) boresight	collecting area, reflectivity, vignetting mirror quality, encircled energy fraction focal length, detector geometry, plate scale alignment
filter	absorption		transmission (E,x,y) contamination (E,x,y,t)	
CCD	charge release	*charge [e^-]*	charge splitting low energy threshold	**patterns** (singles, doubles, triples, quadruples, invalid..)
			contaminating effects quantum efficiency (QE)	**pile-up** (single pixel, pattern) **photon background** (fluorescence, optical loading) **particle induced background** (soft protons, MIPs) **detector induced background** (noise, bright pixels)
	charge transfer			
	charge readout	*pulse height amplitude [adu]*		
on-board data processor	signal processing	*event [bit]*		

Detector Calibration: Quantum Efficiency (QE)

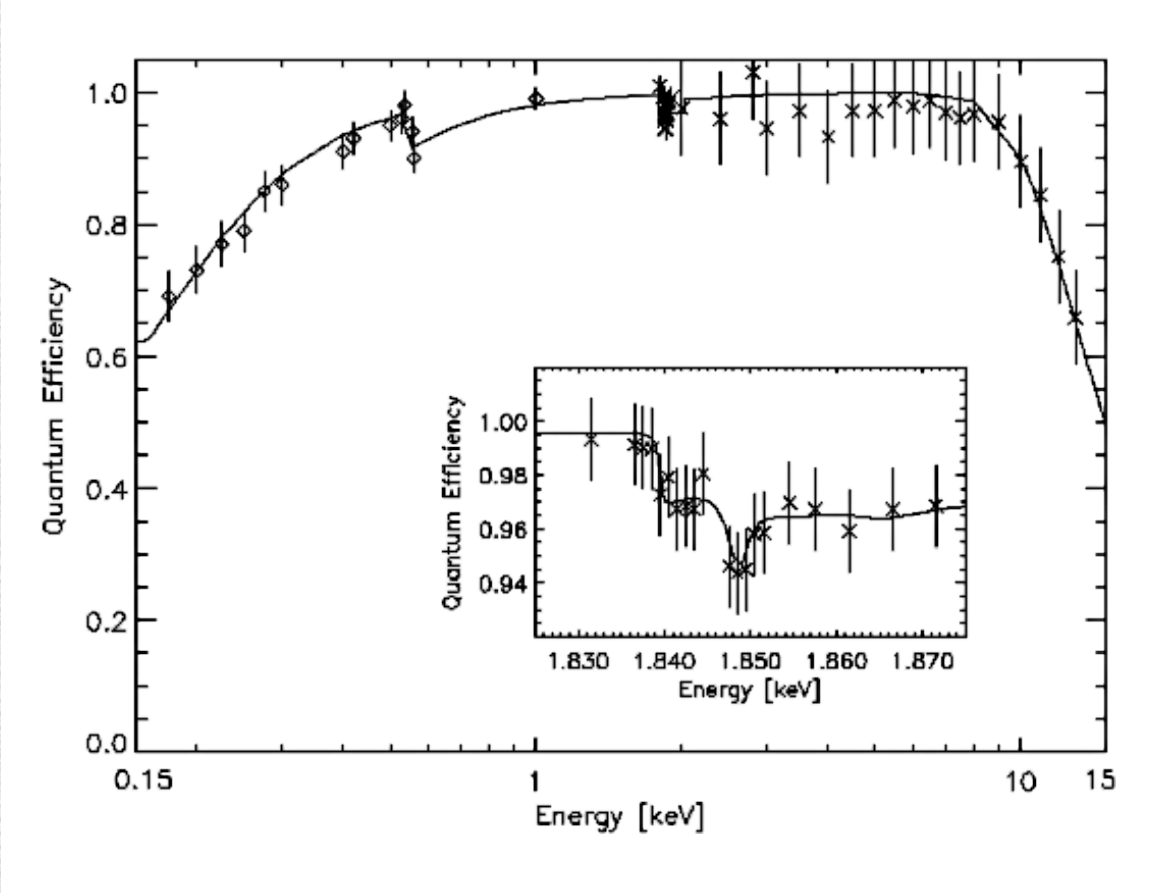

Quantum efficiency of XMM-Newton / EPIC pn

http://xmm.esac.esa.int/external/xmm_user_support/documentation/uhb_2.2/node31.html

Telescope Calibration: effective area * filter transmission * QE

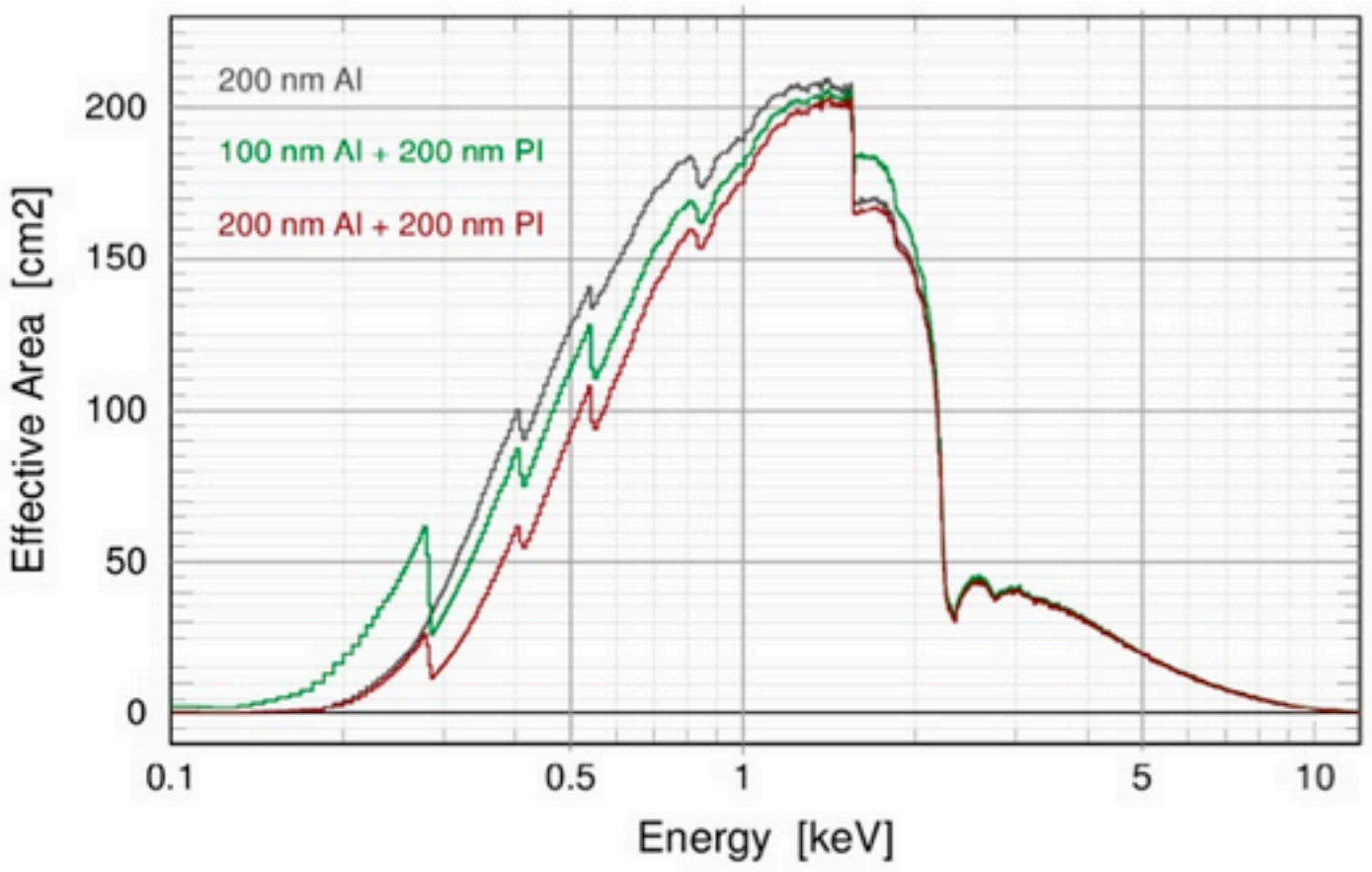

Effective areas of the three filter combinations for one eROSITA camera, composed of the expected effective area of one mirror assembly (averaged over the FoV), the filter transmissions, and the CCD quantum efficiency. All values are preliminary.

From photons to bits: the fate of X-rays grabbed by eROSITA

device	*process*	*signal*	*characteristic properties*	
telescope	reflection (scattering)	*photon [eV]*	effective area (E,θ,φ) point spread function (E,θ,φ) field of view (FOV) boresight	collecting area, reflectivity, vignetting mirror quality, encircled energy fraction focal length, detector geometry, plate scale alignment
filter	absorption		transmission (E,x,y) contamination (E,x,y,t)	
CCD	charge release	*charge [e^-]*	charge splitting low energy threshold	**patterns** (singles, doubles, triples, quadruples, invalid..)
			contaminating effects	**pile-up** (single pixel, pattern) **photon background** (fluorescence, optical loading) **particle induced background** (soft protons, MIPs) **detector induced background** (noise, bright pixels)
			quantum efficiency (QE) energy resolution (ΔE)	
	charge transfer			
	charge readout	*pulse height amplitude [adu]*		
on-board data processor	signal processing	*event [bit]*		

CCD calibration: energy resolution

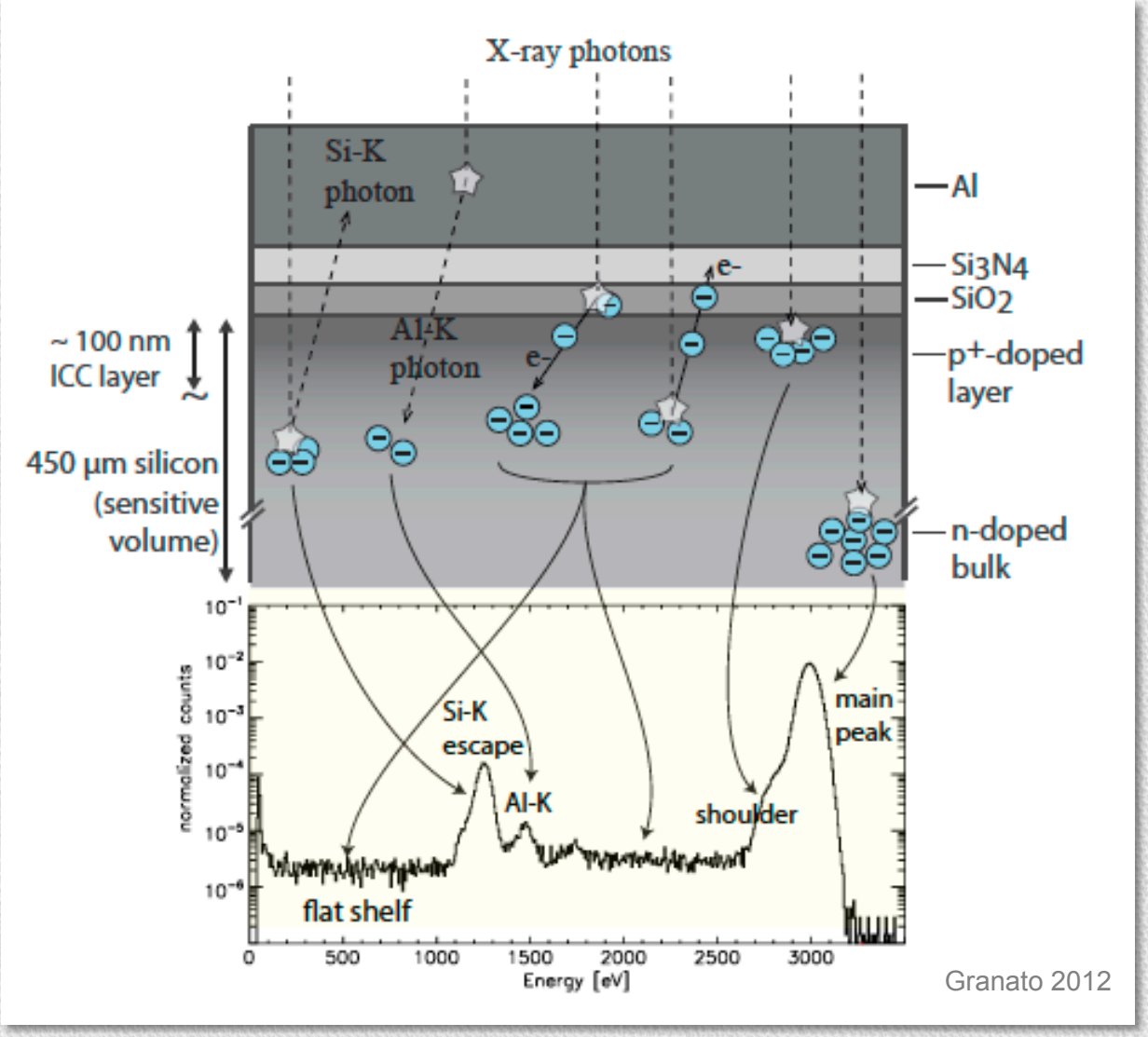

Granato 2012

CCD calibration: energy resolution

Observed signal resulting from monochromatic 3.0 keV X-rays:

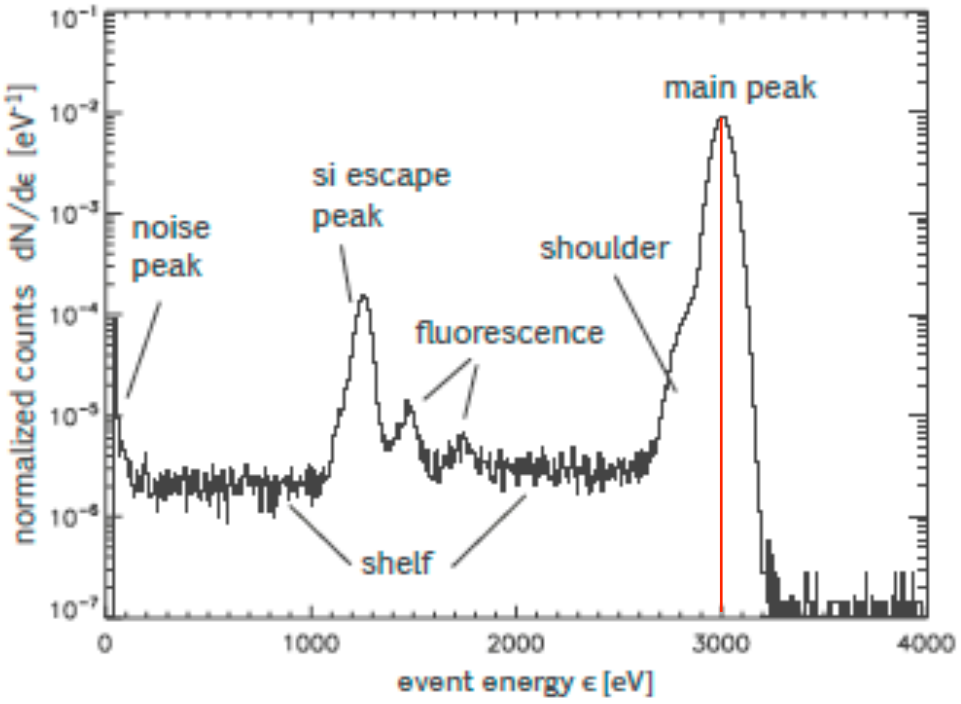

Granato 2012

CCD calibration: energy resolution

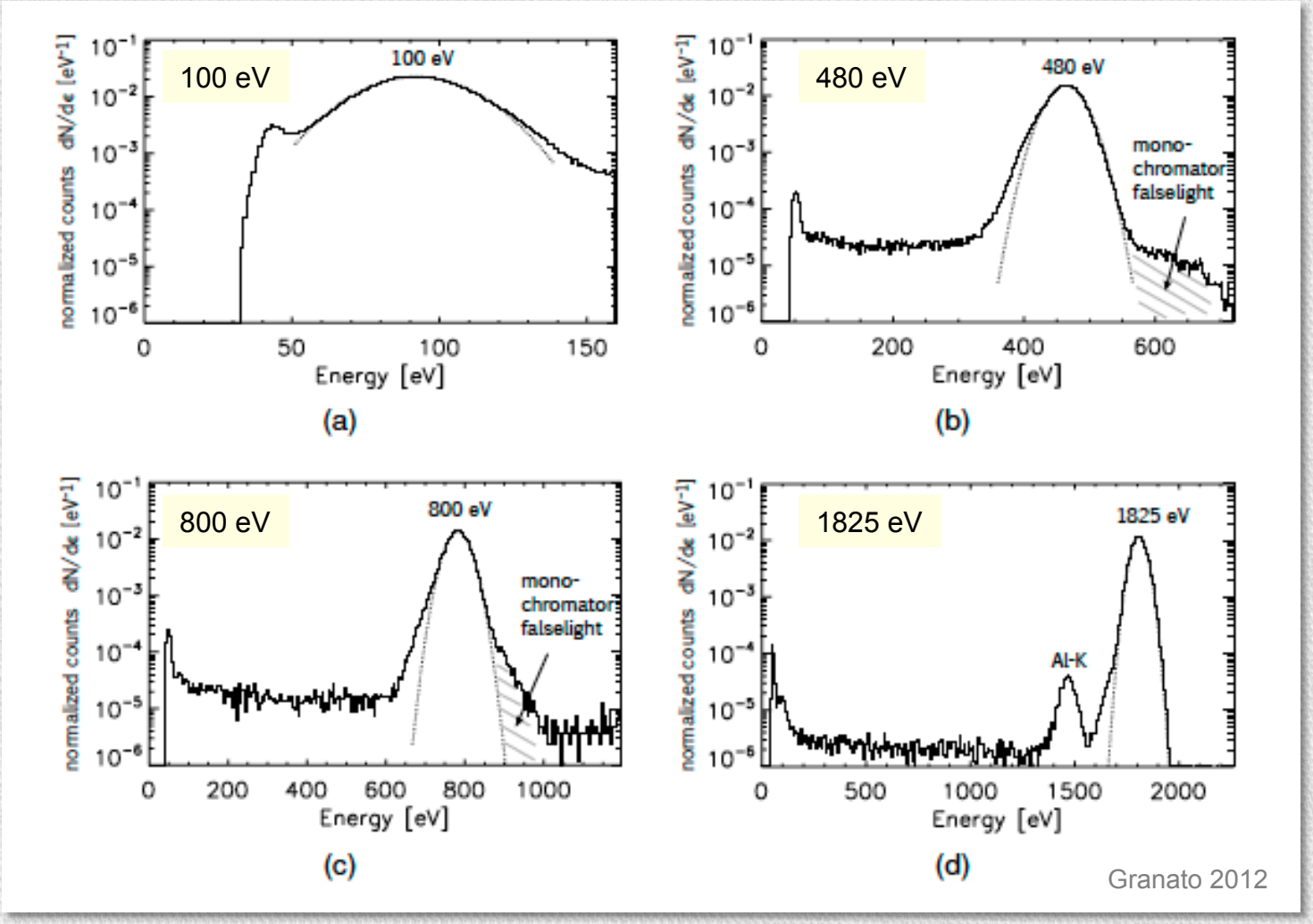

Granato 2012

CCD calibration: energy resolution

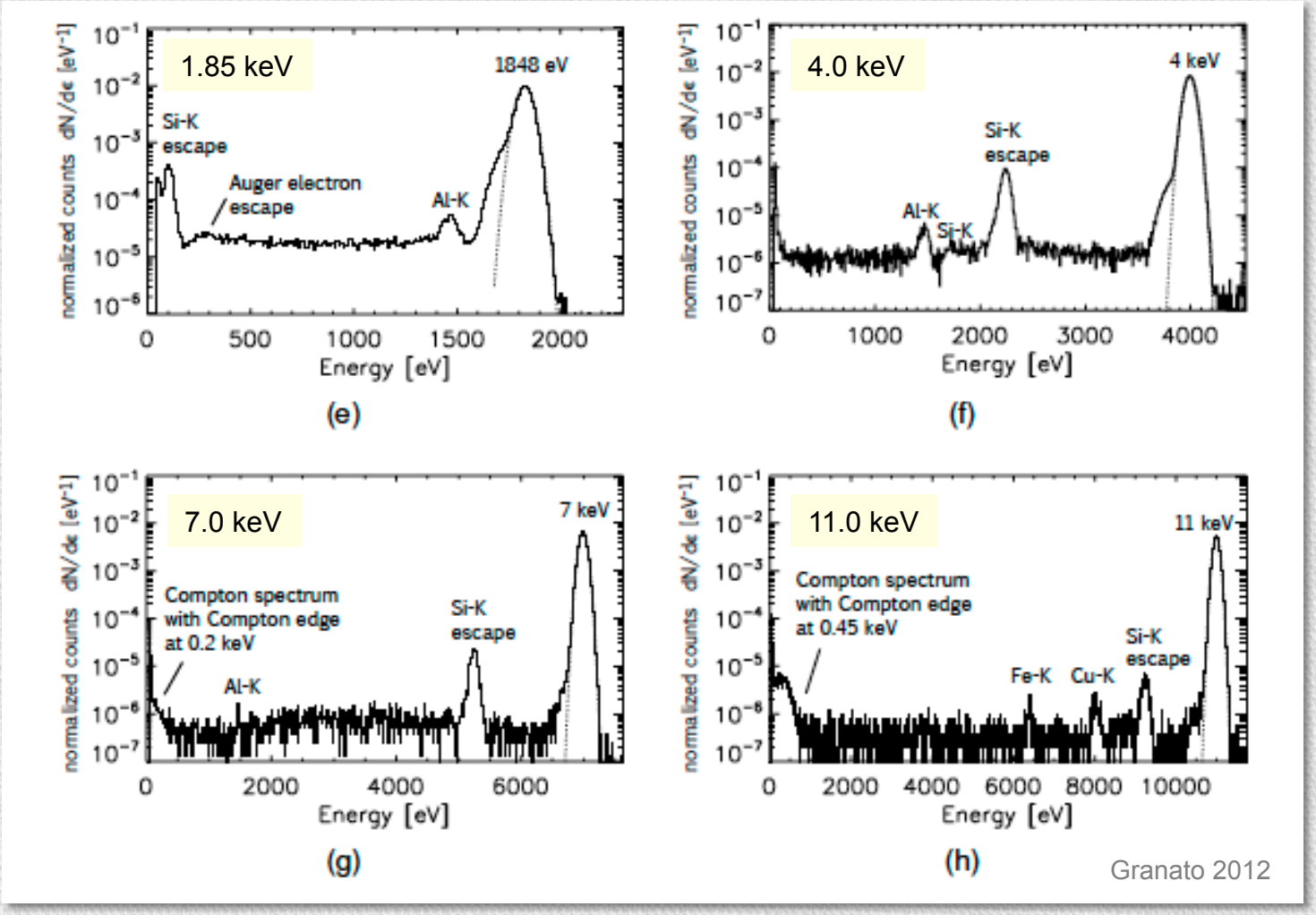

Granato 2012

CCD calibration: energy resolution

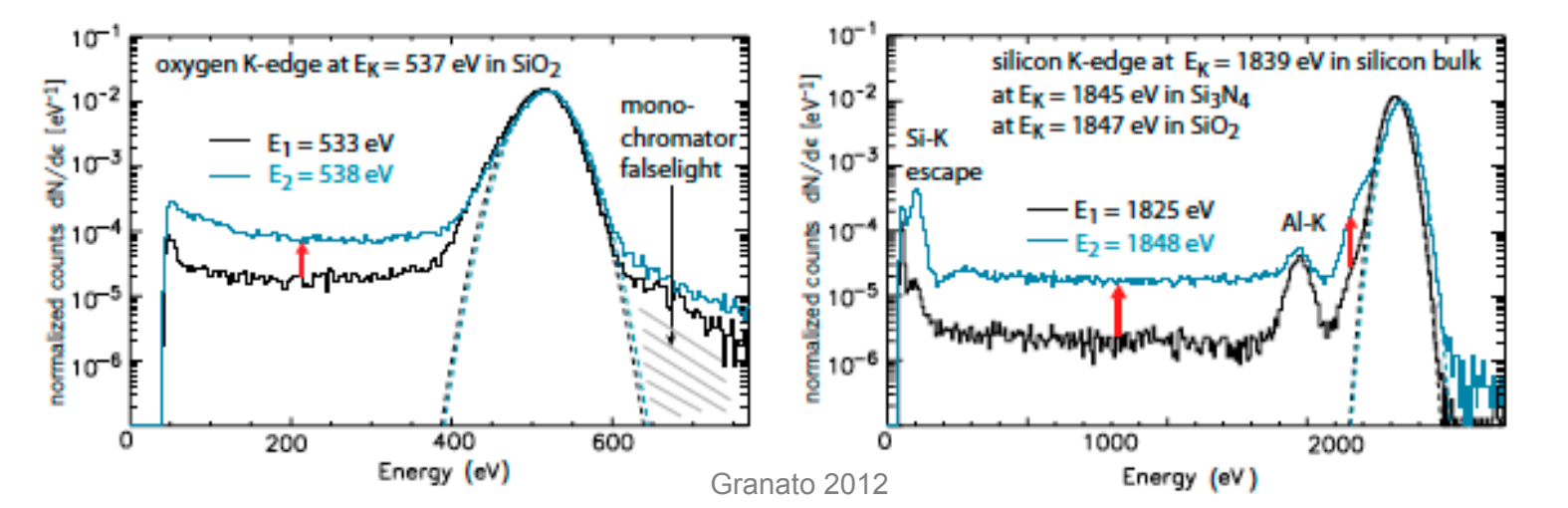

between 533 and 538 eV and between 1825 and 1848 eV a pronounced change in the spectral response is observed

CCD calibration: energy resolution

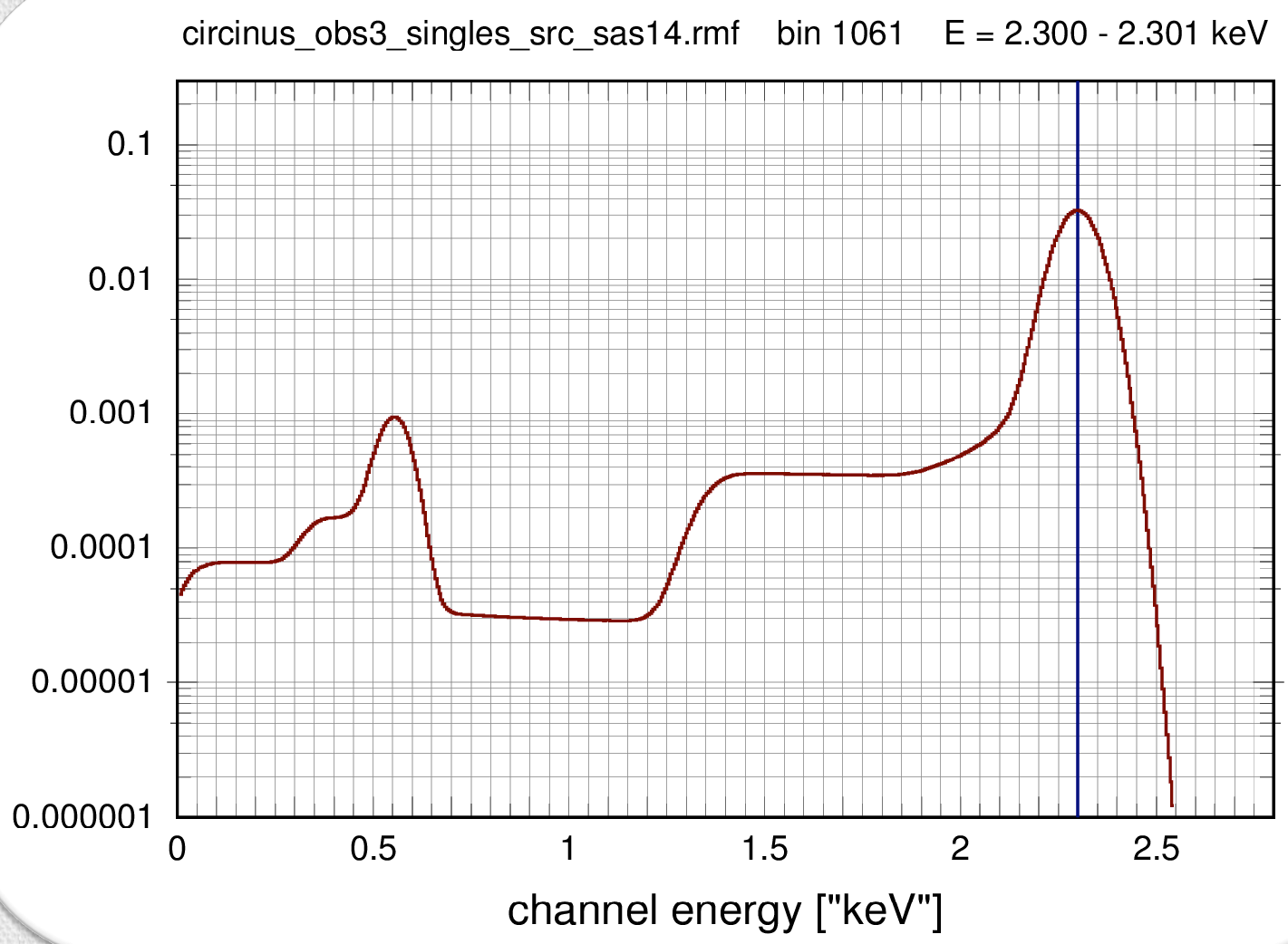

RMFs used for XMM-Newton and Chandra

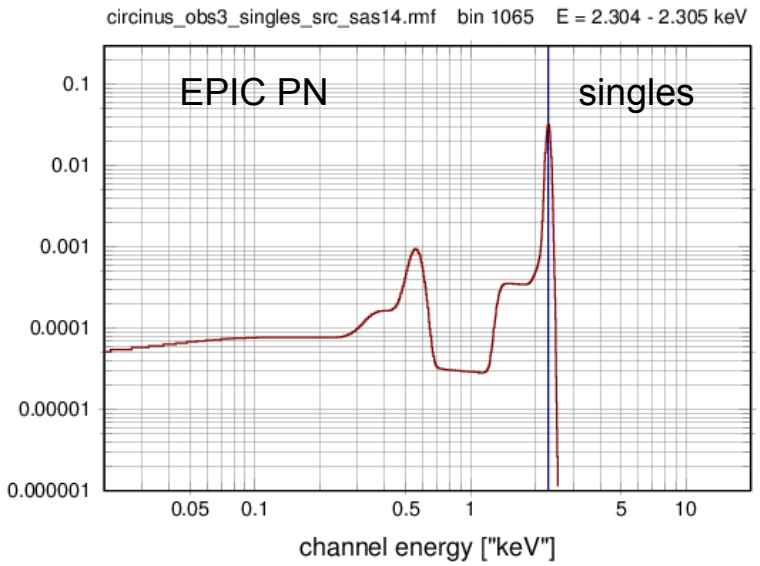

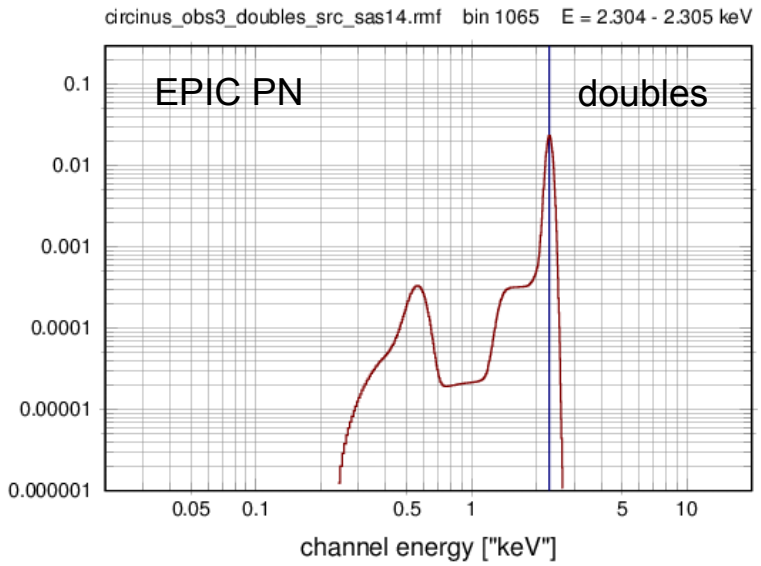

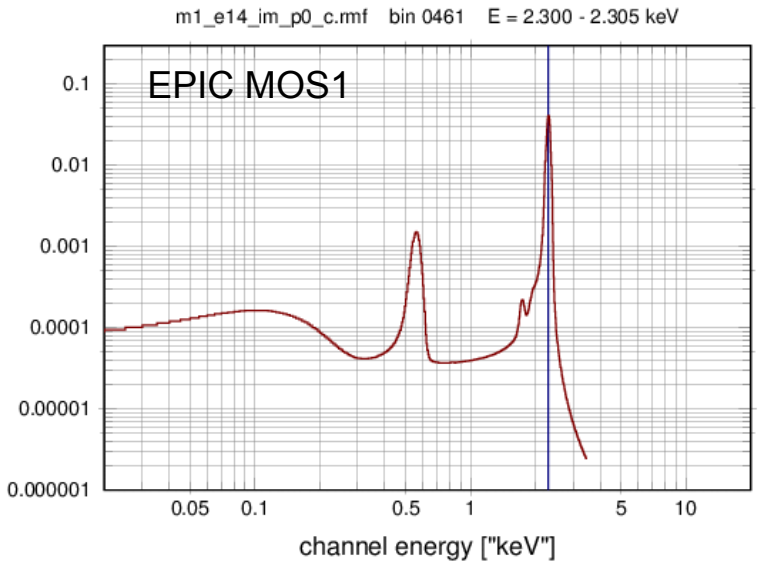

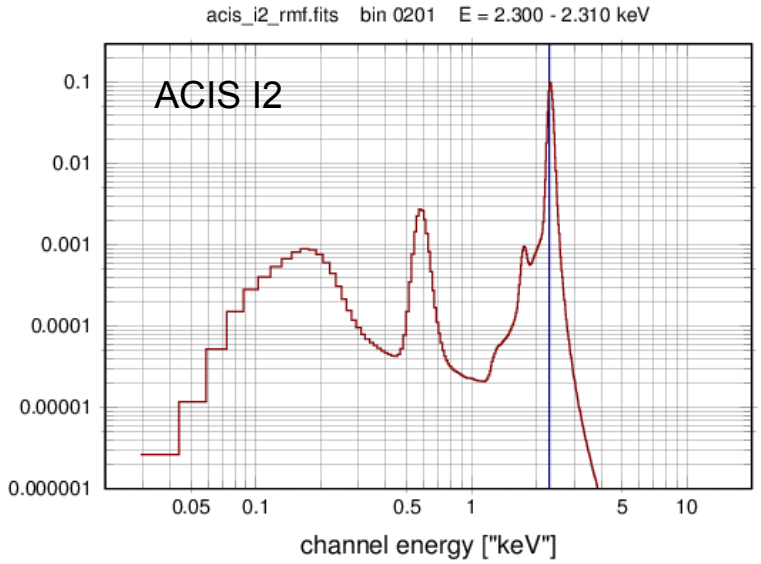

RMFs used for XMM-Newton and Chandra

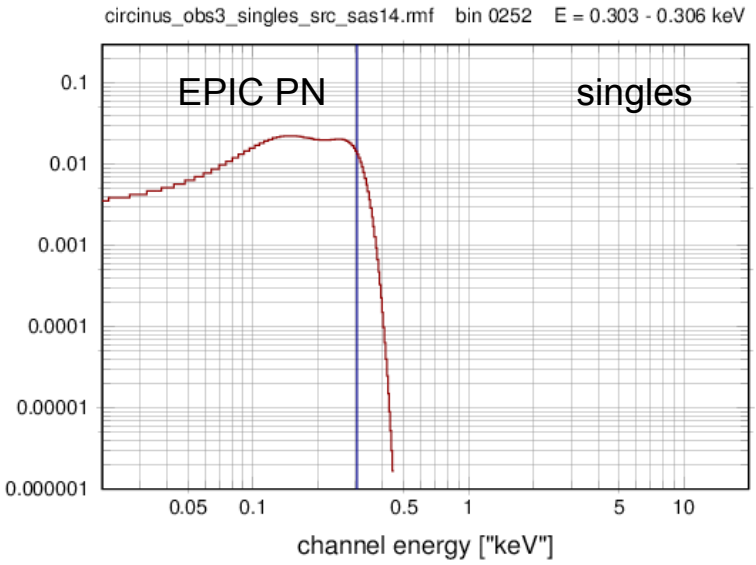

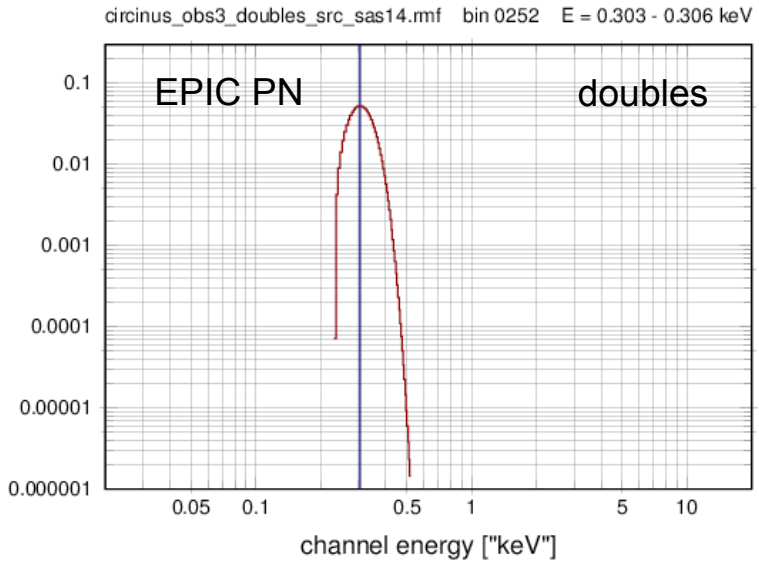

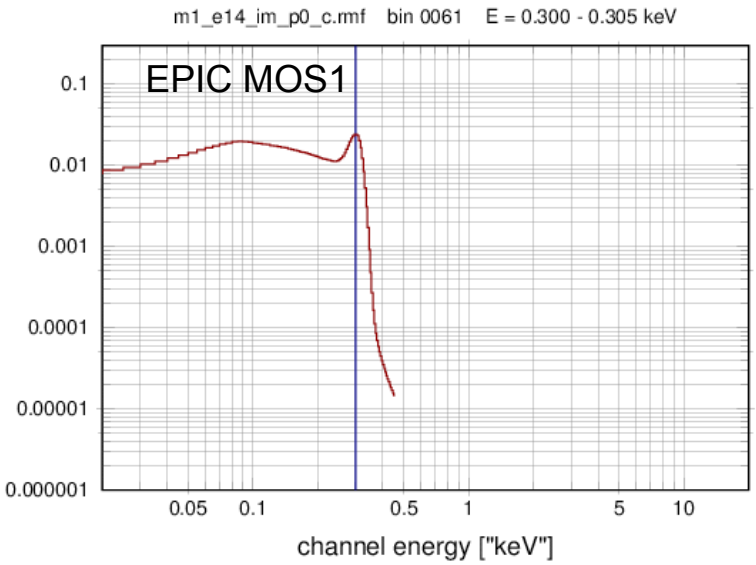

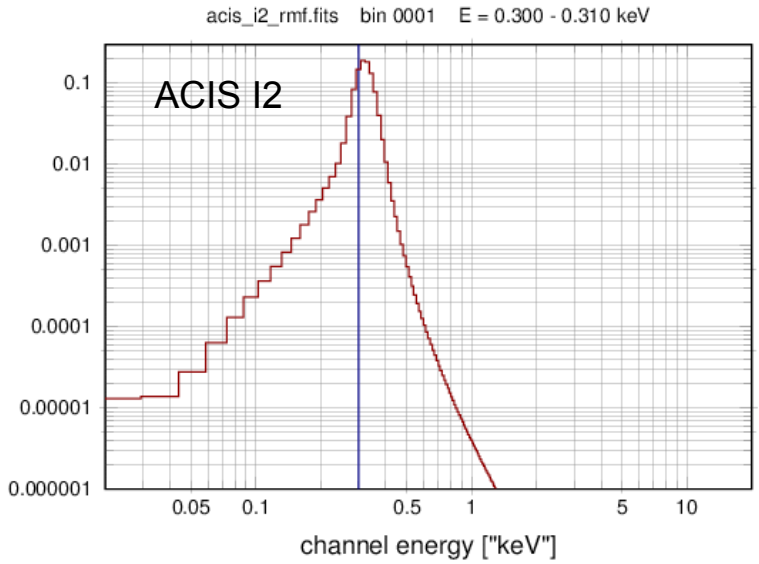

Spectral resolution of XMM-Newton/MOS1

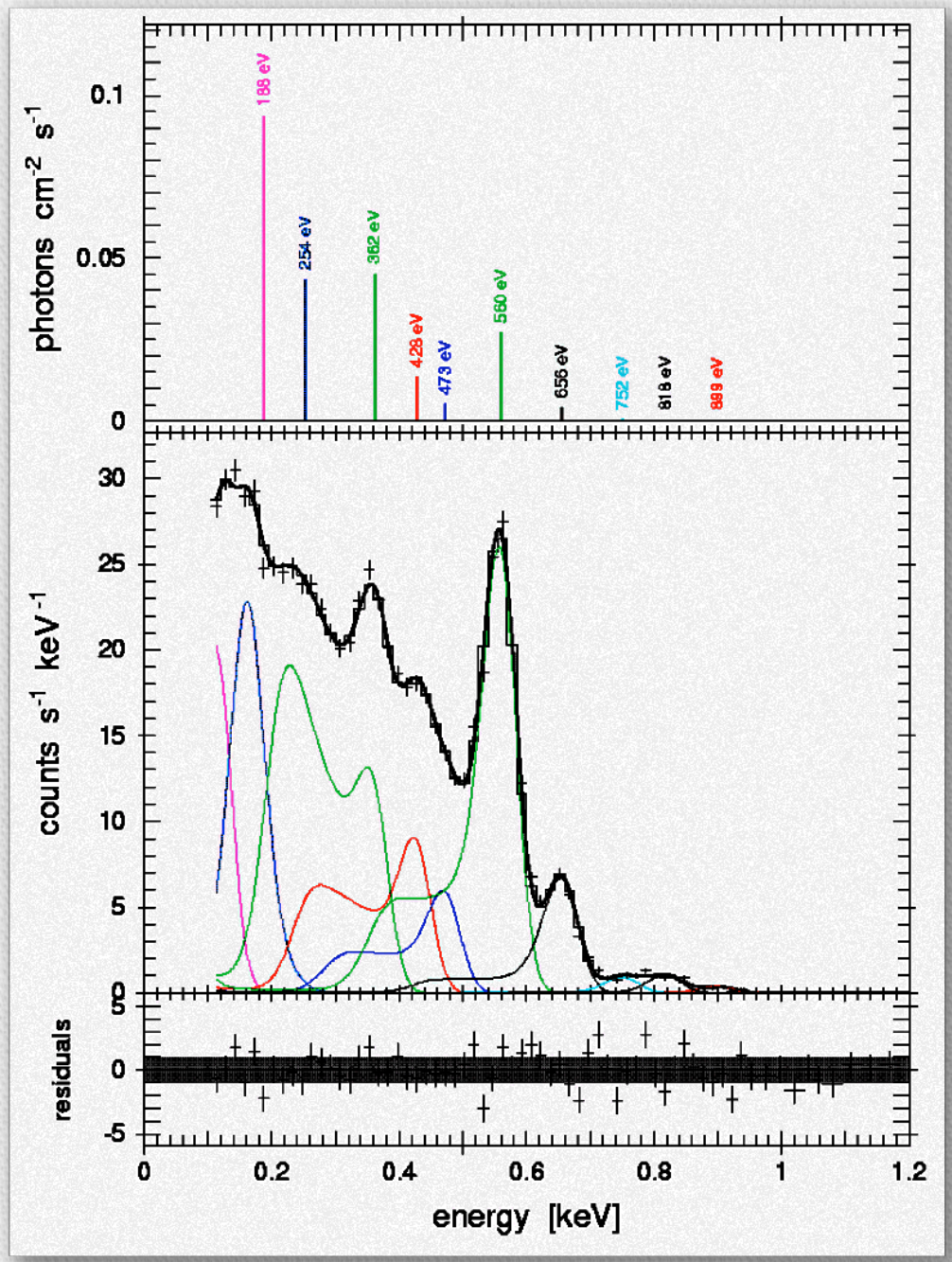

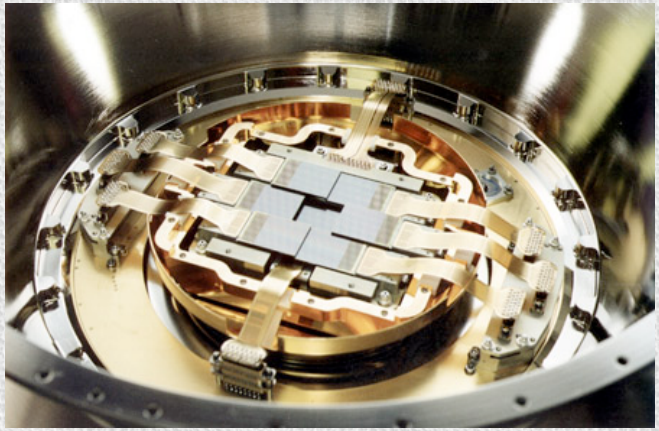

Modification of the incident spectrum by the instrument

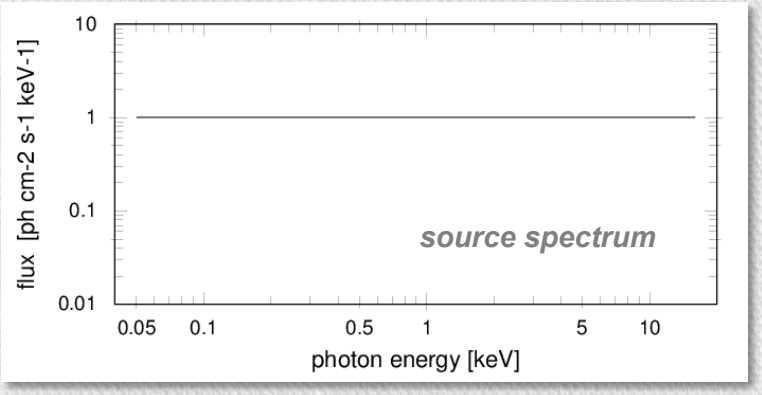

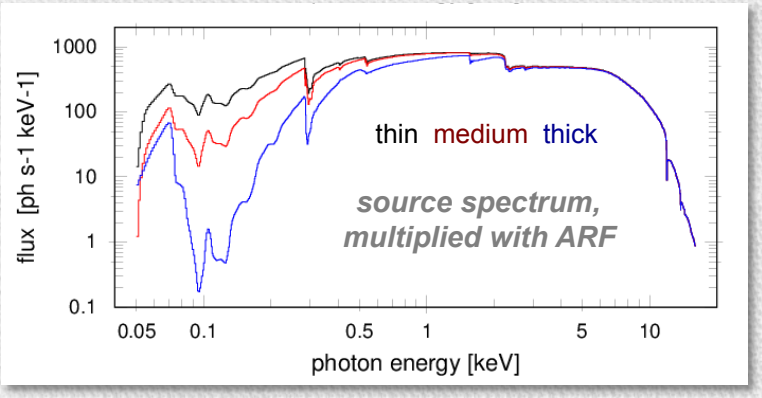

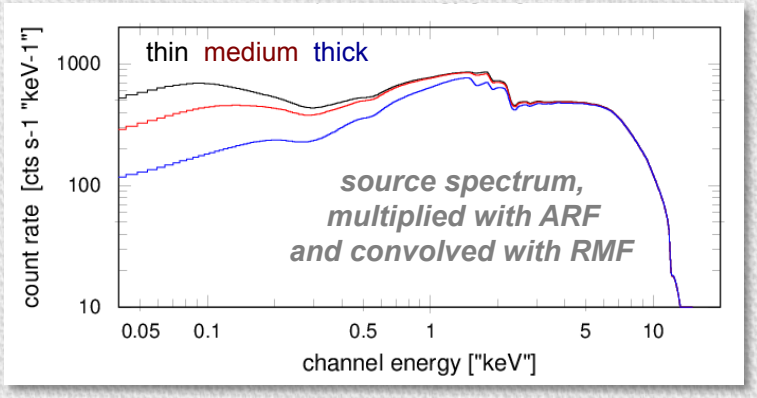

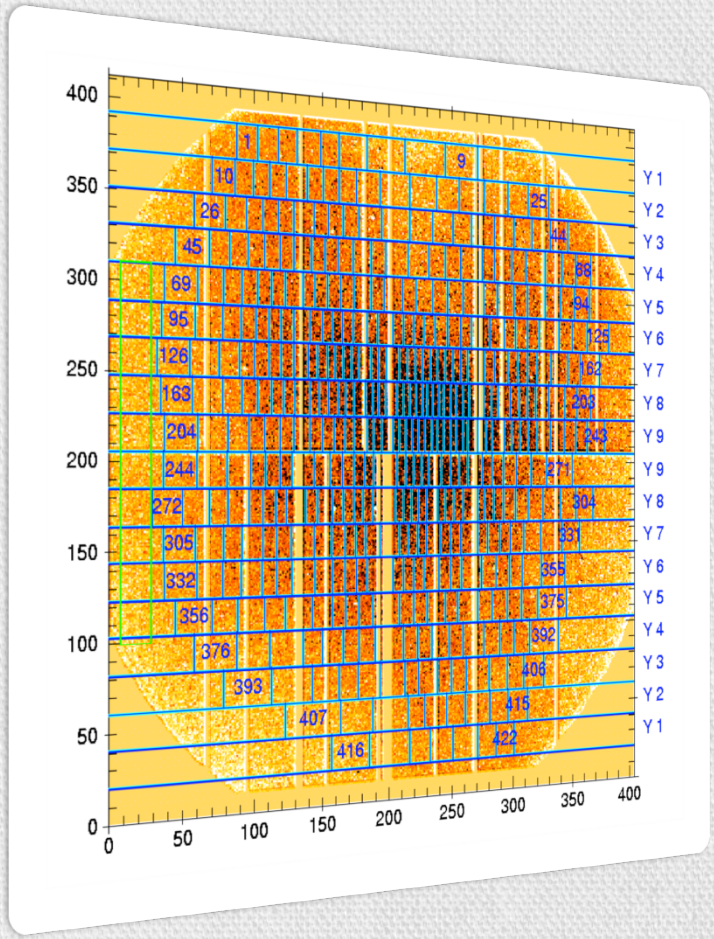
400
350
300
250
200
150
100
50
0
0
50
100
150
200
250
300
350
400
1
9
10
25
26
44
45
66
69
94
95
125
126
162
163
203
204
243
244
271
272
304
305
331
332
355
356
375
376
392
393
406
407
415
416
422
Y 1
Y 2
Y 3
Y 4
Y 5
Y 6
Y 7
Y 8
Y 9
Y 9
Y 8
Y 7
Y 6
Y 5
Y 4
Y 3
Y 2
Y 1

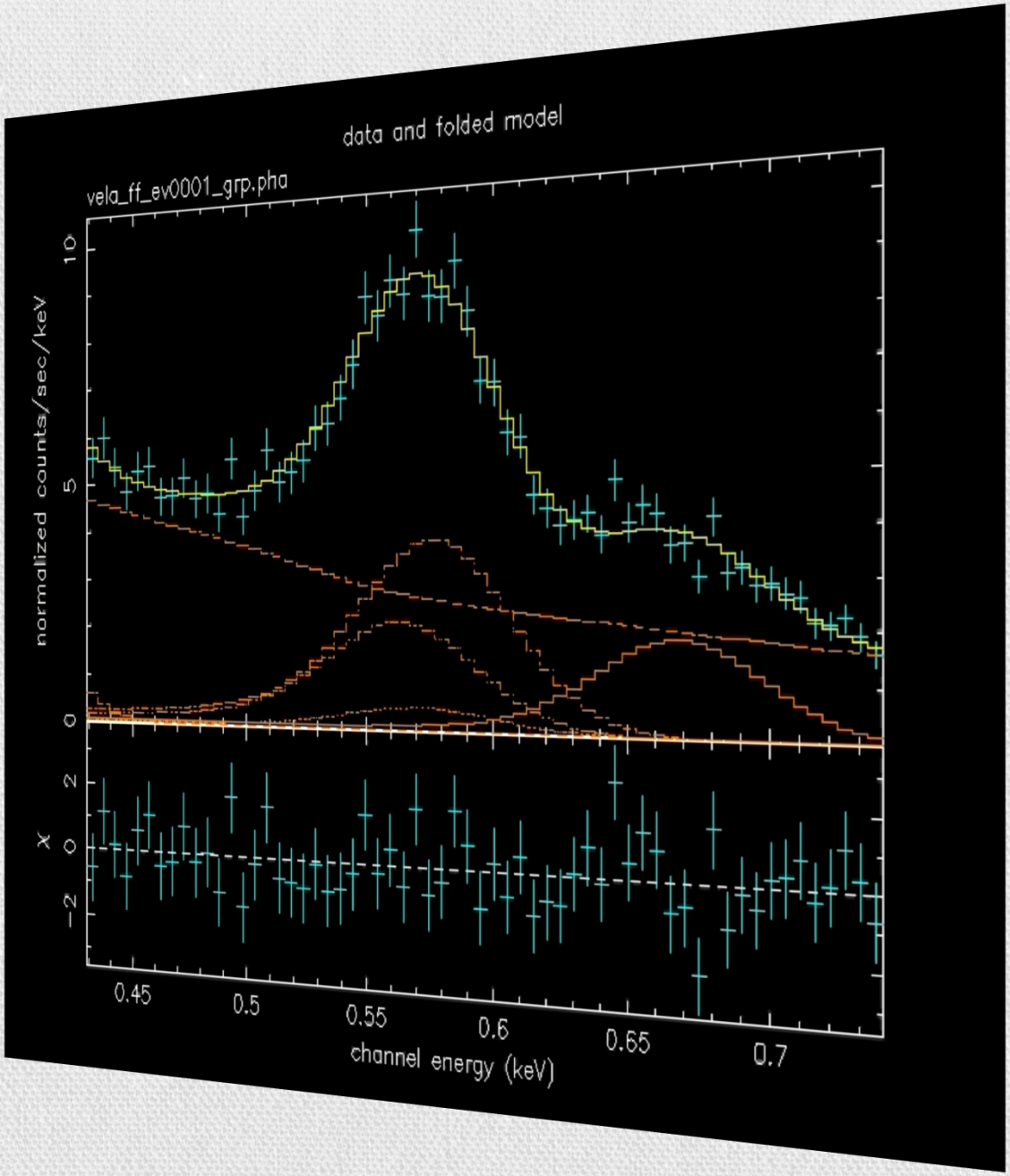
data and folded model
vela_ff_ev0001_grp.pha
normalized counts/sec/keV
10
5
0
χ
2
0
−2
0.45
0.5
0.55
0.6
0.65
0.7
channel energy (keV)

From photons to bits: the fate of X-rays grabbed by eROSITA

device	*process*	*signal*	*characteristic properties*	
telescope	reflection (scattering)	*photon [eV]*	effective area (E,θ,φ) point spread function (E,θ,φ) field of view (FOV) boresight	collecting area, reflectivity, vignetting mirror quality, encircled energy fraction focal length, detector geometry, plate scale alignment
filter	absorption		transmission (E,x,y) contamination (E,x,y,t)	
CCD	charge release	*charge [e^-]*	charge splitting low energy threshold	**patterns** (singles, doubles, triples, quadruples, invalid..)
			contaminating effects	**pile-up** (single pixel, pattern) **photon background** (fluorescence, optical loading) **particle induced background** (soft protons, MIPs) **detector induced background** (noise, bright pixels)
			quantum efficiency (QE) energy resolution (ΔE)	
	charge transfer		charge transfer loss (CTI) pattern migration	**trap saturation** due to photons and particles **charge transfer noise** **threshold induced charge loss** reemission, charge diffusion, charge splitting
	charge readout	*pulse height amplitude [adu]*		
on-board data processor	signal processing	*event [bit]*		

Detector Calibration: Charge Transfer Inefficiency (CTI)

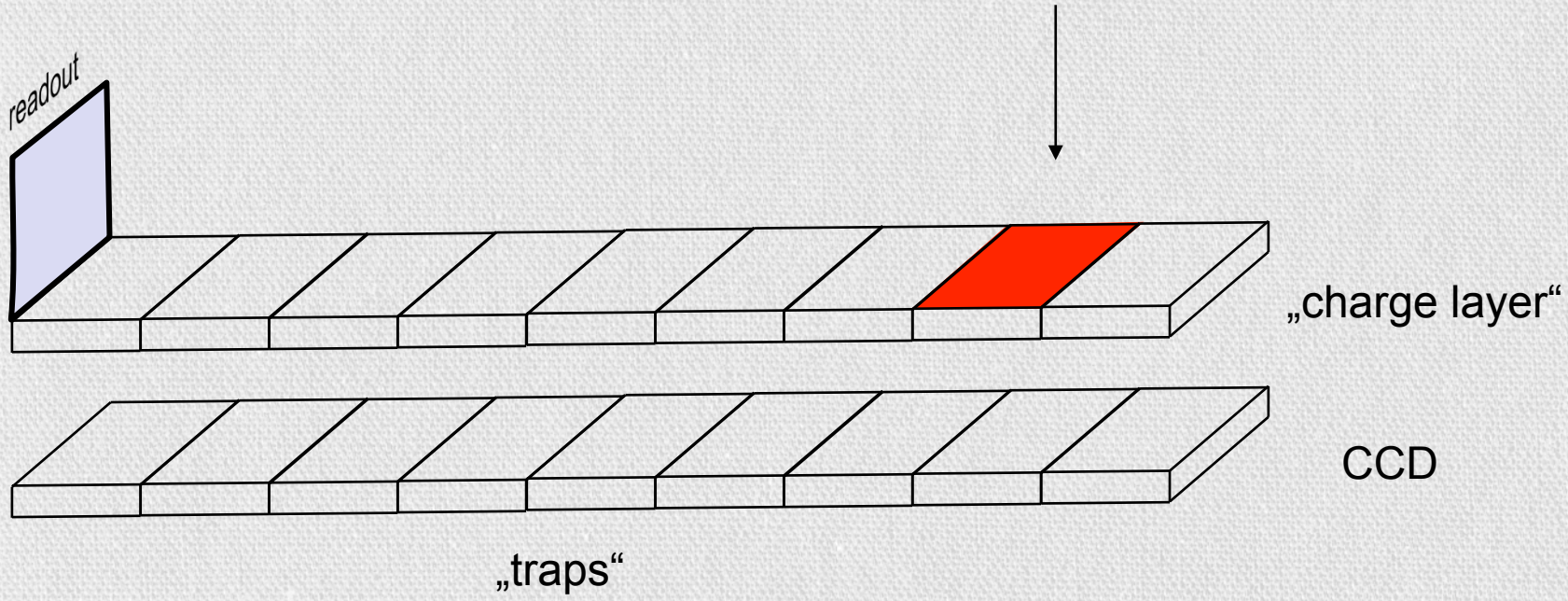

Detector Calibration: Charge Transfer Inefficiency (CTI)

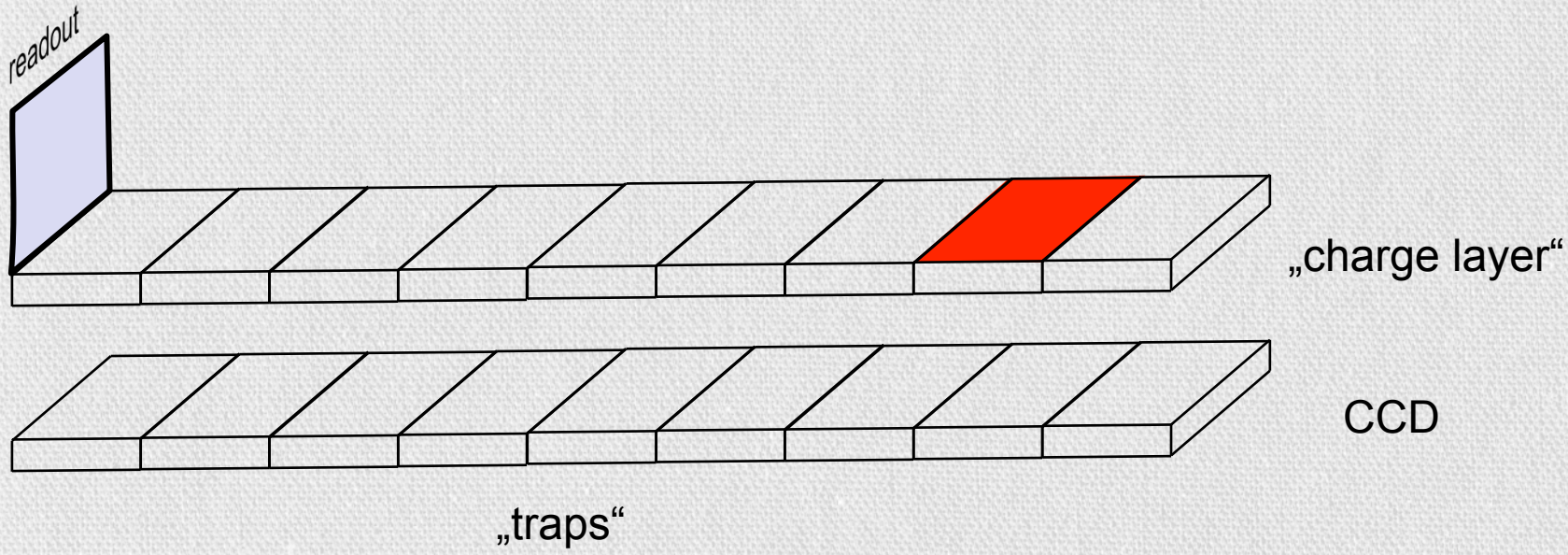

Detector Calibration: Charge Transfer Inefficiency (CTI)

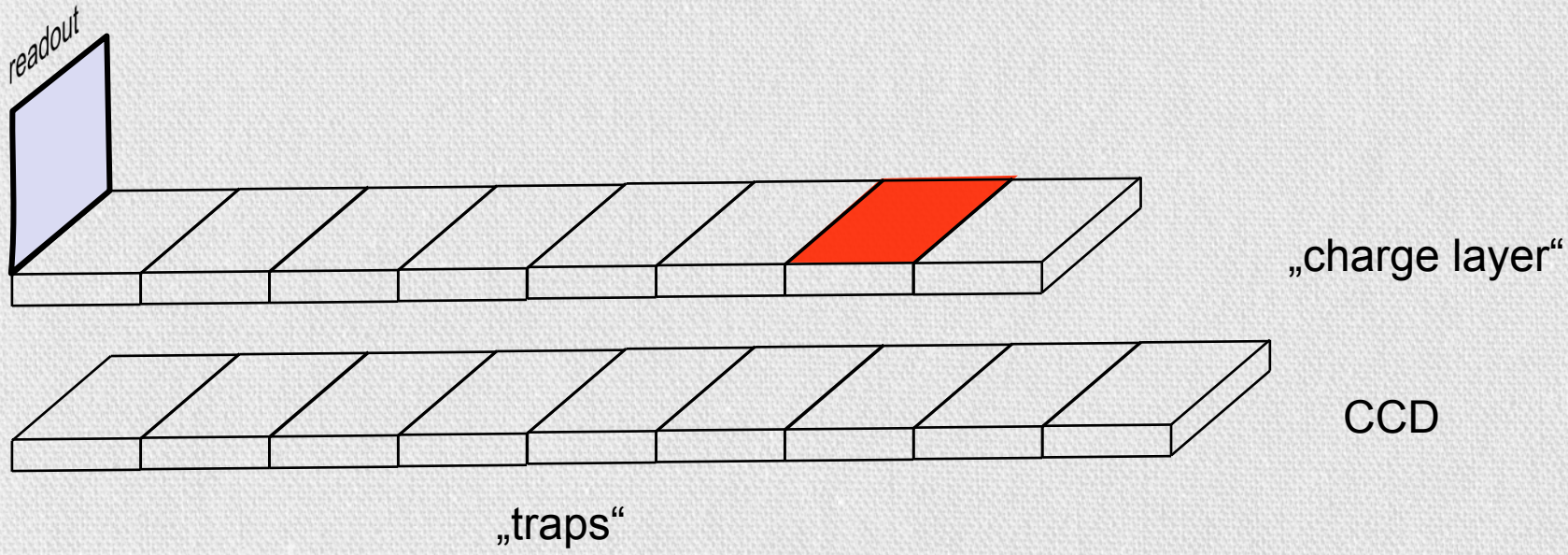

Detector Calibration: Charge Transfer Inefficiency (CTI)

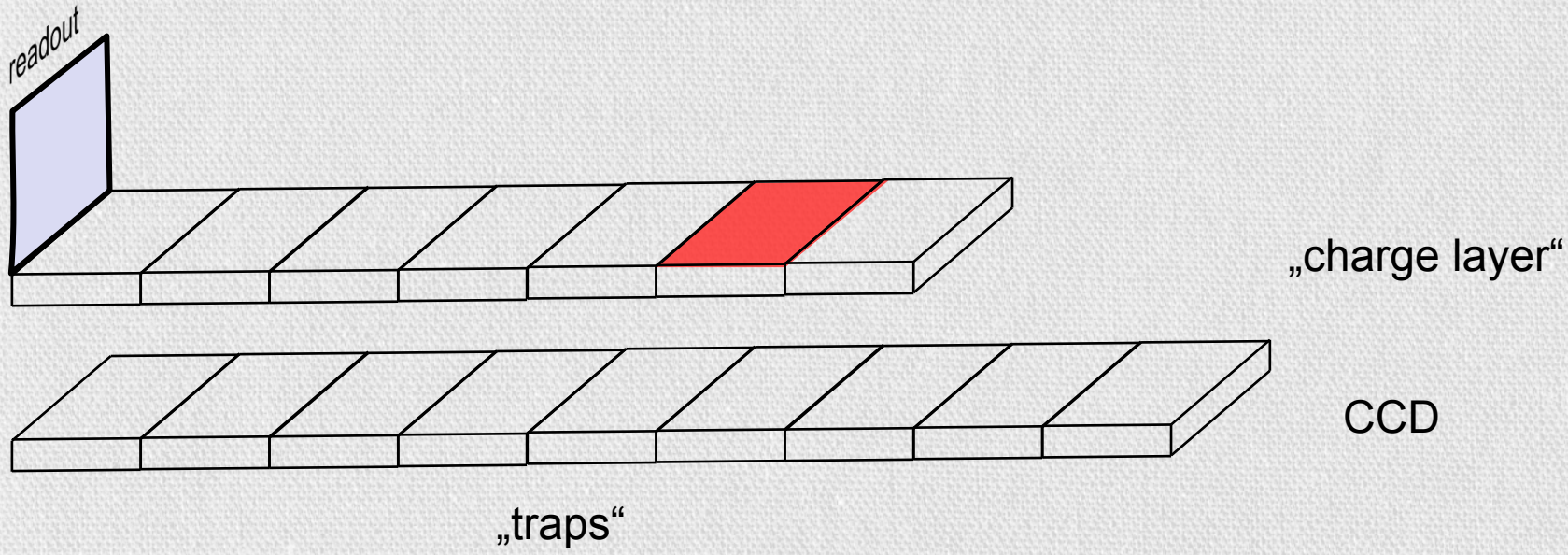

Detector Calibration: Charge Transfer Inefficiency (CTI)

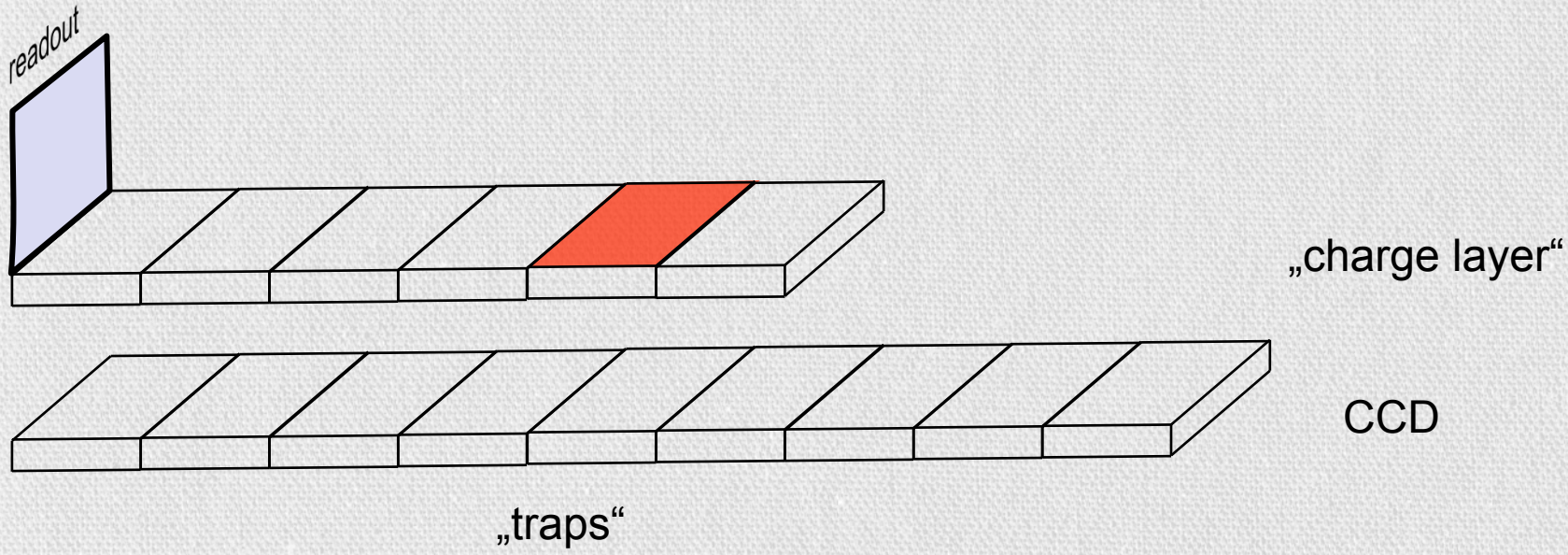

Detector Calibration: Charge Transfer Inefficiency (CTI)

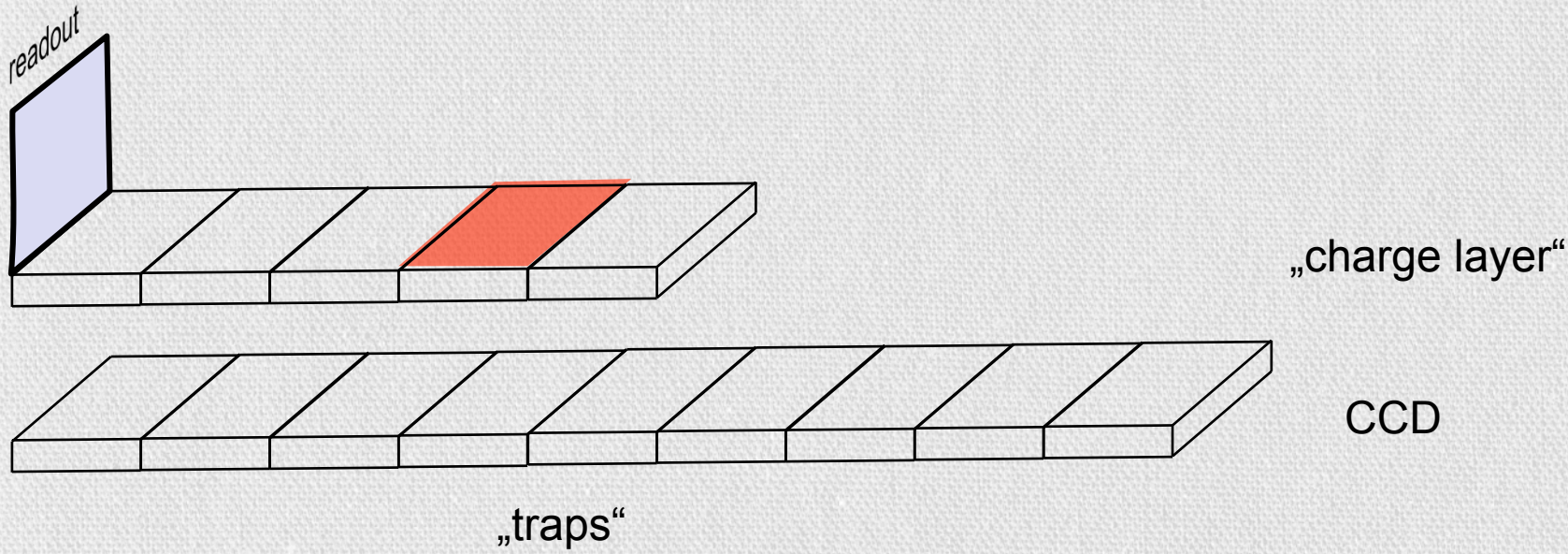

Detector Calibration: Charge Transfer Inefficiency (CTI)

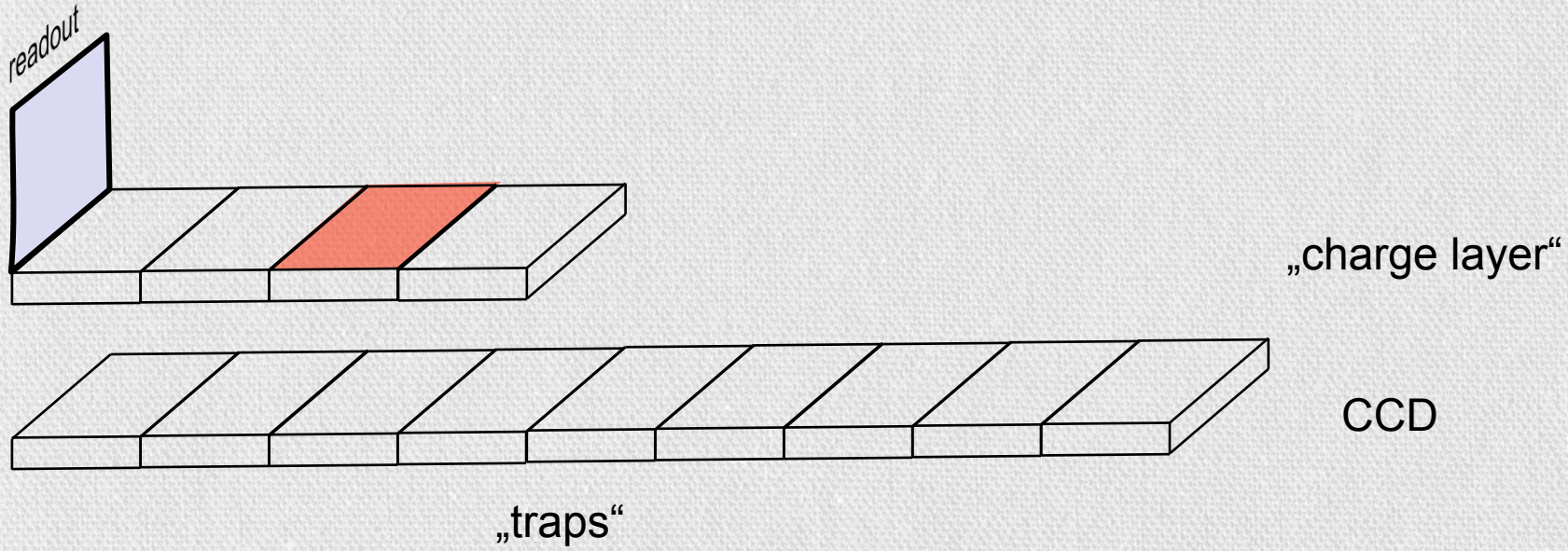

Detector Calibration: Charge Transfer Inefficiency (CTI)

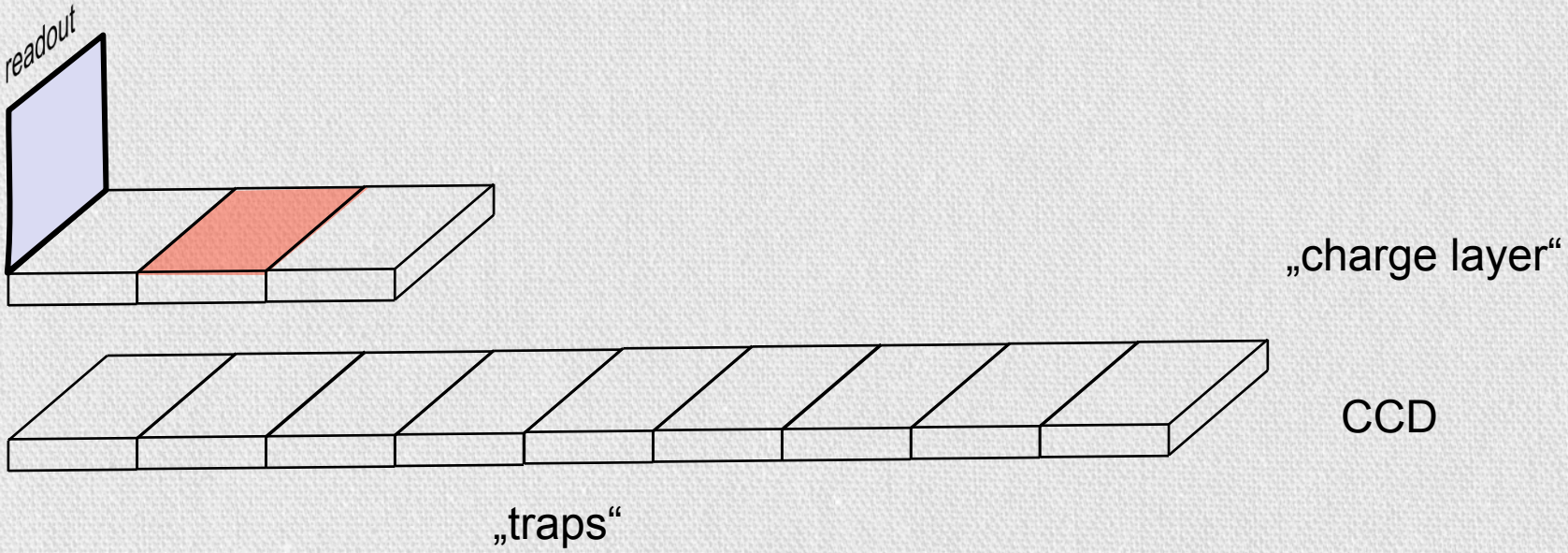

Detector Calibration: Charge Transfer Inefficiency (CTI)

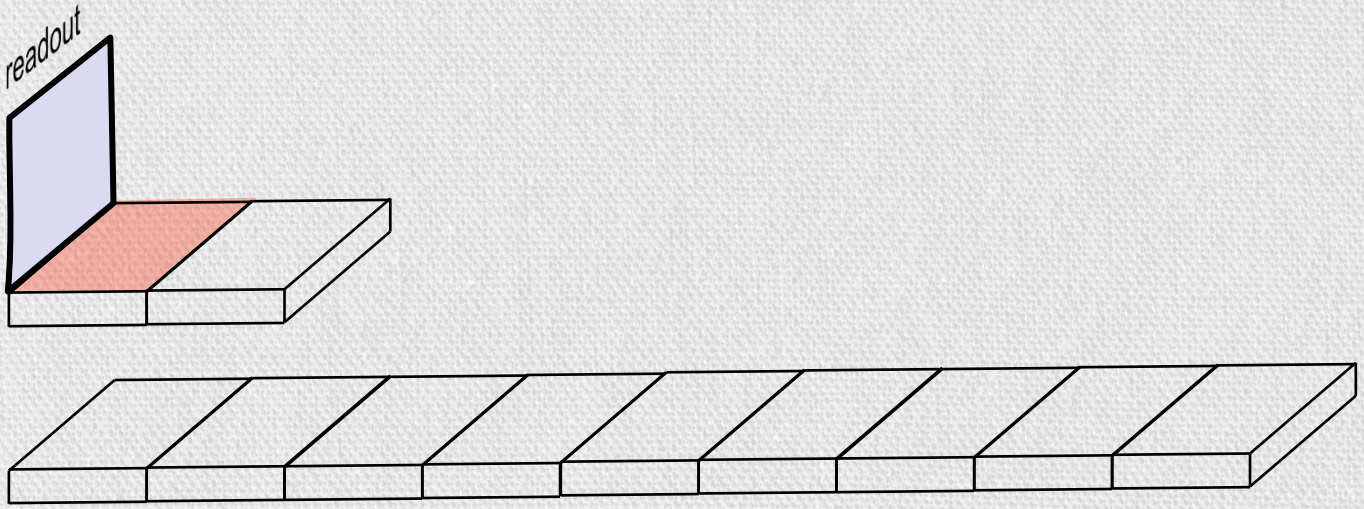

Detector Calibration: Charge Transfer Inefficiency (CTI)

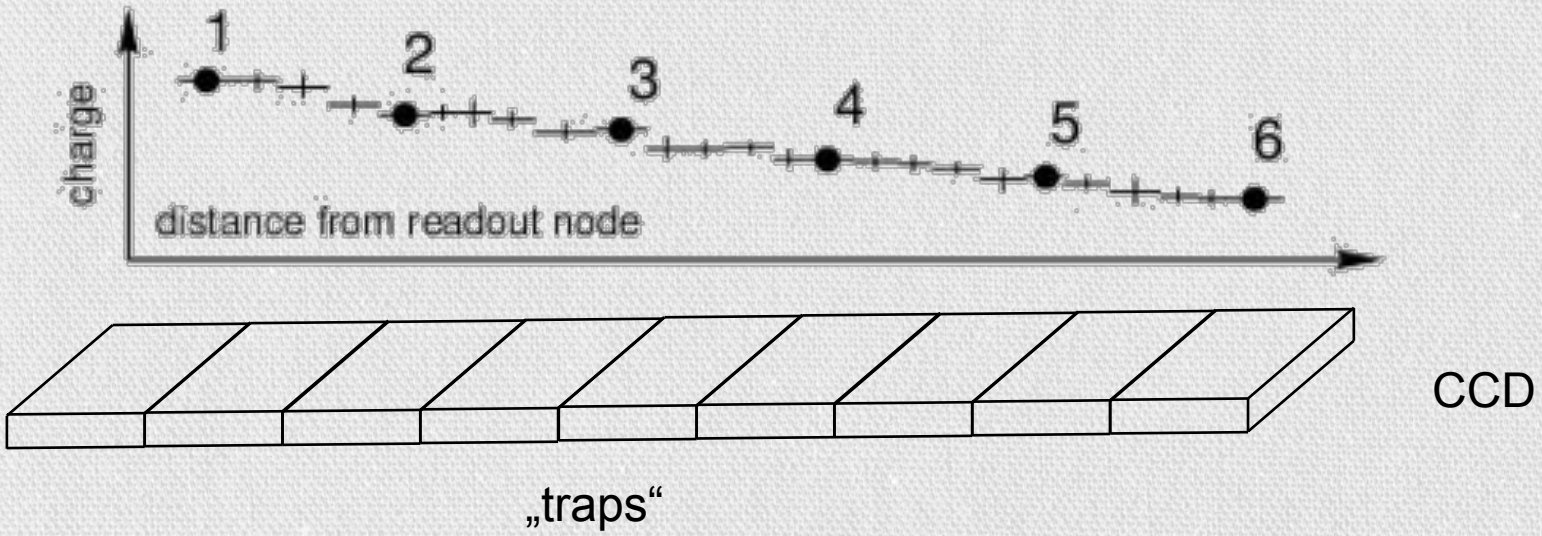

Detector Calibration: Charge Transfer Inefficiency (CTI)

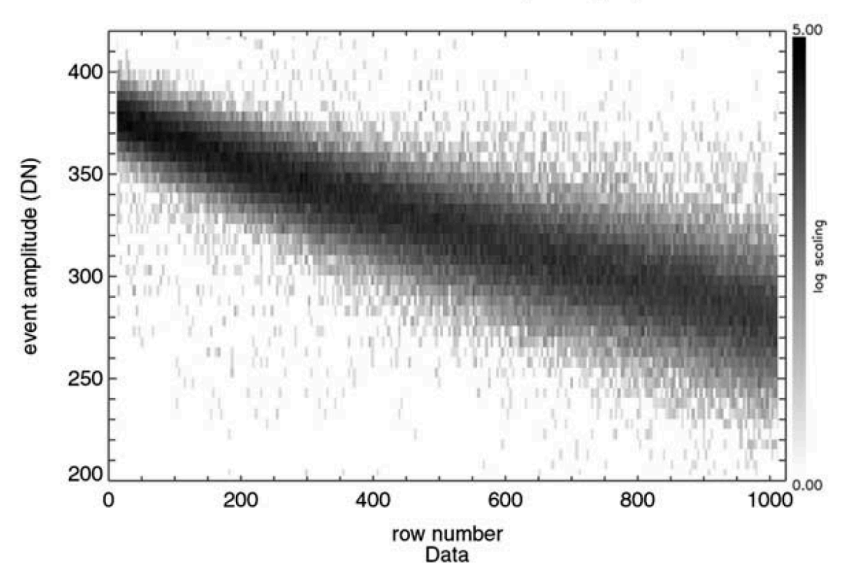

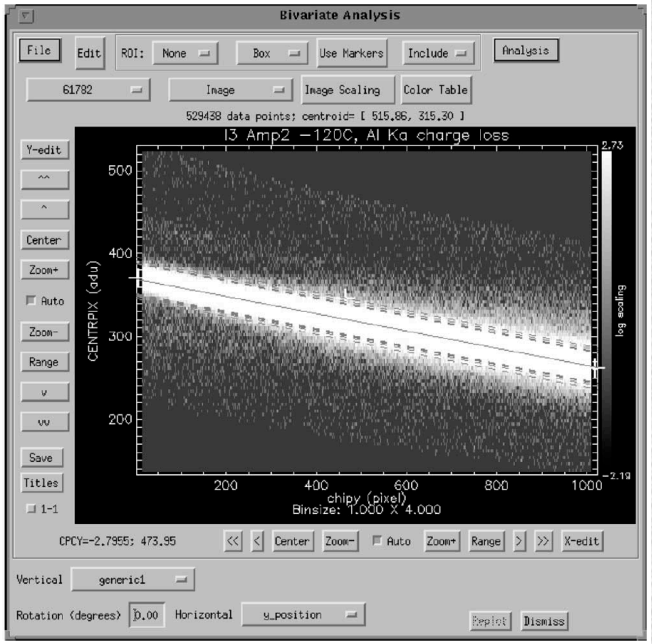

Amplitude of Al Ka line in units of DN, as a function of row number (FI device I3 at -120 C)

Townsley et al., Nuclear Instruments and Methods in Physics Research A 486 (2002) 751–784

Determination of the Charge Transfer Inefficiency (CTI)

25 macro pixels,
20-29 singles
per macro pixel

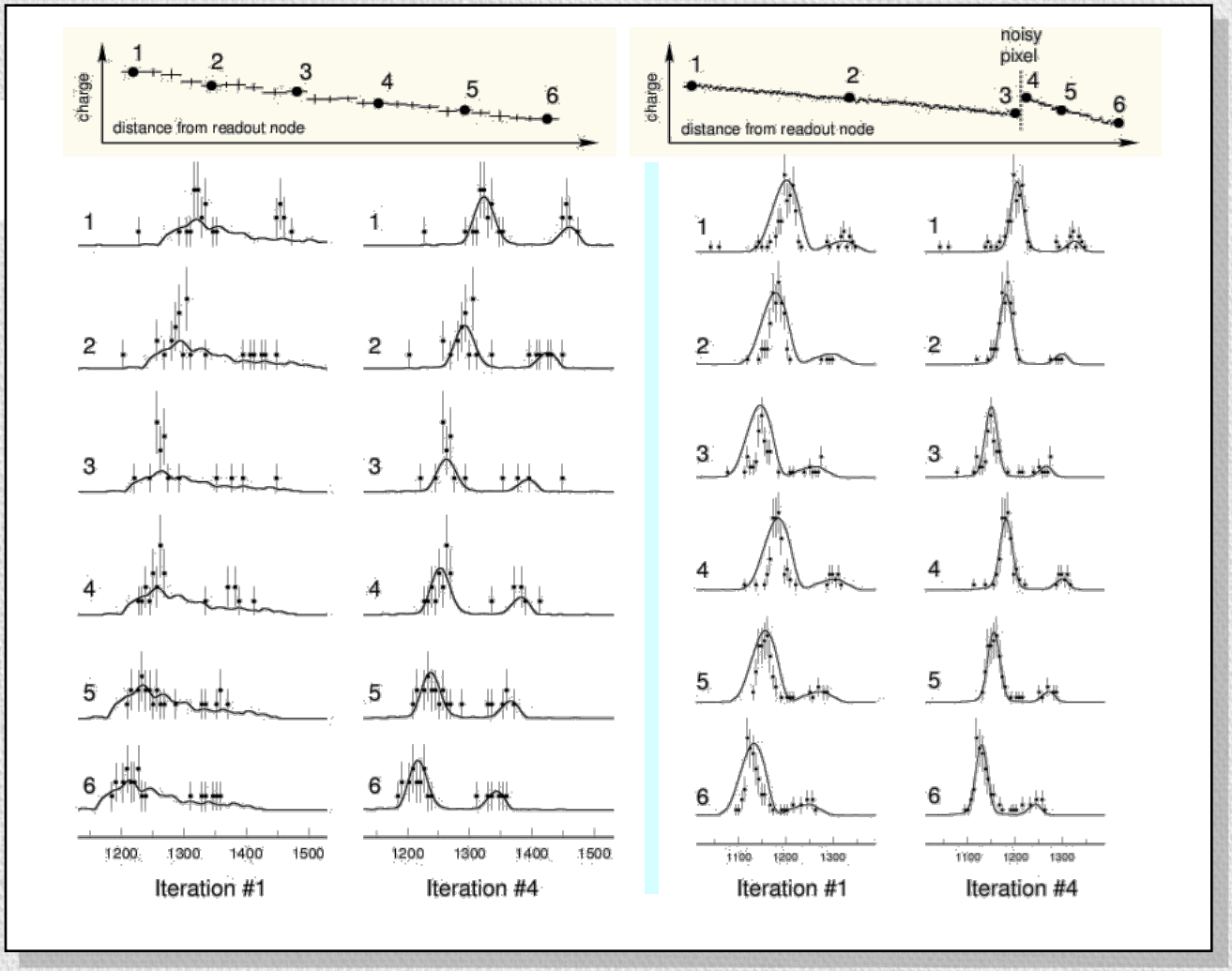

low photon statistics ***high photon statistics***

Detector Calibration: Charge Transfer Inefficiency (CTI)

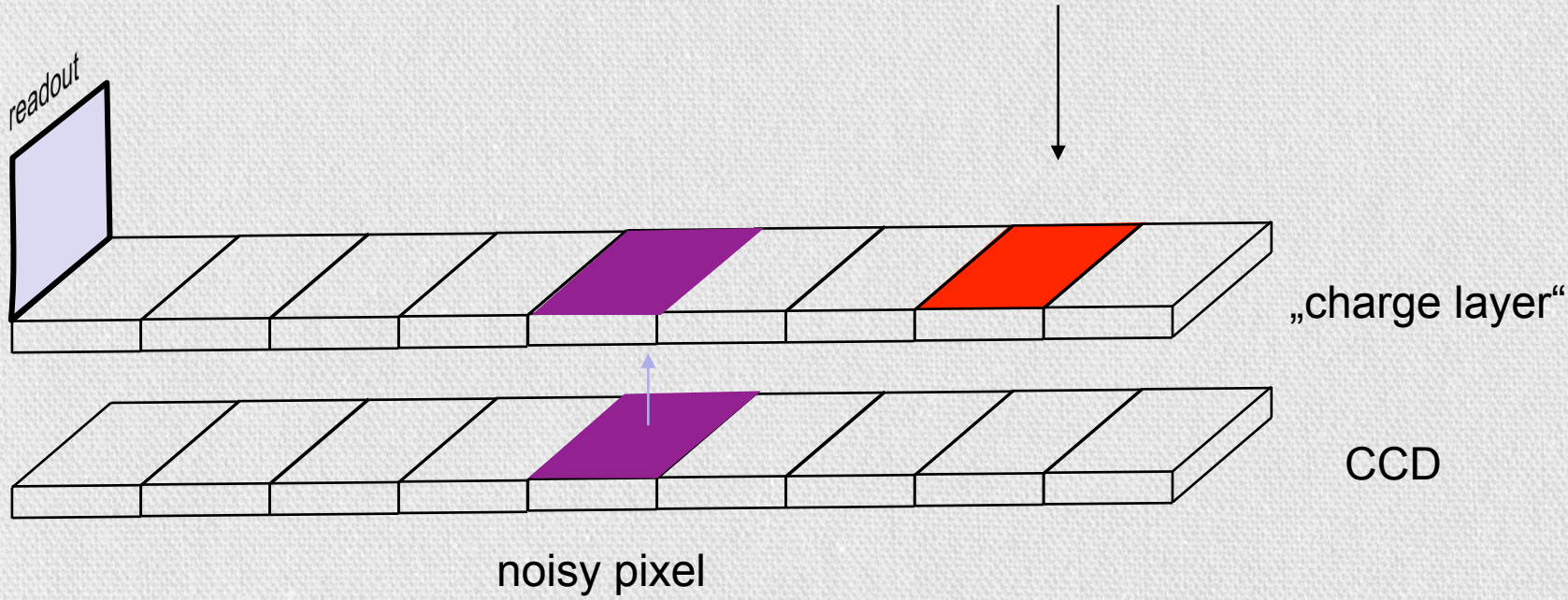

Detector Calibration: Charge Transfer Inefficiency (CTI)

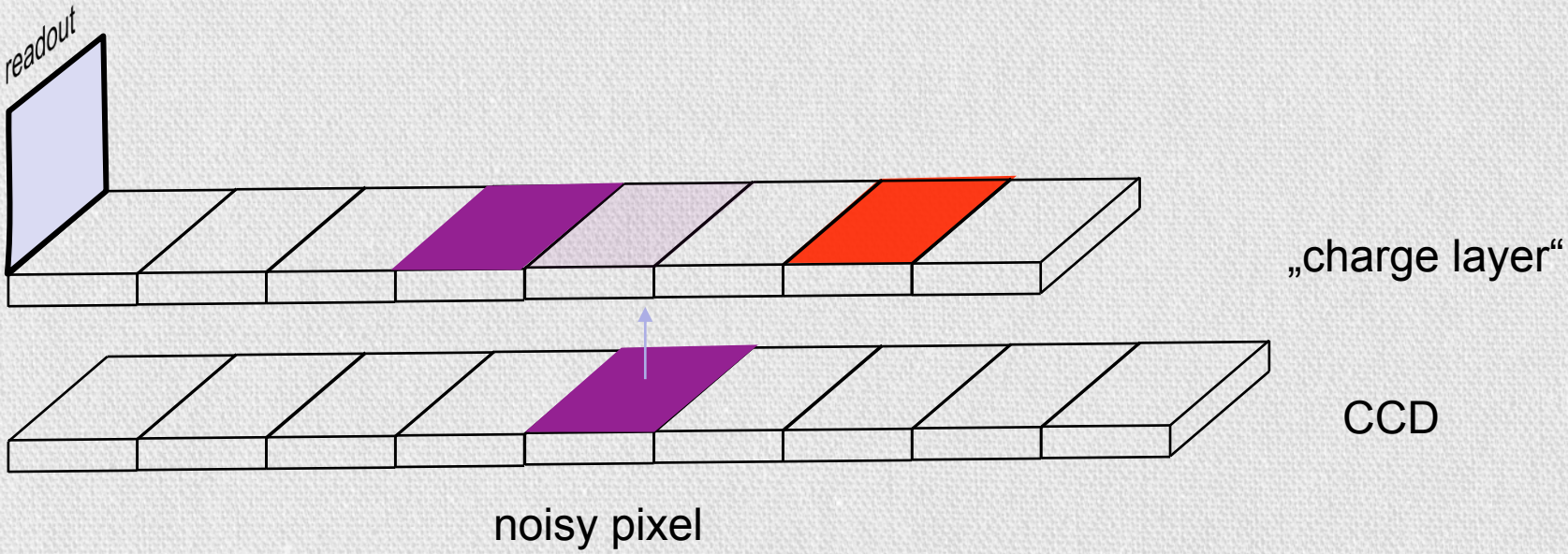

Detector Calibration: Charge Transfer Inefficiency (CTI)

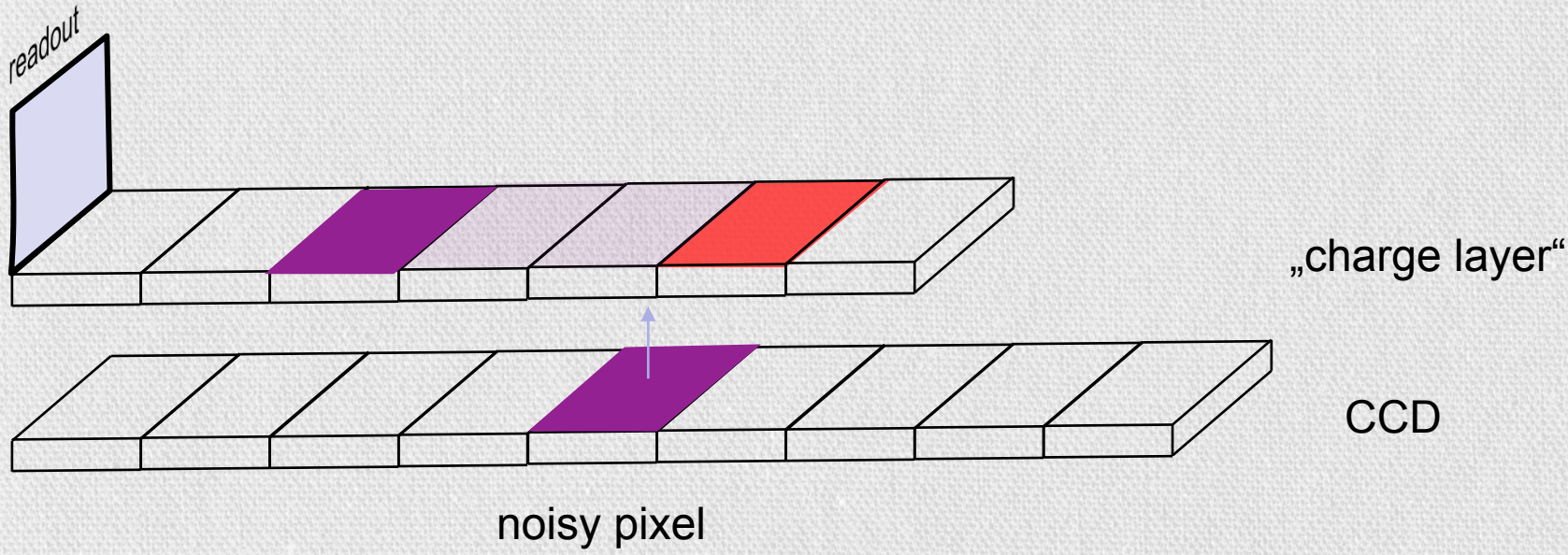

Detector Calibration: Charge Transfer Inefficiency (CTI)

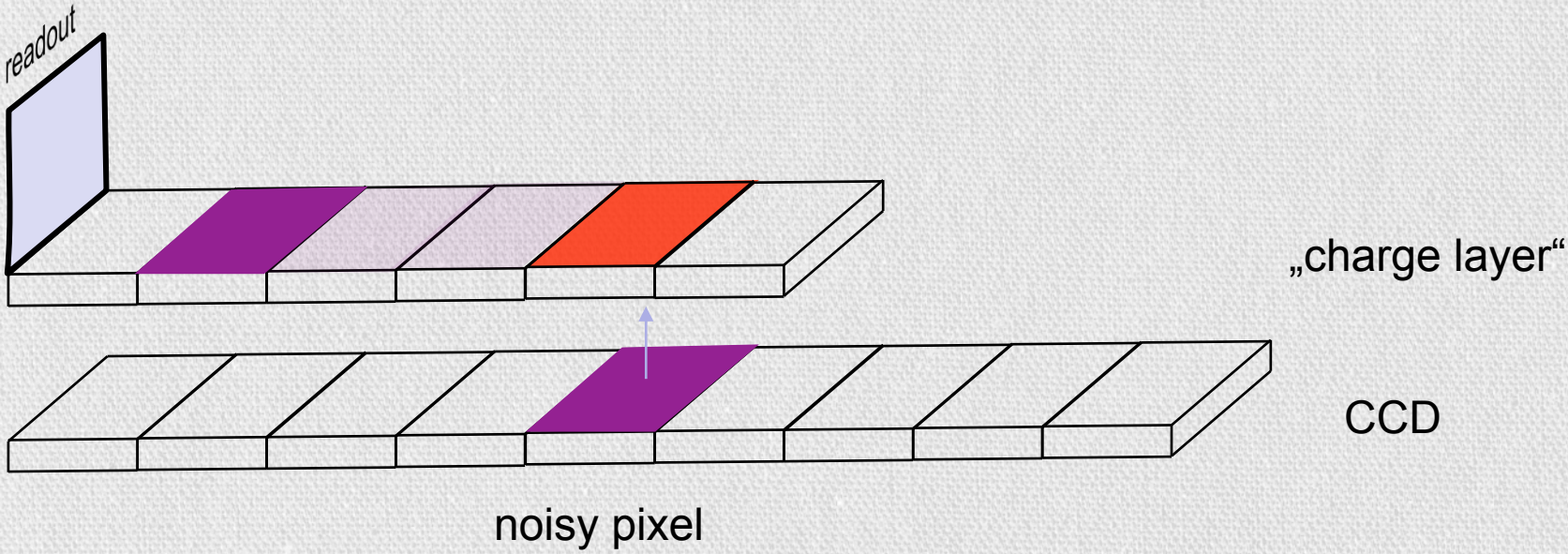

Detector Calibration: Charge Transfer Inefficiency (CTI)

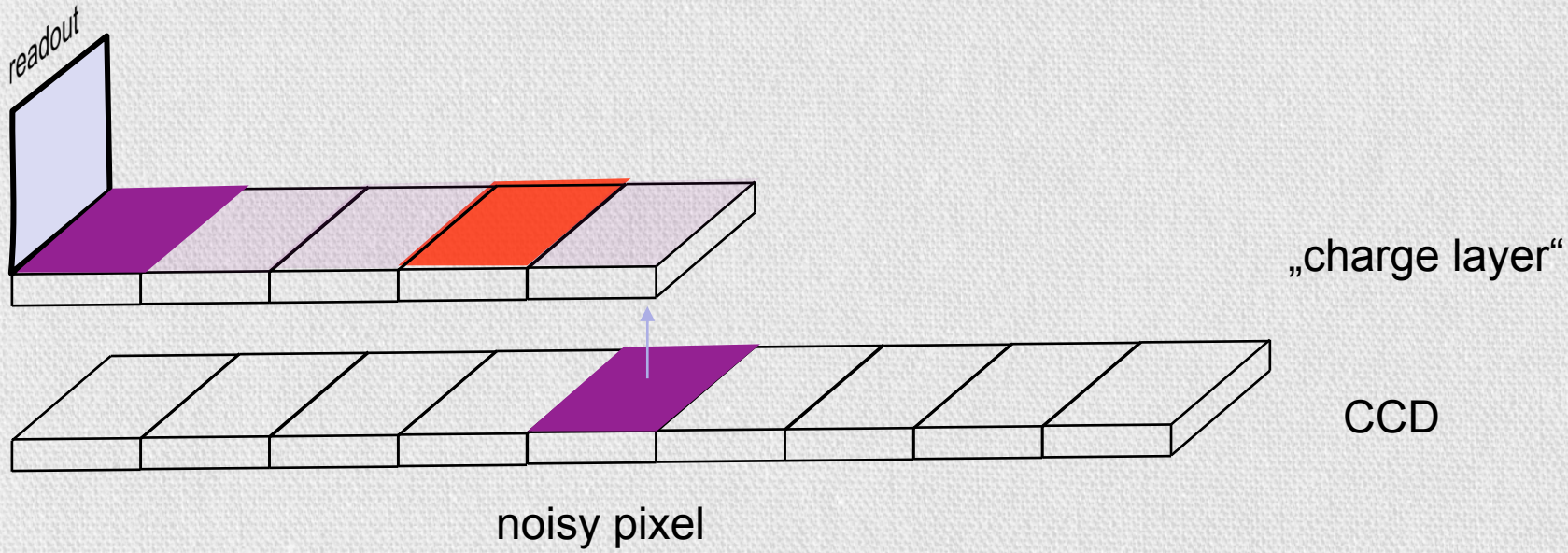

Detector Calibration: Charge Transfer Inefficiency (CTI)

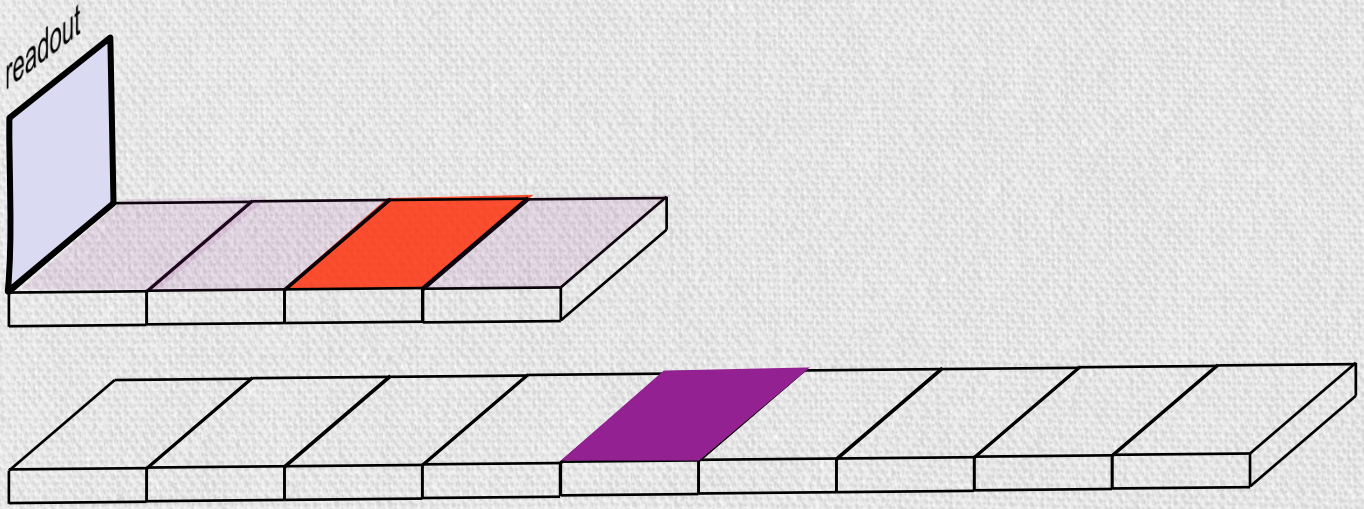

Detector Calibration: Charge Transfer Inefficiency (CTI)

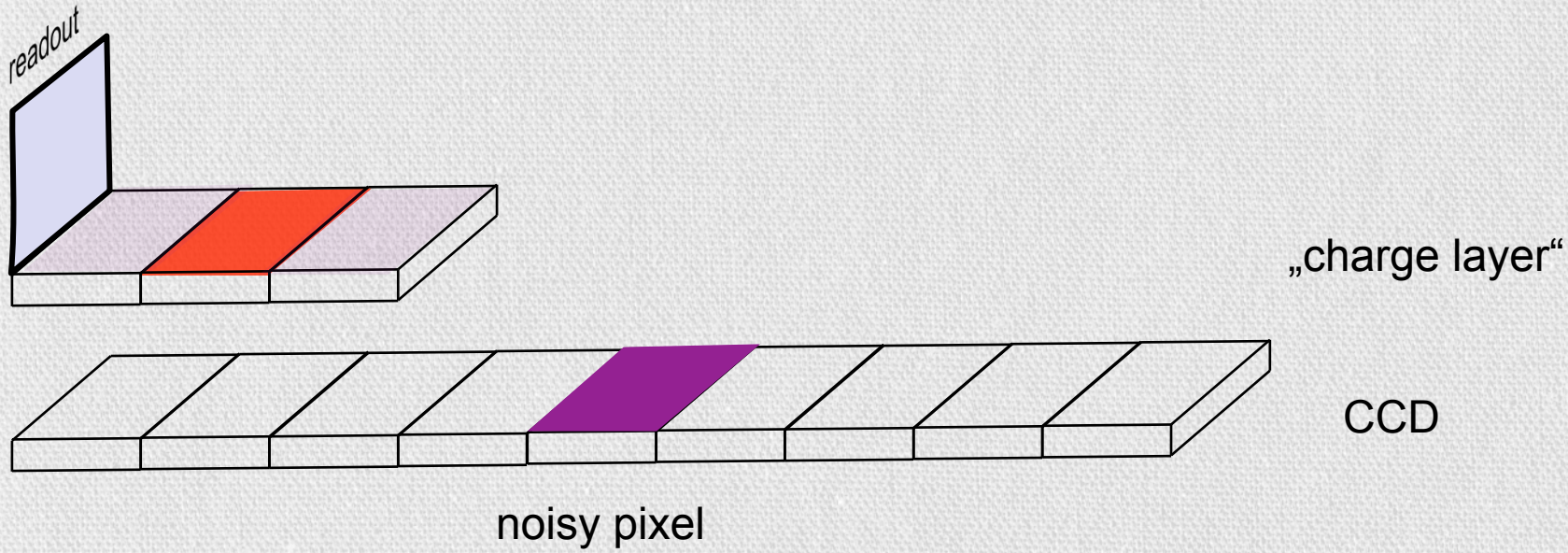

Detector Calibration: Charge Transfer Inefficiency (CTI)

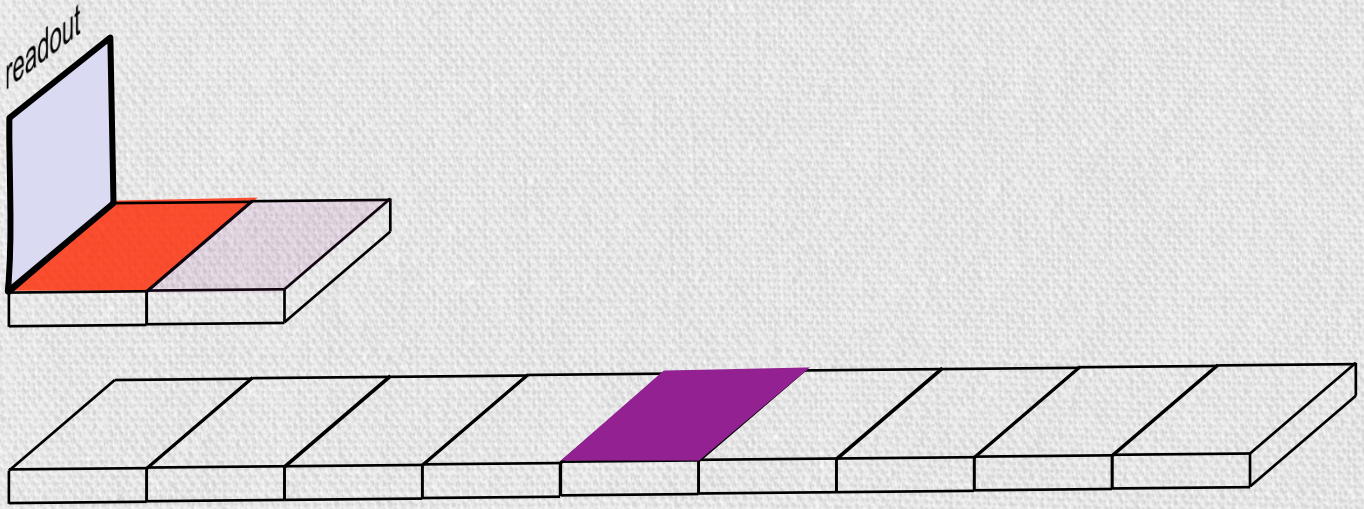

Detector Calibration: Charge Transfer Inefficiency (CTI)

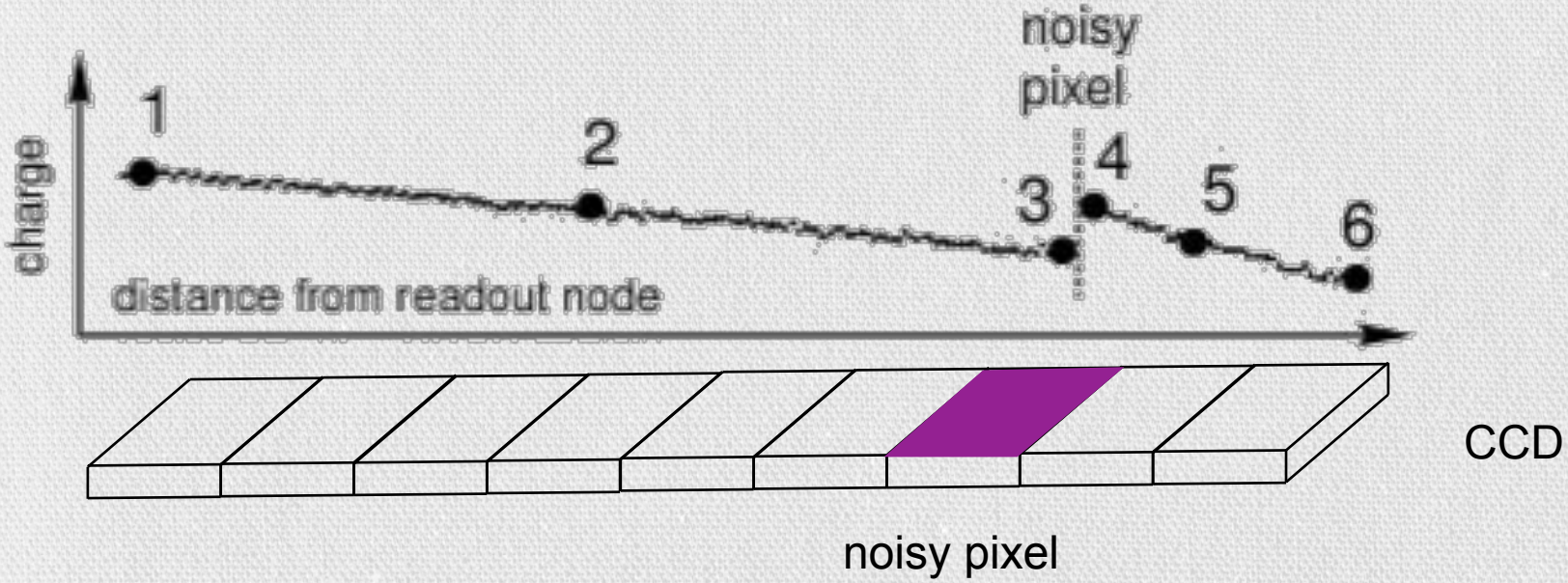

Detector Calibration: Charge Transfer Inefficiency (CTI)

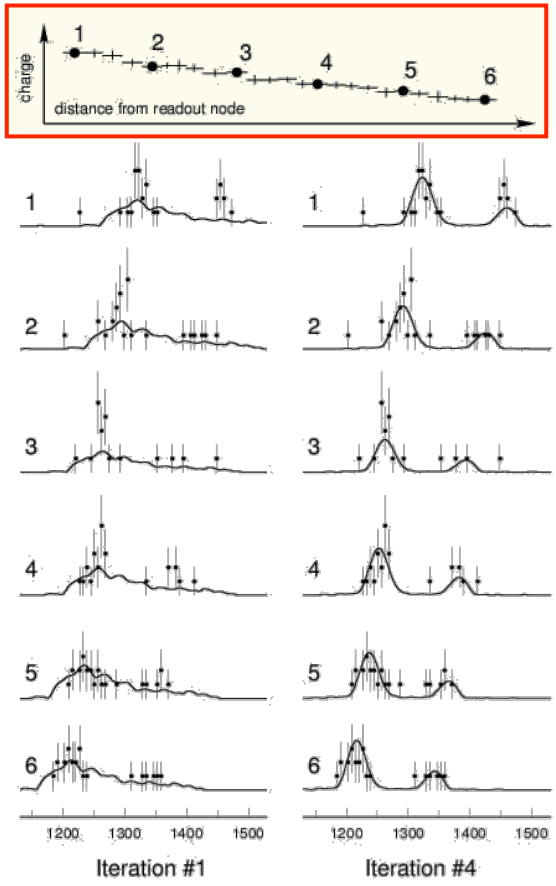

example:
Fe-K, measured with FM4

CCD column 240 (arbitrary choice)

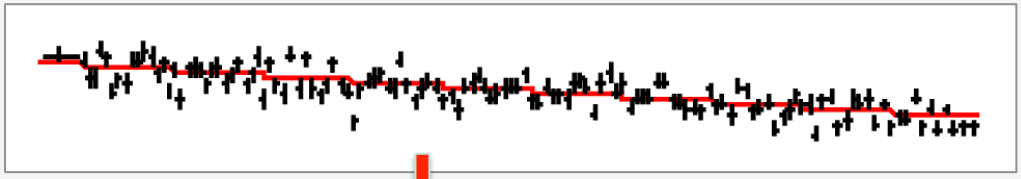

CTI = 2.1 x 10^{-5}

emission line determined in 130 (adaptively computed) macro pixels containing a minimum of 30 first singles around the line

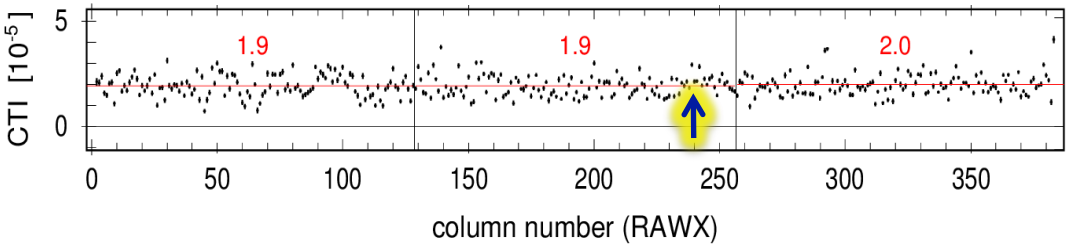

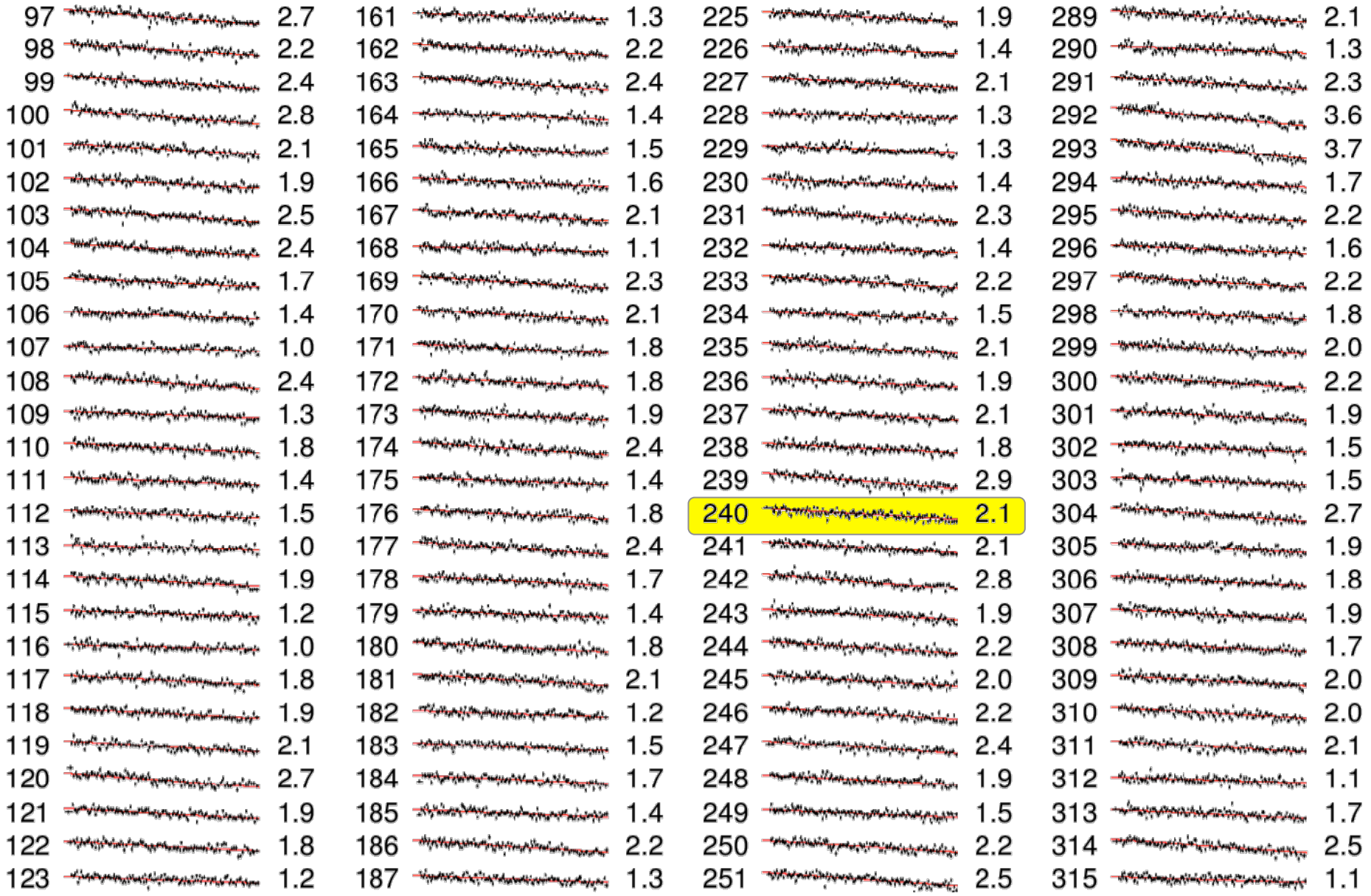

CTI determination

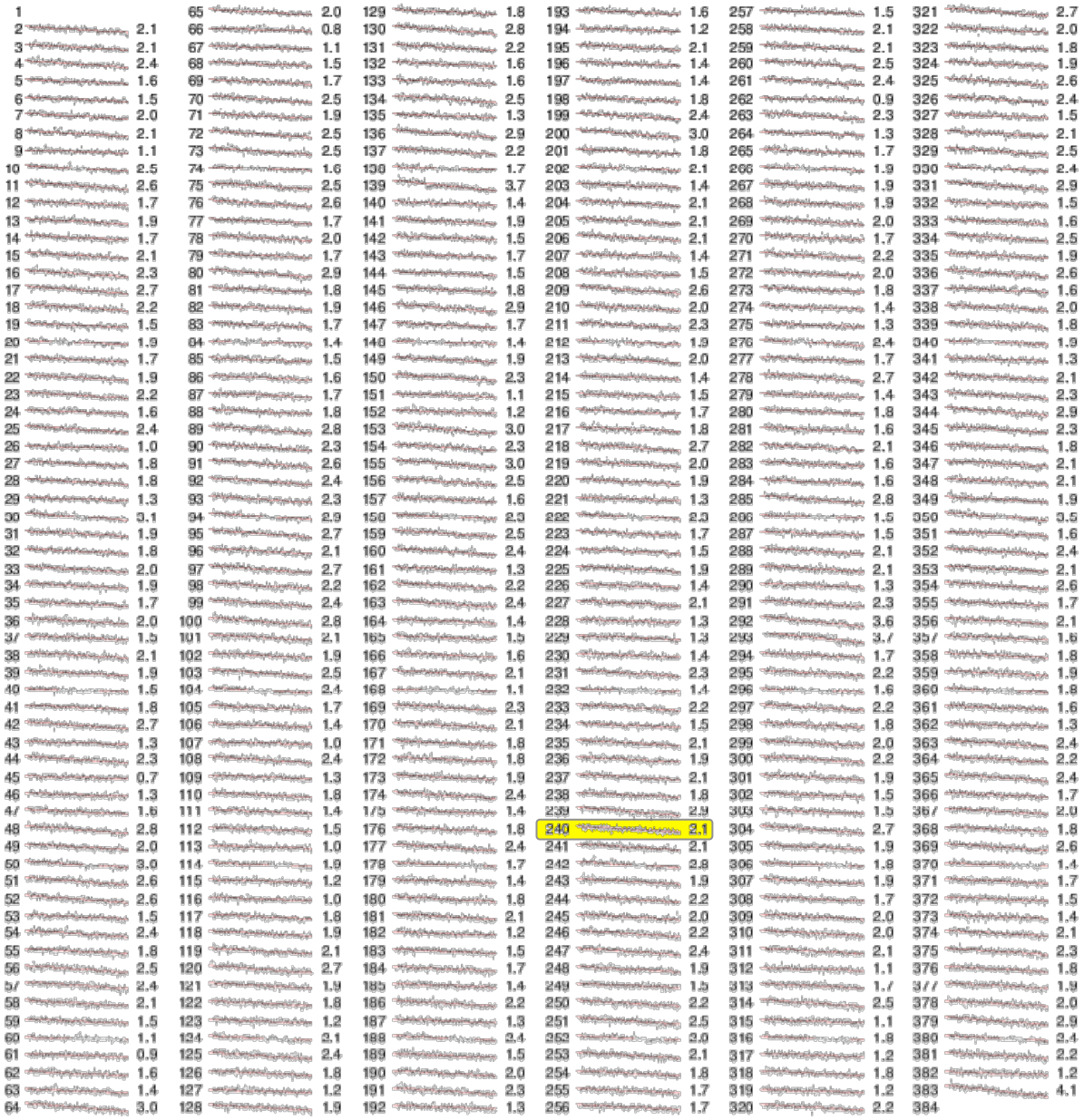

example:
Fe-K, measured with FM4

plot contains
47 267 data points

each data point is
the result of several
iterative template fits

CTI determination

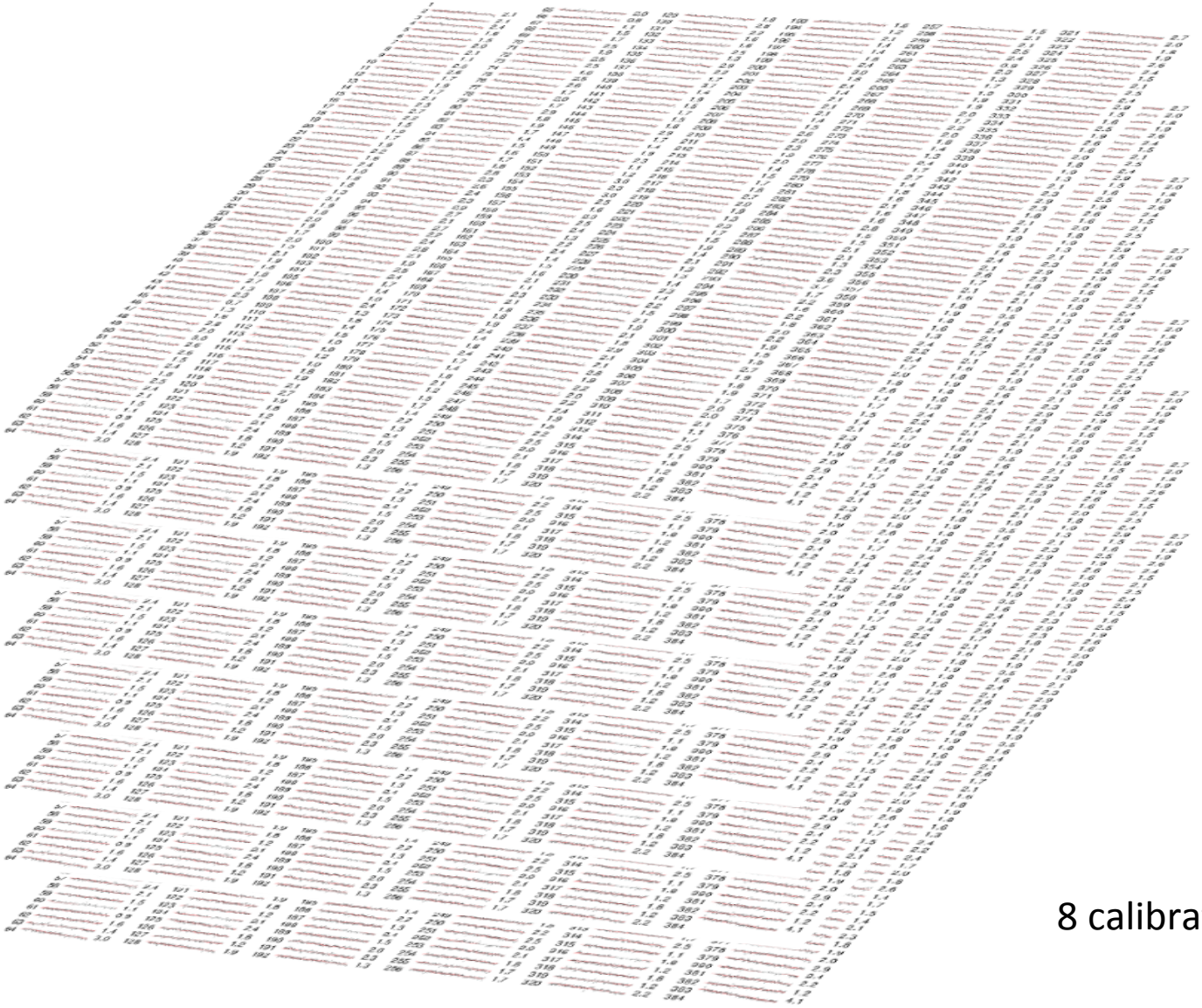

8 calibration energies

CTI determination

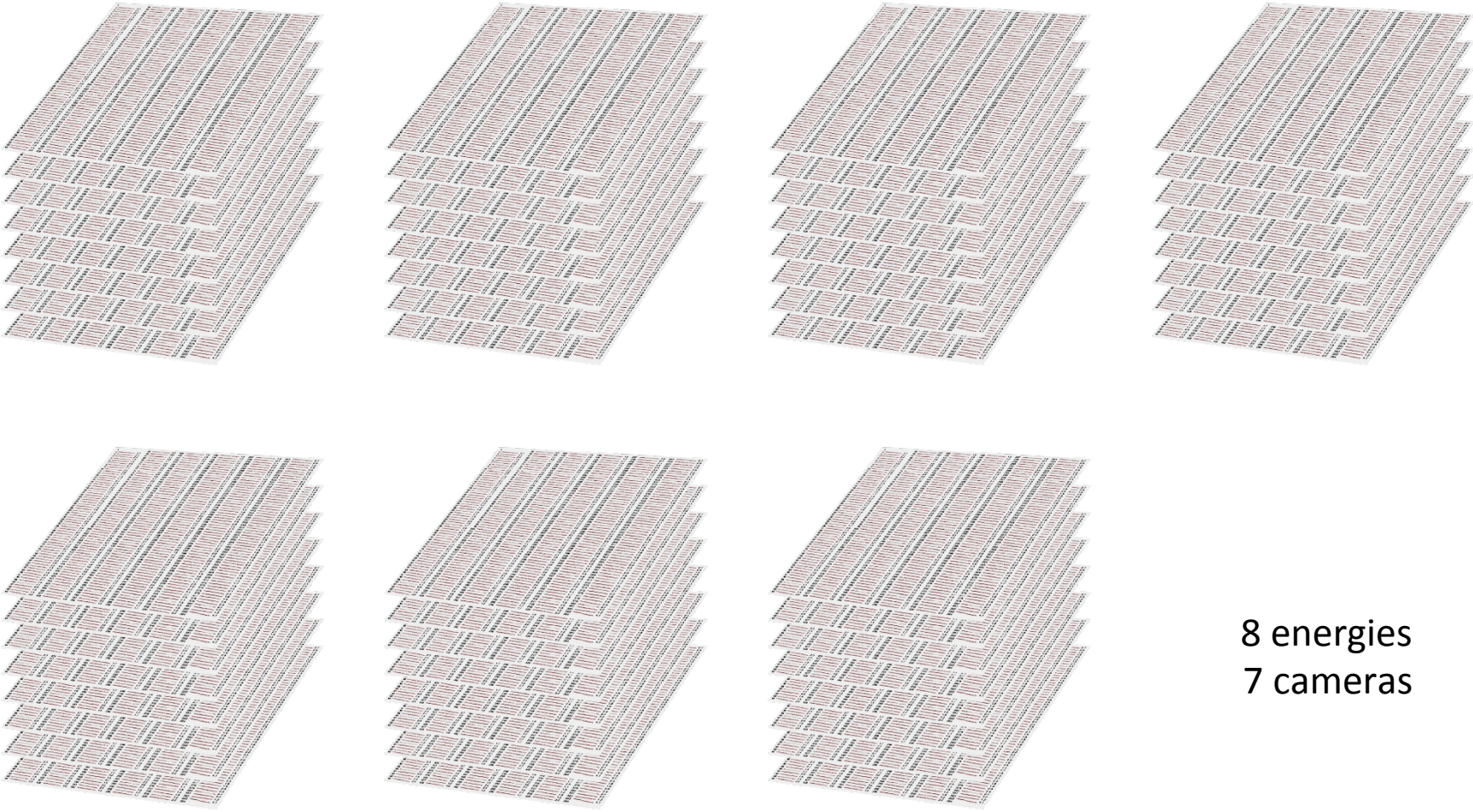

8 energies
7 cameras

7 CCDs (with 3.3 billion events) calibrated

CTI determination

From photons to bits: the fate of X-rays grabbed by eROSITA

device	*process*	*signal*	*characteristic properties*	
telescope	reflection (scattering)	*photon [eV]*	effective area (E,θ,φ) point spread function (E,θ,φ) field of view (FOV) boresight	collecting area, reflectivity, vignetting mirror quality, encircled energy fraction focal length, detector geometry, plate scale alignment
filter	absorption		transmission (E,x,y) contamination (E,x,y,t)	
CCD	charge release	*charge [e^-]*	charge splitting low energy threshold	**patterns** (singles, doubles, triples, quadruples, invalid..)
			contaminating effects	**pile-up** (single pixel, pattern) **photon background** (fluorescence, optical loading) **particle induced background** (soft protons, MIPs) **detector induced background** (noise, bright pixels)
			quantum efficiency (QE) energy resolution (ΔE)	
	charge transfer		charge transfer loss (CTI) pattern migration	**trap saturation** due to photons and particles **charge transfer noise** **threshold induced charge loss** reemission, charge diffusion, charge splitting
	charge readout	*pulse height amplitude [adu]*	readout noise amplification (‘gain’)	non-linear gain, also dependence of the “apparent” gain on threshold(!) dependence on energy, temperature, time, ...
on-board data processor	signal processing	*event [bit]*		

Detector Calibration: Gain

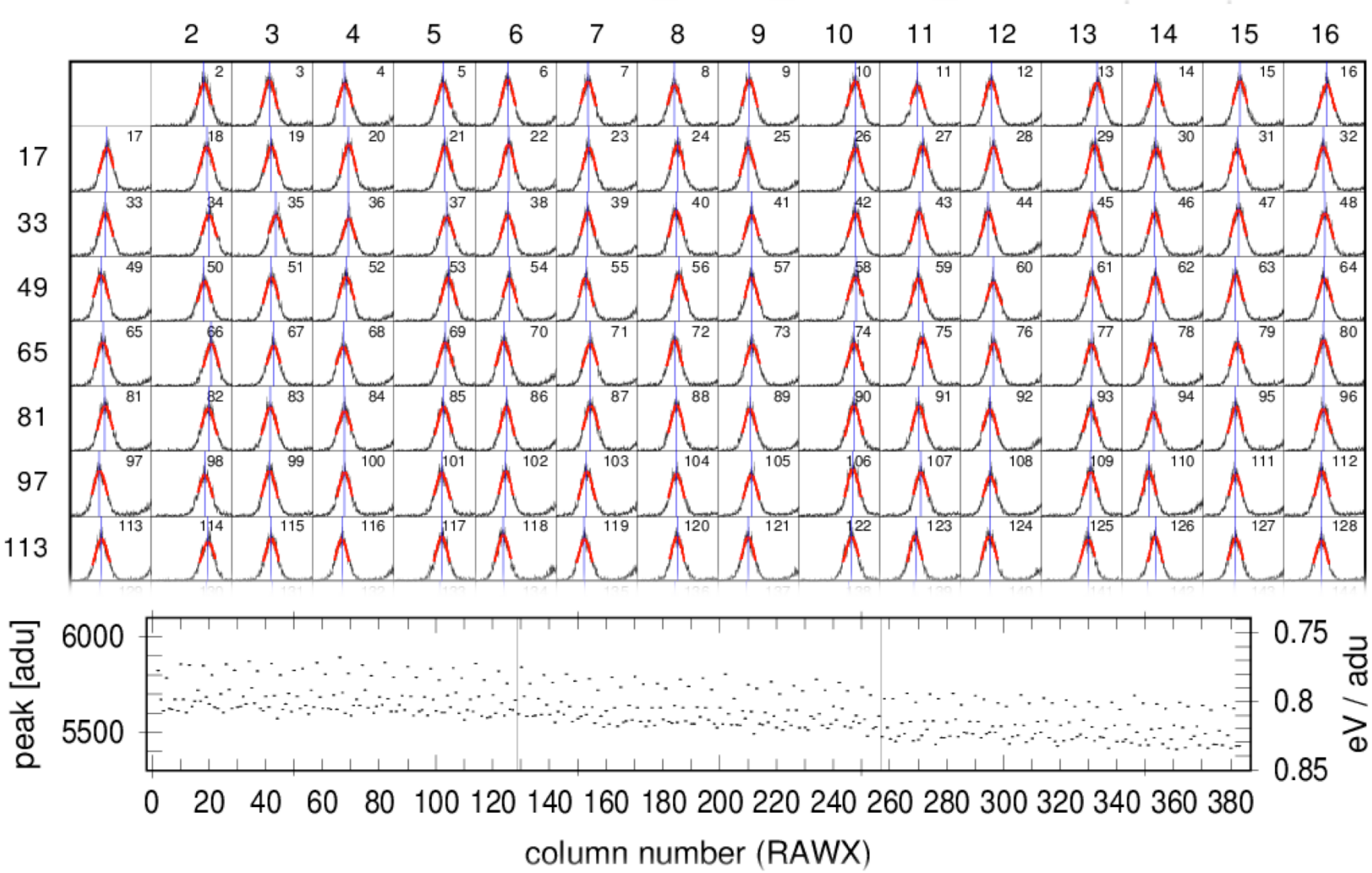

Energy interpolation of gain and CTI

gain

individually for each CCD column

CTI

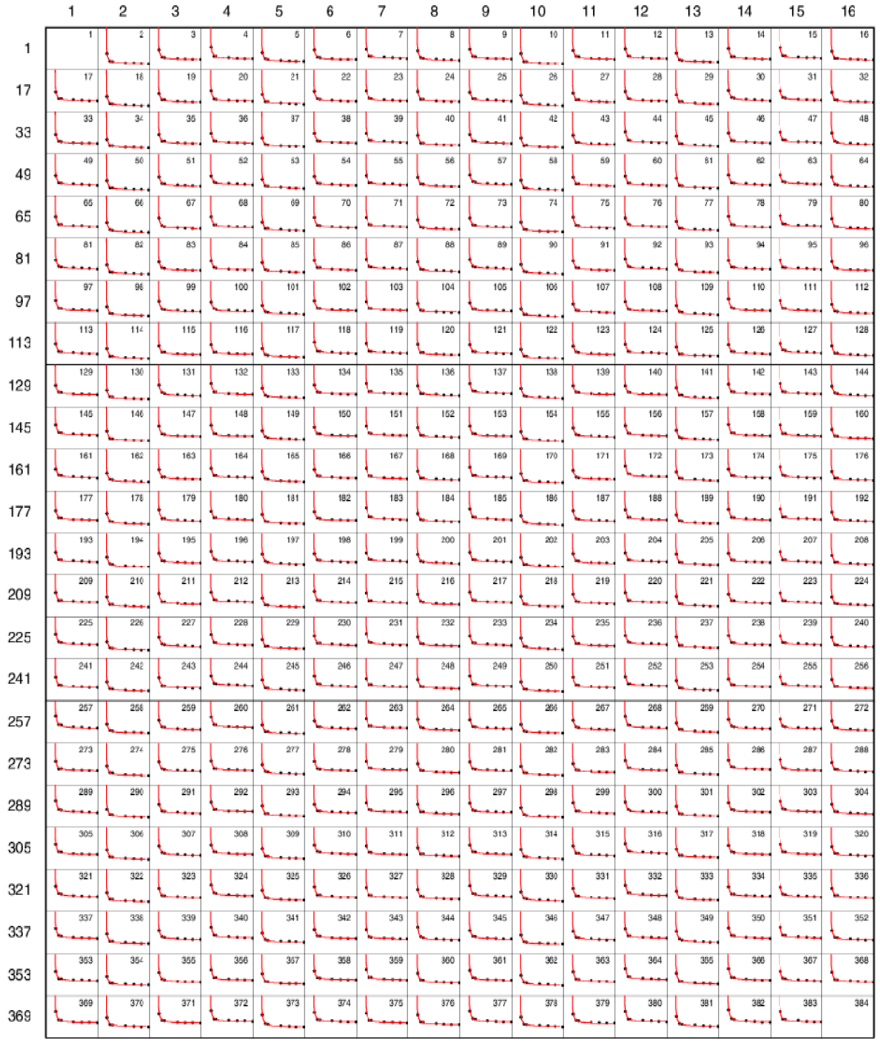

x axis: energy (linear) , min : -2.0 keV, max : 10.0 keV

y axis: gain (linear) , min : 0.72 eV / adu , max : 0.95 eV / adu

energies [keV] : 0.277 0.277 0.930 1.486 4.508 6 .398 8.040 9.886

transition lines: C-K O-K Cu-L Al-K Ti-K Fe-K Cu-K Ge-K

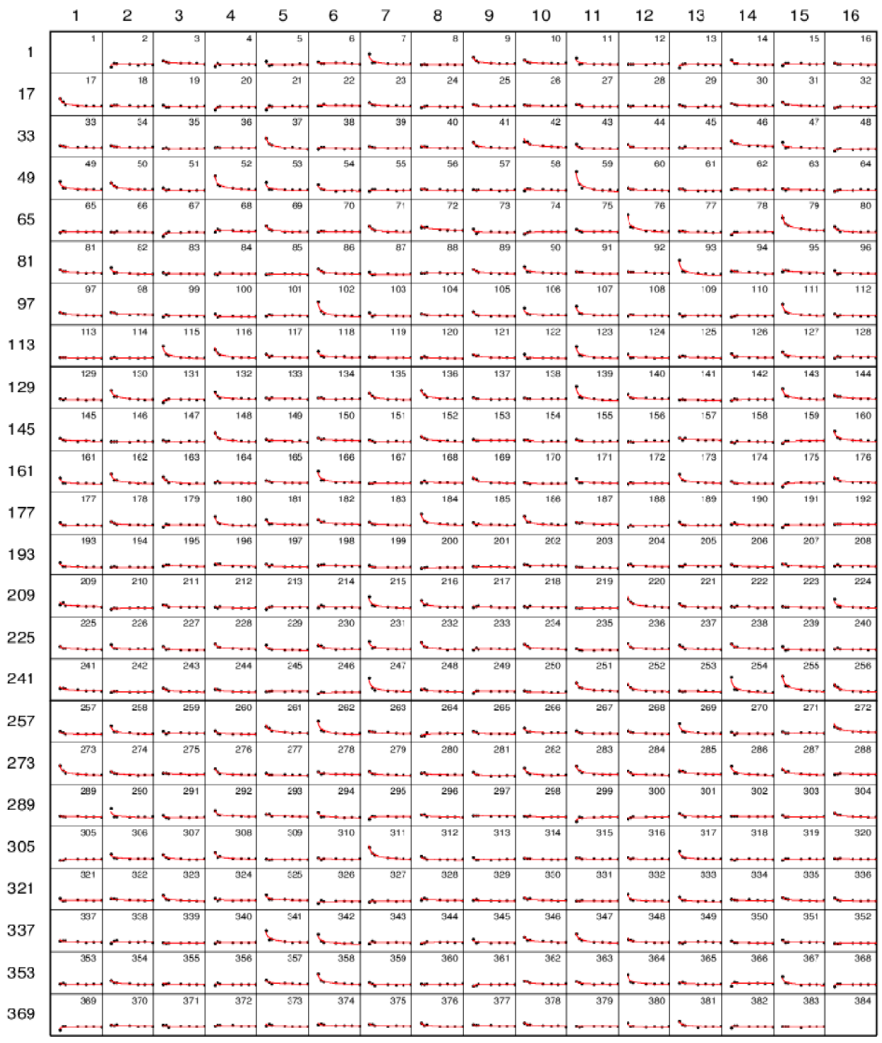

x axis: energy (linear) , min : -2.00 keV, max : 10.00 keV

y axis: CTI (linear) , min : -5.0 e-5 , max : 20.0 e-5

energies [keV] : 0.277 0.277 0.930 1.486 4.508 6 .398 8.040 9.886

transition lines: C-K O-K Cu-L Al-K Ti-K Fe-K Cu-K Ge-K

Reconstructing the spectral distribution requires

- **pattern** recognition
- correction for **gain** variations between CCD channels
- correction for charge transfer loss **(CTI)**

example: Fe-K, measured with FM4

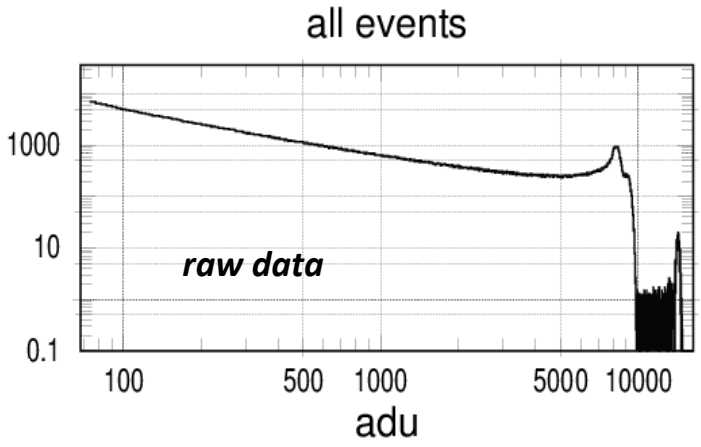

FWHM = 132.5 – 143.1 eV
all photons: FWHM = 137.8 eV

accuracy of absolute
energy scale: 2 eV (0.03%)

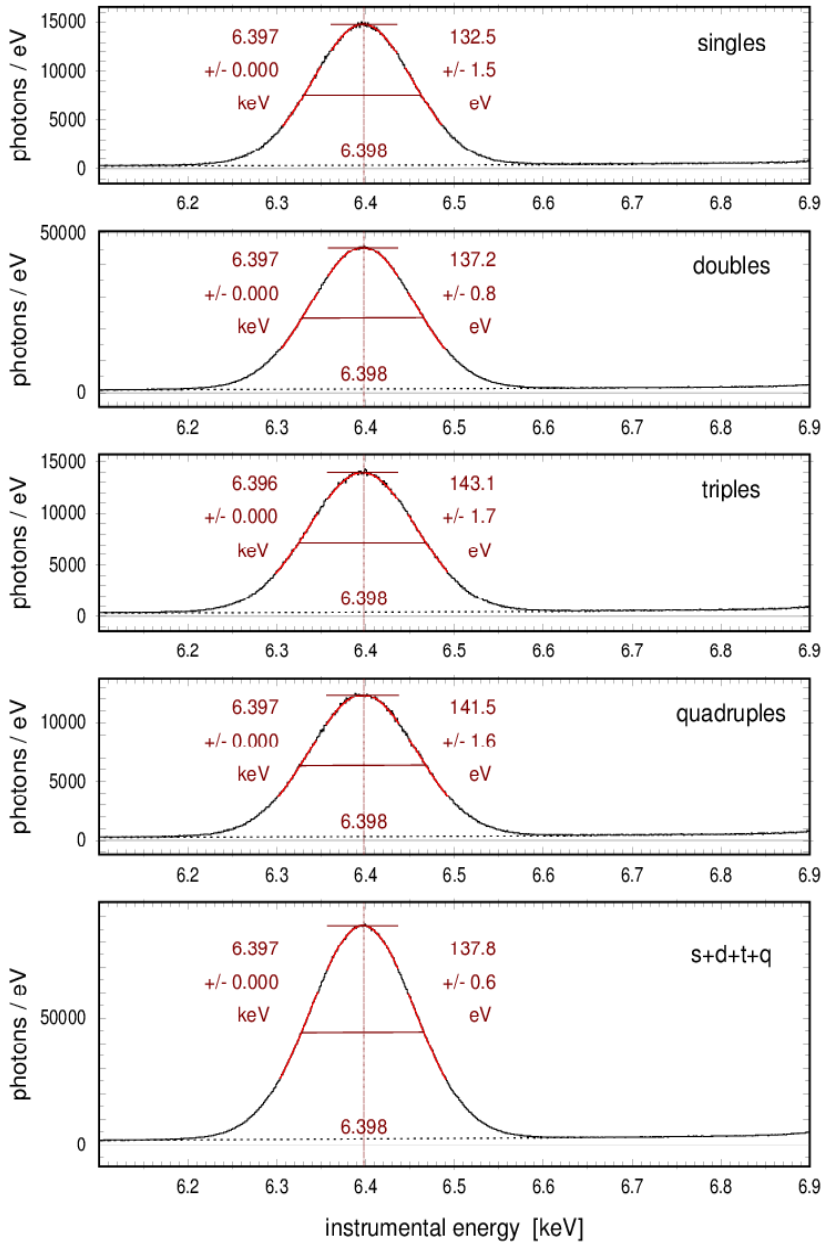

reconstructed spectral distribution

From photons to bits: the fate of X-rays grabbed by eROSITA

device	*process*	*signal*	*characteristic properties*	
telescope	reflection (scattering)	*photon [eV]*	effective area (E,θ,φ) point spread function (E,θ,φ) field of view (FOV) boresight	collecting area, reflectivity, vignetting mirror quality, encircled energy fraction focal length, detector geometry, plate scale alignment
filter	absorption		transmission (E,x,y) contamination (E,x,y,t)	
CCD	charge release	*charge [e^-]*	charge splitting low energy threshold	**patterns** (singles, doubles, triples, quadruples, invalid..)
			contaminating effects	**pile-up** (single pixel, pattern) **photon background** (fluorescence, optical loading) **particle induced background** (soft protons, MIPs) **detector induced background** (noise, bright pixels)
			quantum efficiency (QE) energy resolution (ΔE)	
	charge transfer		charge transfer loss (CTI) pattern migration	**trap saturation** due to photons and particles **charge transfer noise** **threshold induced charge loss** reemission, charge diffusion, charge splitting
	charge readout	*pulse height amplitude [adu]*	readout noise amplification (‘gain’)	non-linear gain, also dependence of the “apparent” gain on threshold(!) dependence on energy, temperature, time, ...
on-board data processor	signal processing	*event [bit]*	energy offsets (offset map) common mode correction signal extraction MIP suppression	*(would require separate presentation)*

Baikonur, Kazakhstan, 2019 July 13

From photons to bits: the fate of X-rays grabbed by eROSITA

device	*process*	*signal*	*characteristic properties*	
telescope	reflection (scattering)	*photon [eV]*	effective area (E,θ,φ) point spread function (E,θ,φ) field of view (FOV) boresight	collecting area, reflectivity, vignetting mirror quality, encircled energy fraction focal length, detector geometry, plate scale alignment
filter	absorption		transmission (E,x,y) contamination (E,x,y,t)	
CCD	charge release	*charge [e^-]*	charge splitting low energy threshold	**patterns** (singles, doubles, triples, quadruples, invalid..)
			contaminating effects	**pile-up** (single pixel, pattern) **photon background** (fluorescence, optical loading)
			quantum efficiency (QE)	**particle induced background** (soft protons, MIPs)
			energy resolution (ΔE)	**detector induced background** (noise, bright pixels)
	charge transfer		charge transfer loss (CTI)	**trap saturation** due to photons and particles **charge transfer noise** **threshold induced charge loss**
			pattern migration	reemission, charge diffusion, charge splitting
	charge readout	*pulse height amplitude [adu]*	readout noise	non-linear gain, also dependence of the "apparent" gain on threshold(!)
			amplification ('gain')	dependence on energy, temperature, time, ...
on-board data processor	signal processing	*event [bit]*	energy offsets (offset map) common mode correction signal extraction MIP suppression	*(would require separate presentation)*

Energy calibration with the internal ^{55}Fe source

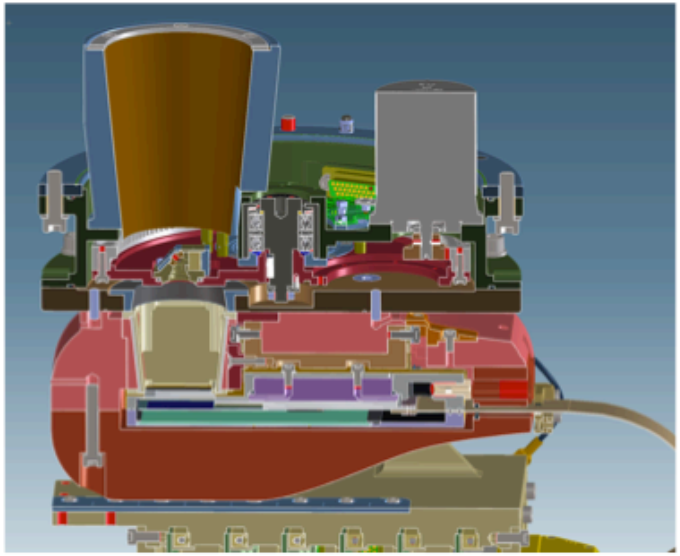

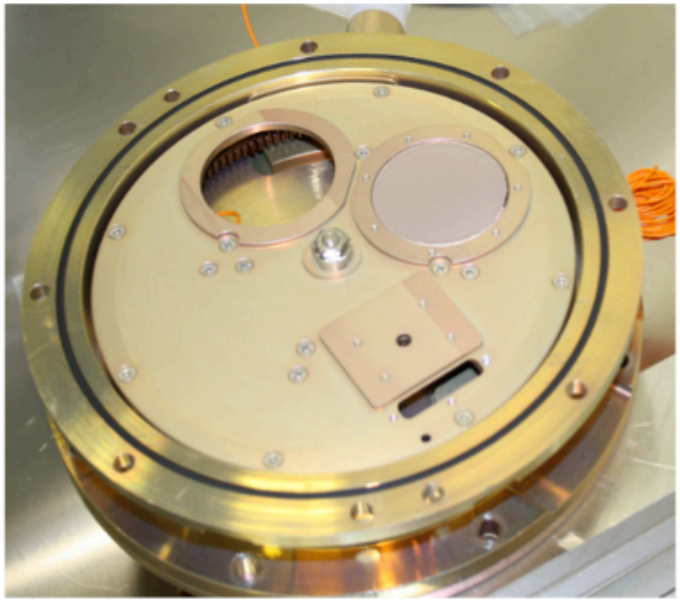

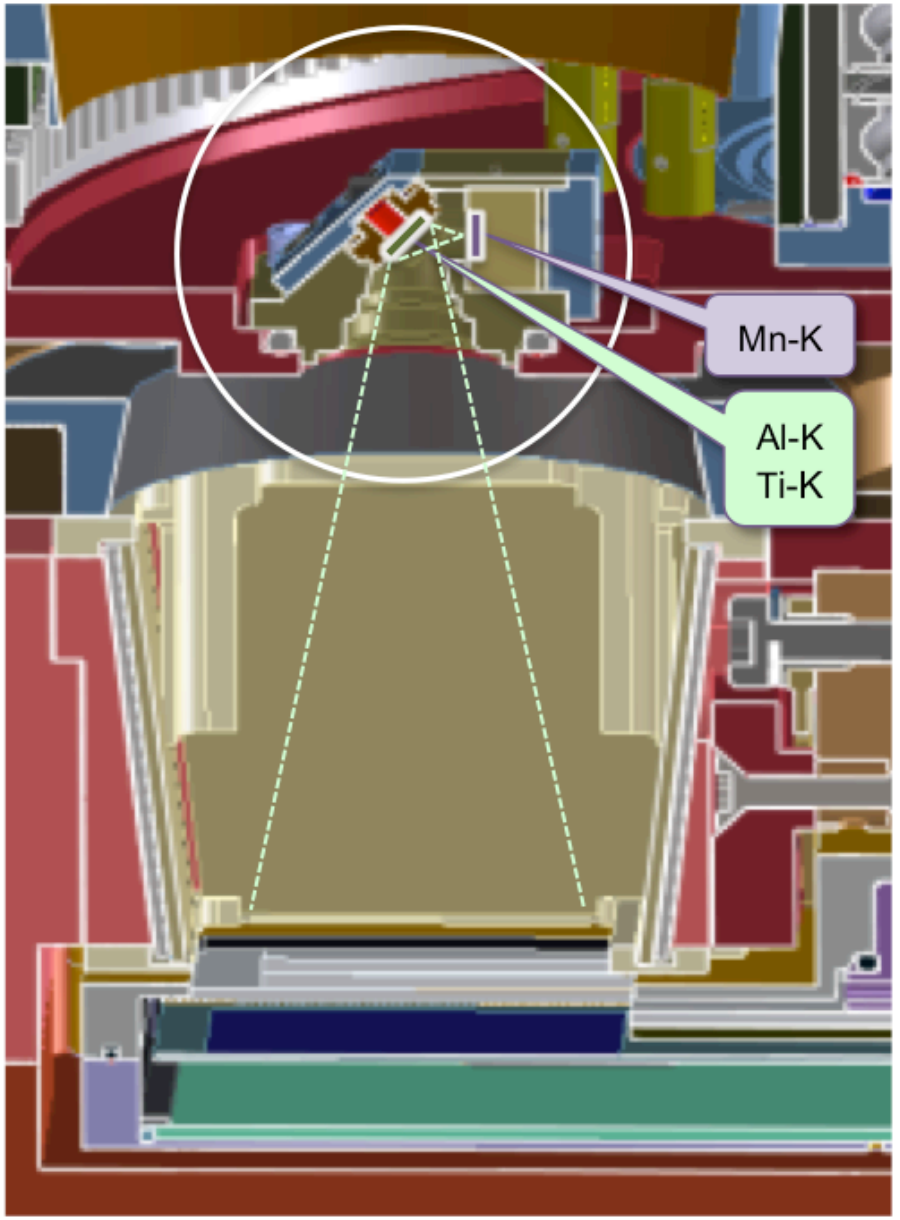

Energy Calibration: internal calibration source

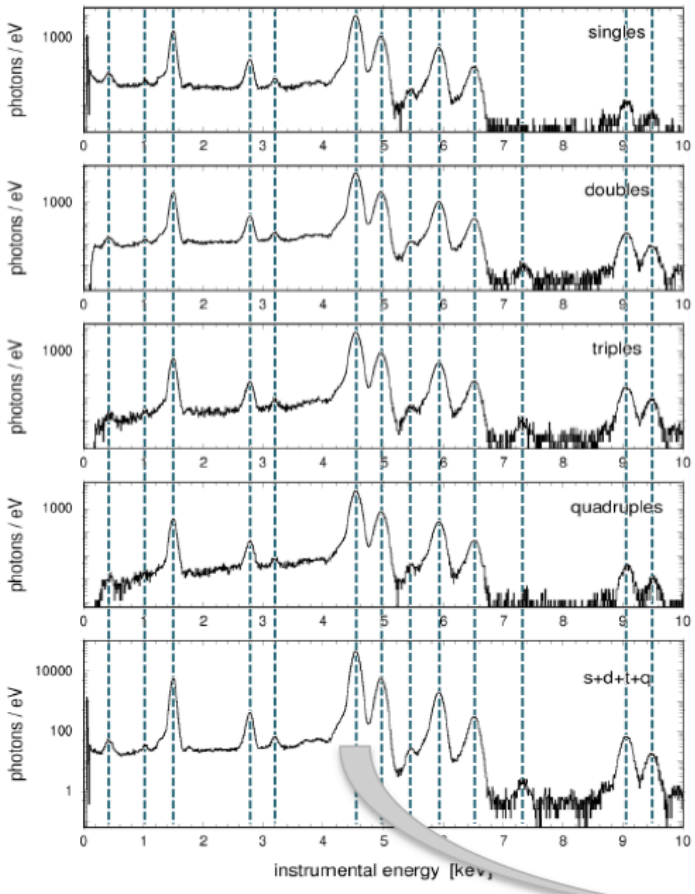

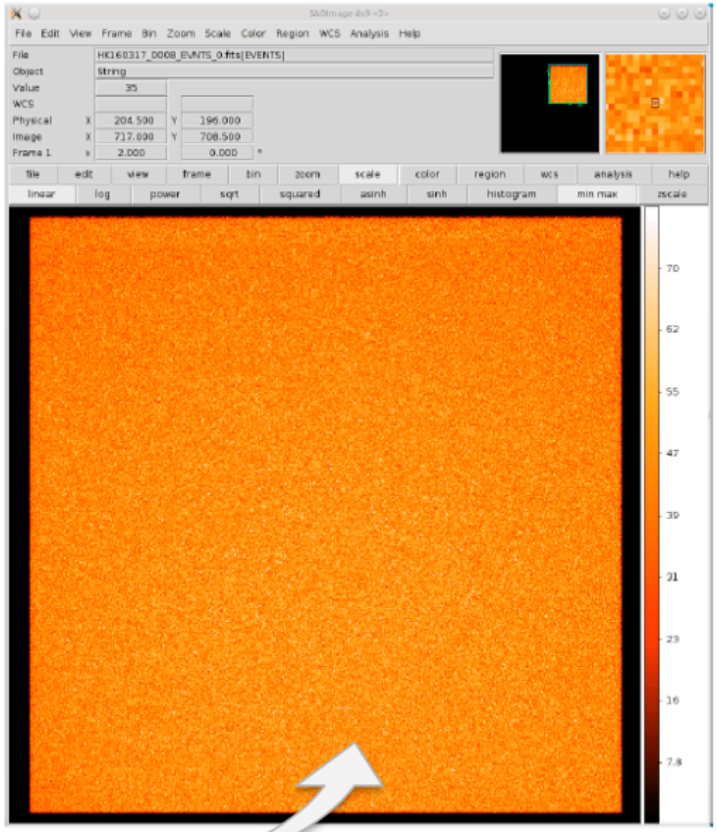

Gain comparison: before / after launch

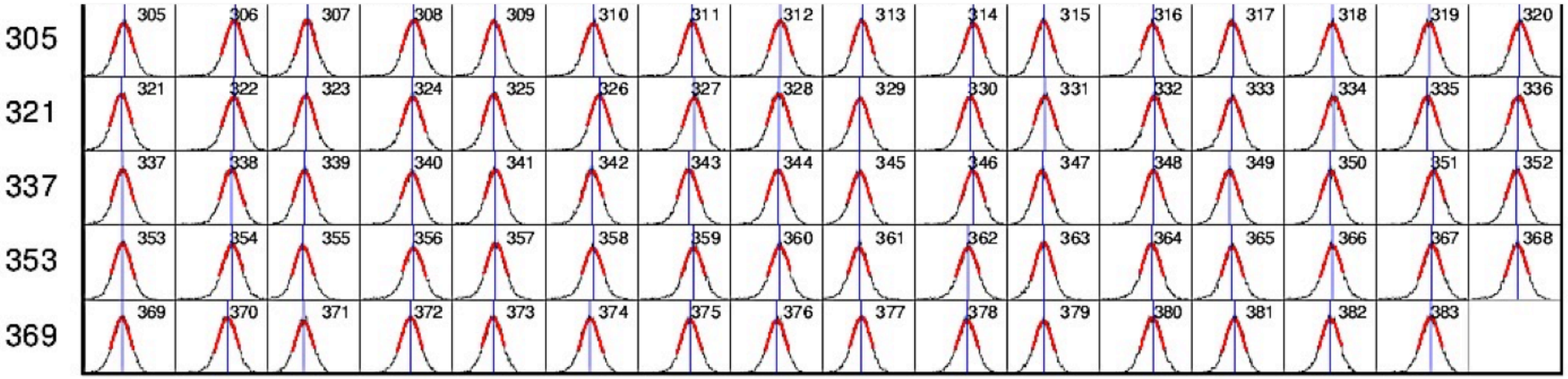

CTE correction applied energy: 1.486 keV split threshold: 46 adu

selection: first singles, amplitude range: 1700 .. 2100 adu, intensity range: 0.0 - 513.5 counts / bin

minimum counts per macro pixel: 90 binning: 4 precursor energy threshold: 100 adu

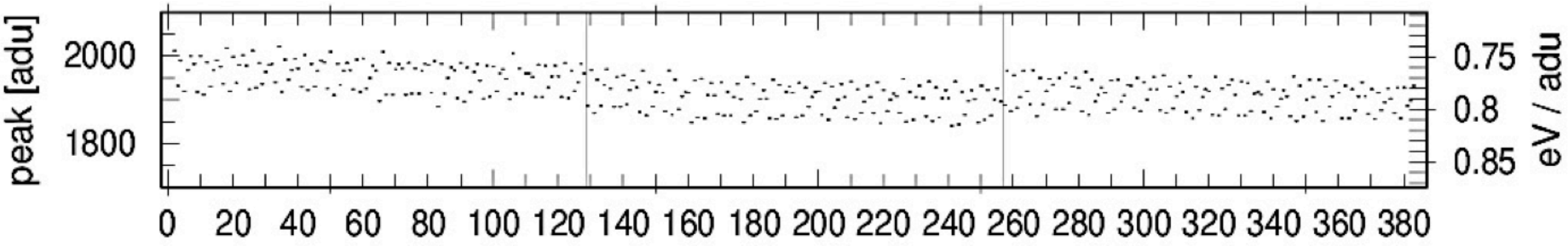

Gain: TM 4, Al-K

ground calibration

Gain comparison: before / after launch

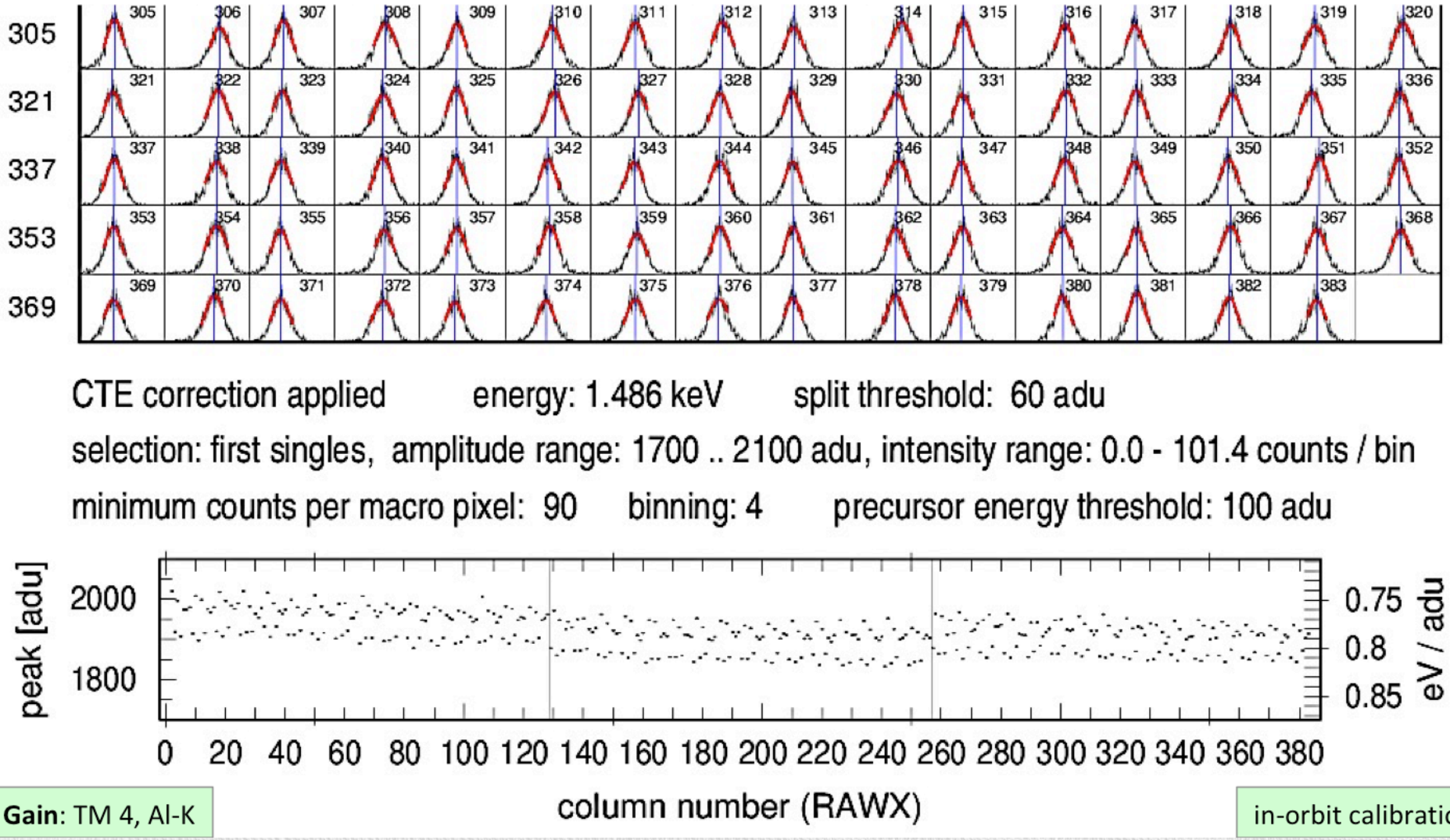

Gain: TM 4, Al-K

in-orbit calibration

CTI comparison: before / after launch

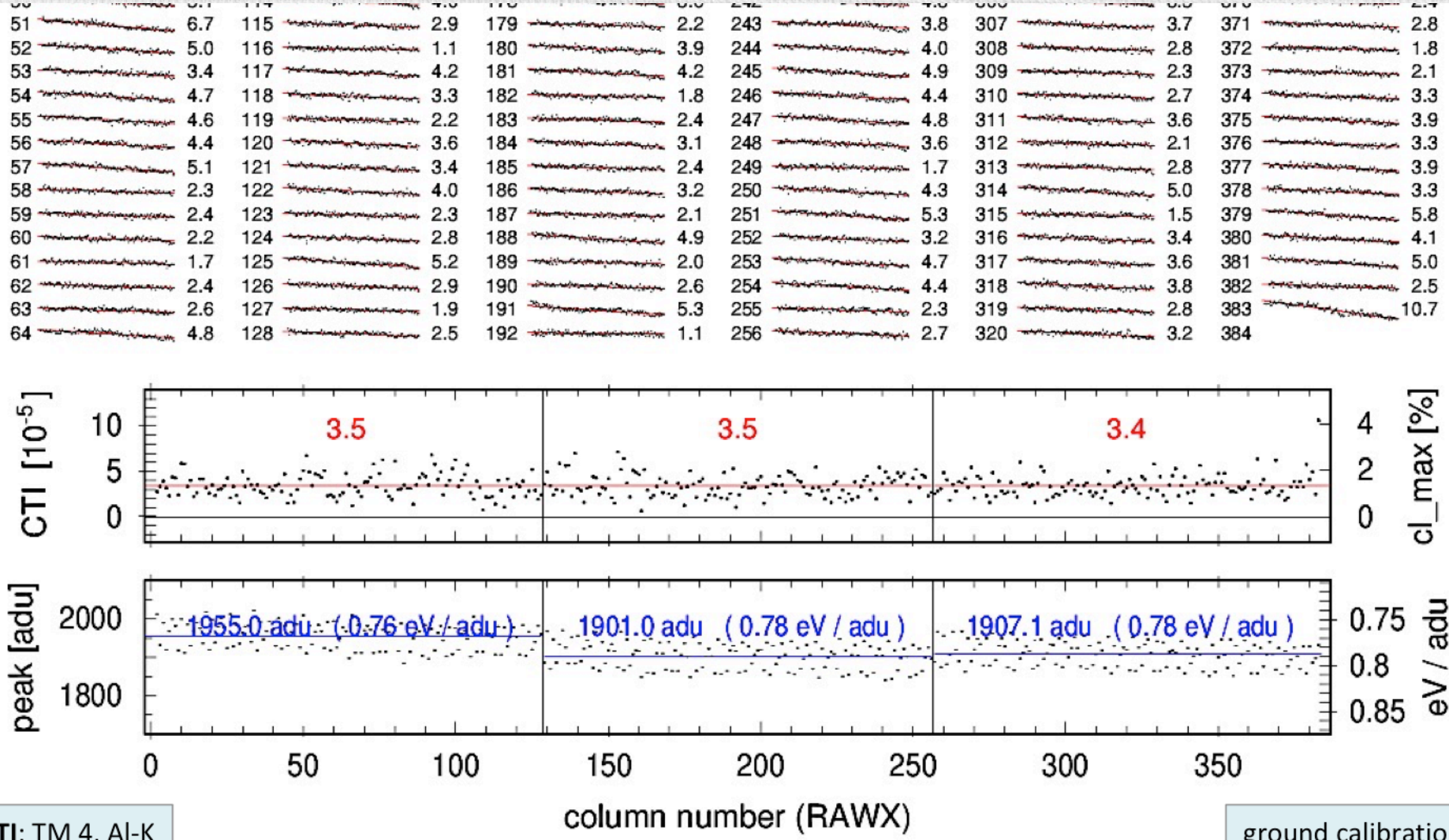

CTI: TM 4, Al-K

ground calibration

CTI comparison: before / after launch

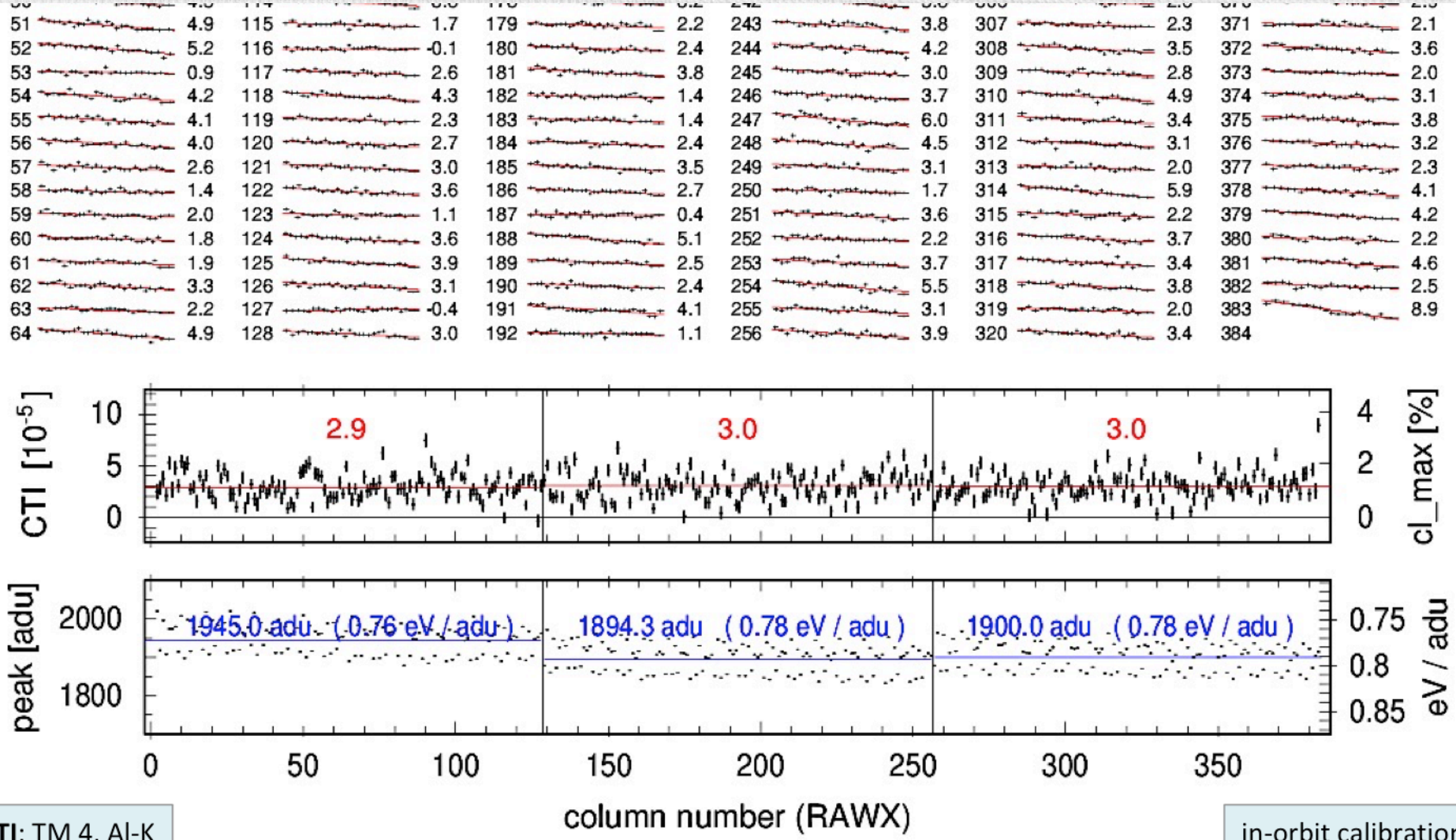

CTI: TM 4, Al-K

in-orbit calibration

Challenges for the energy calibration:

1) CCD temperatures (Sep 2019 – Feb 2022)

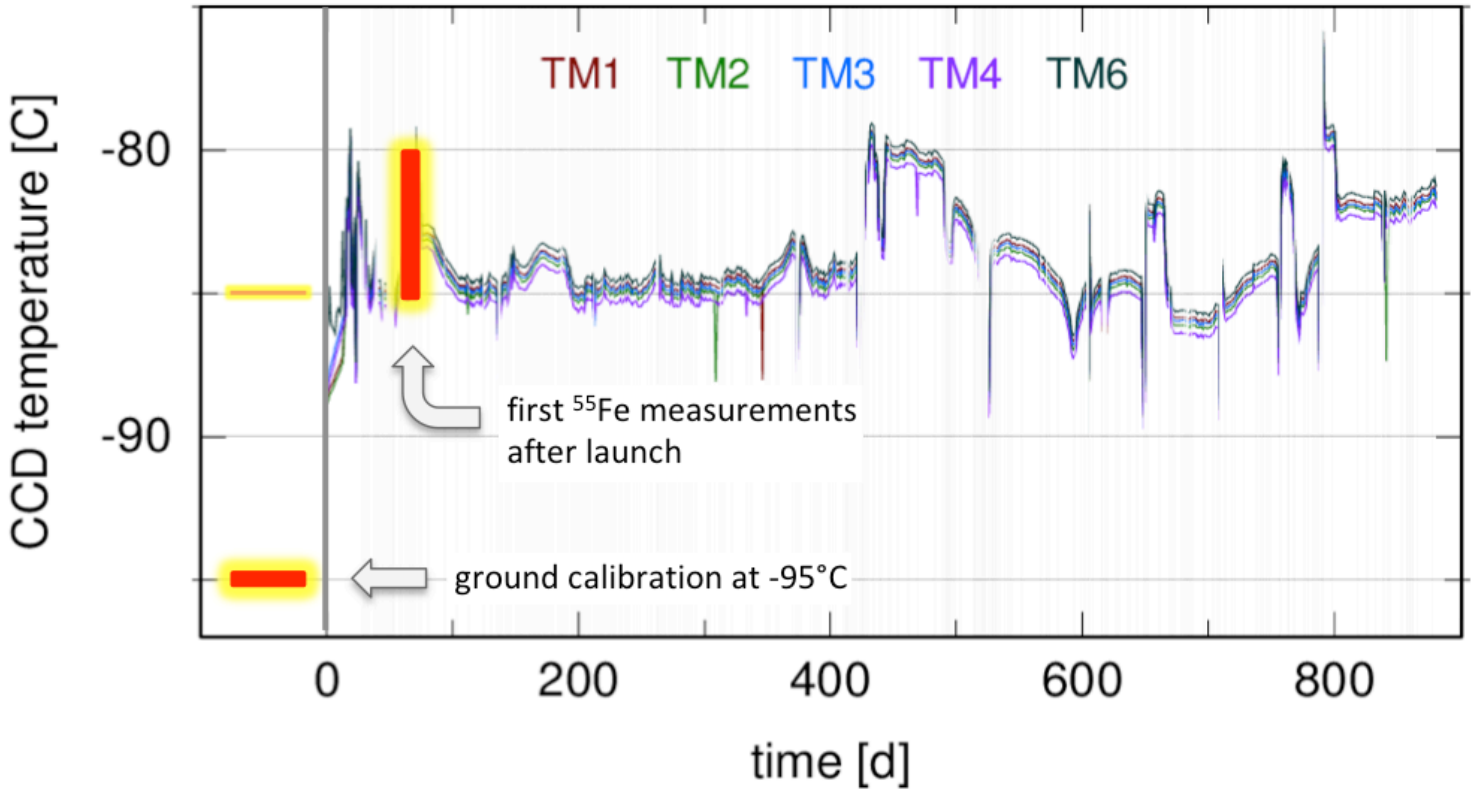

CCD temperatures during the first ^{55}Fe measurements after launch

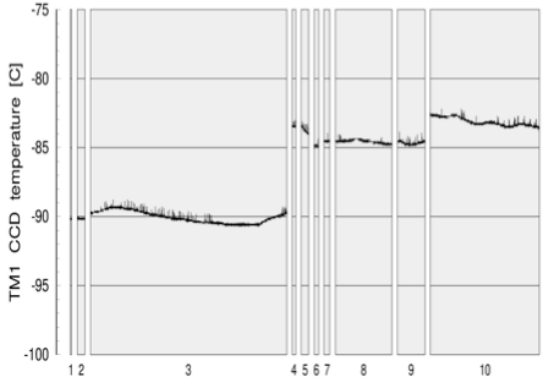

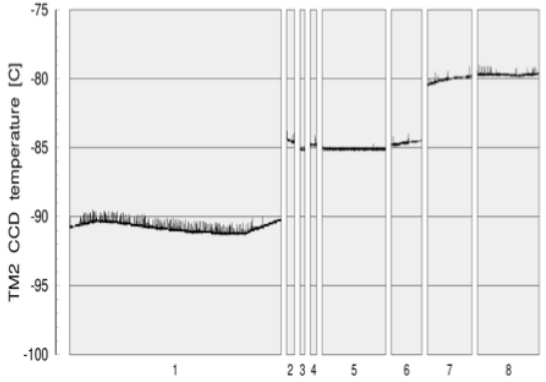

(major) challenge: develop a temperature model for gain and CTI

$$g(x,E,T) = g(x,E,T_0)\left(1 + (T-T_0)\frac{\partial g}{\partial T}\right)$$

$$\mathrm{CTI}(x,y,E,T) = \mathrm{CTI}(x,y,E,T_0) + (T-T_0)\frac{\partial \mathrm{CTI}}{\partial T}$$

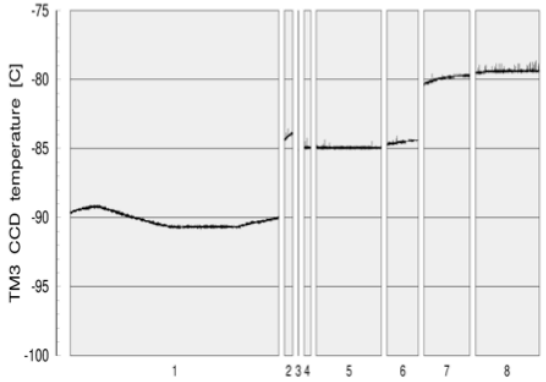

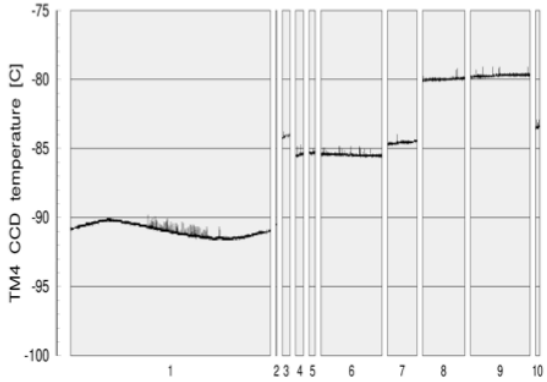

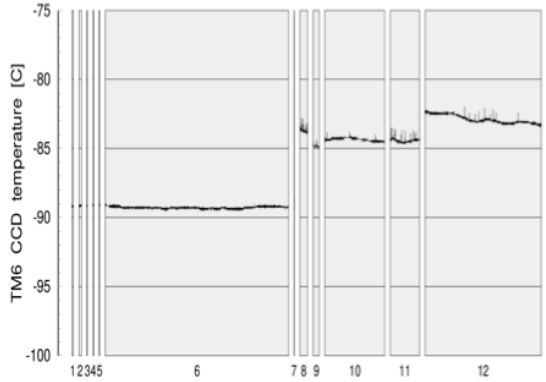

Effect of CCD temperature on energy @ 1.5 keV

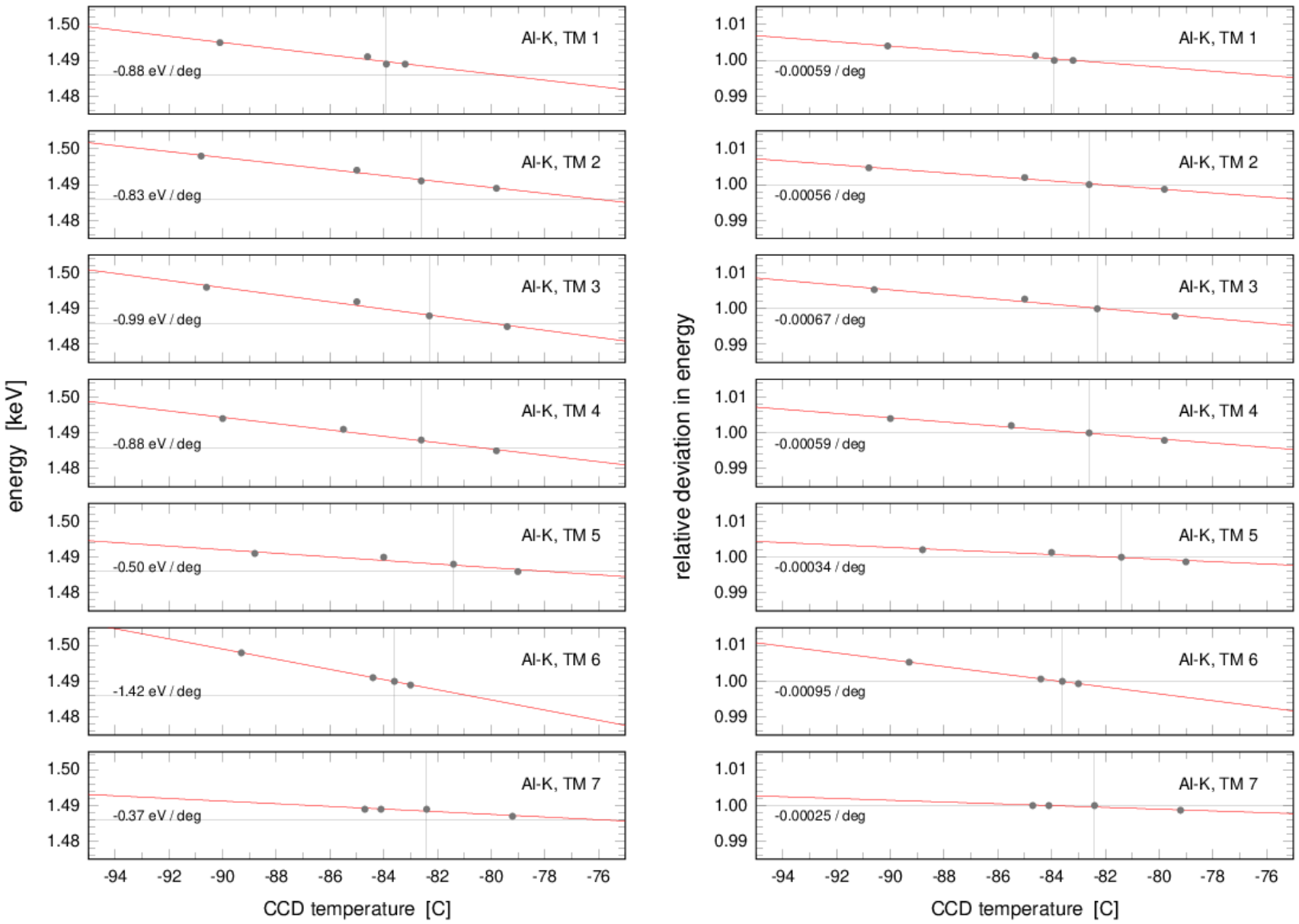

Effect of CCD temperature on energy @ 4.5 keV

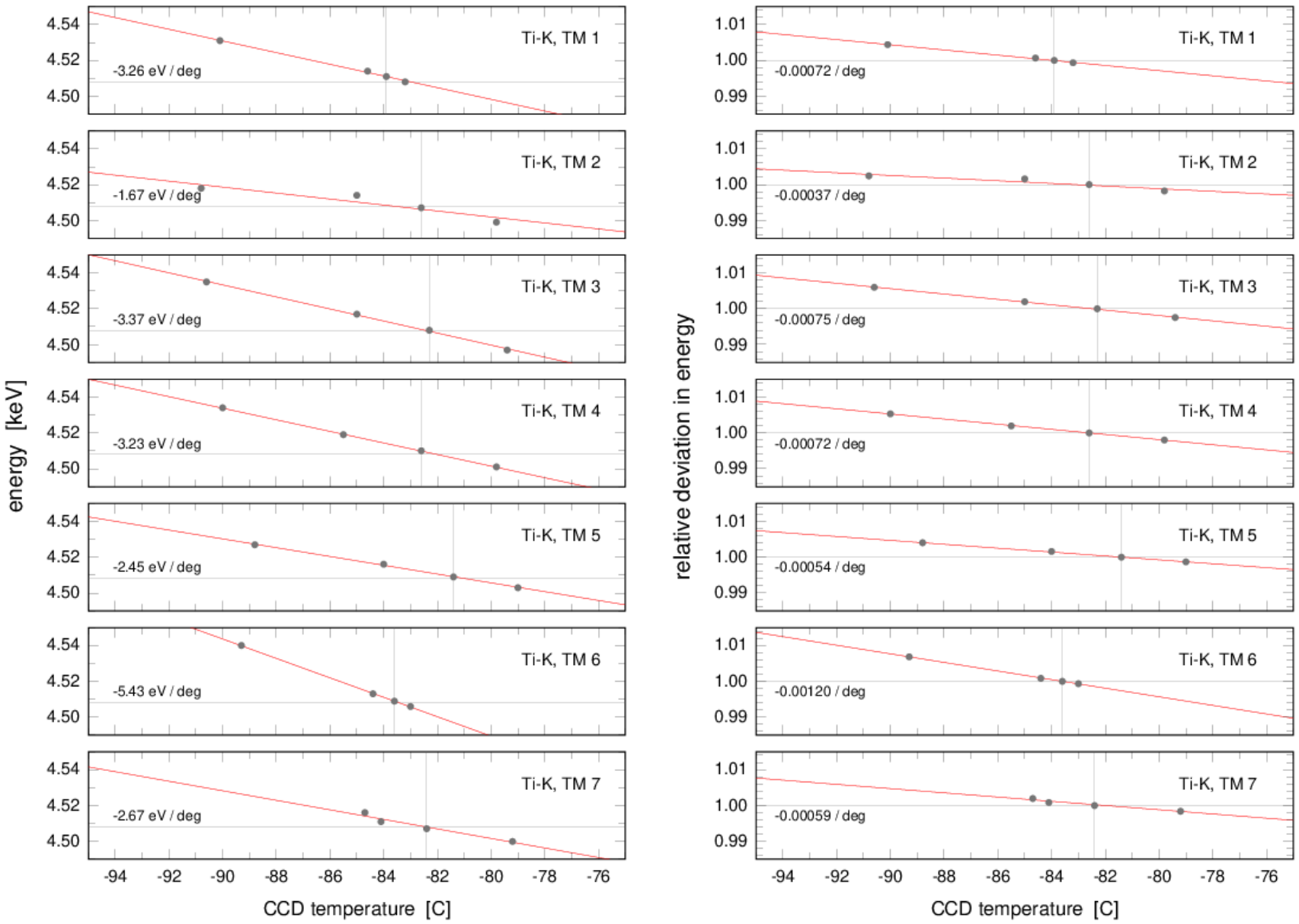

Challenges for the energy calibration:

2) CTI increase due to radiation damage

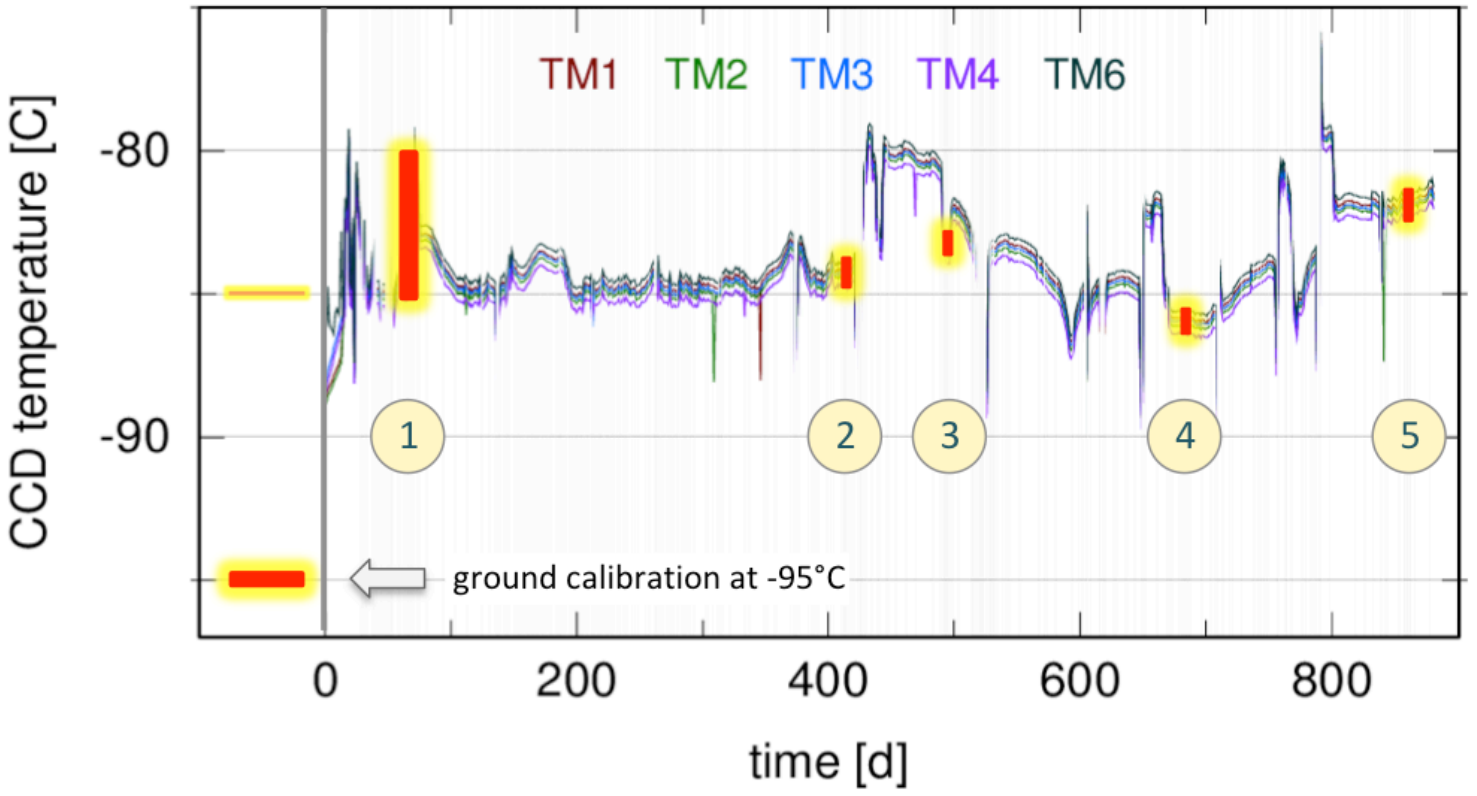

Challenges for the energy calibration:

2) CTI increase due to radiation damage

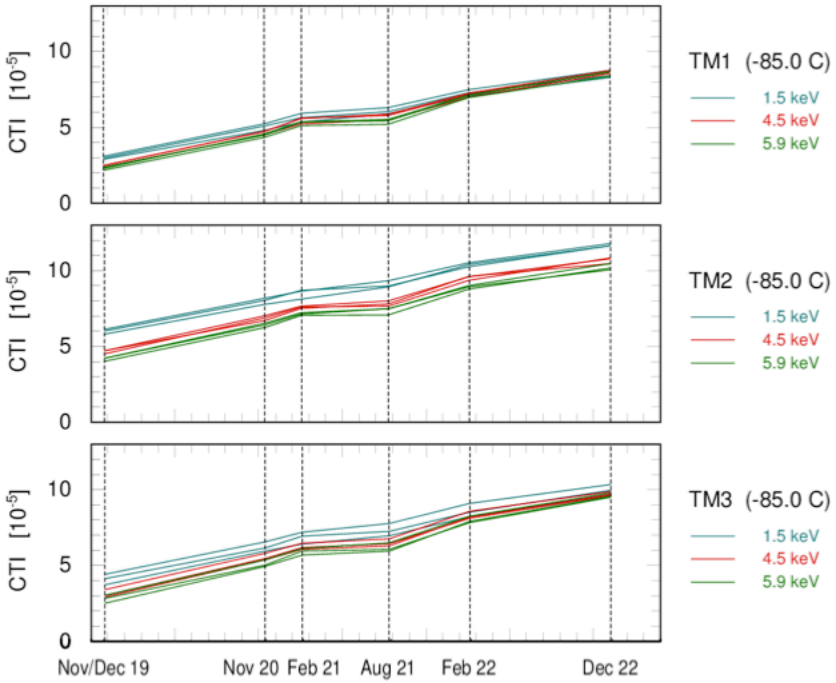

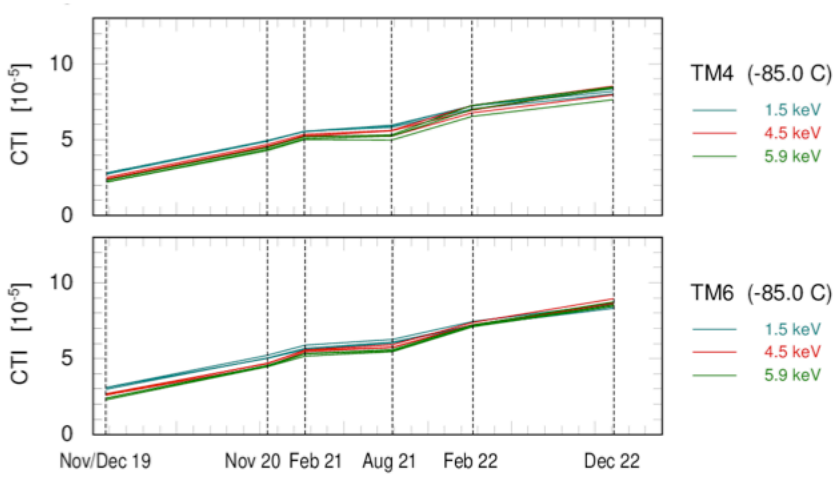

1

CCD column specific CTI evolution

TM1, Al-K

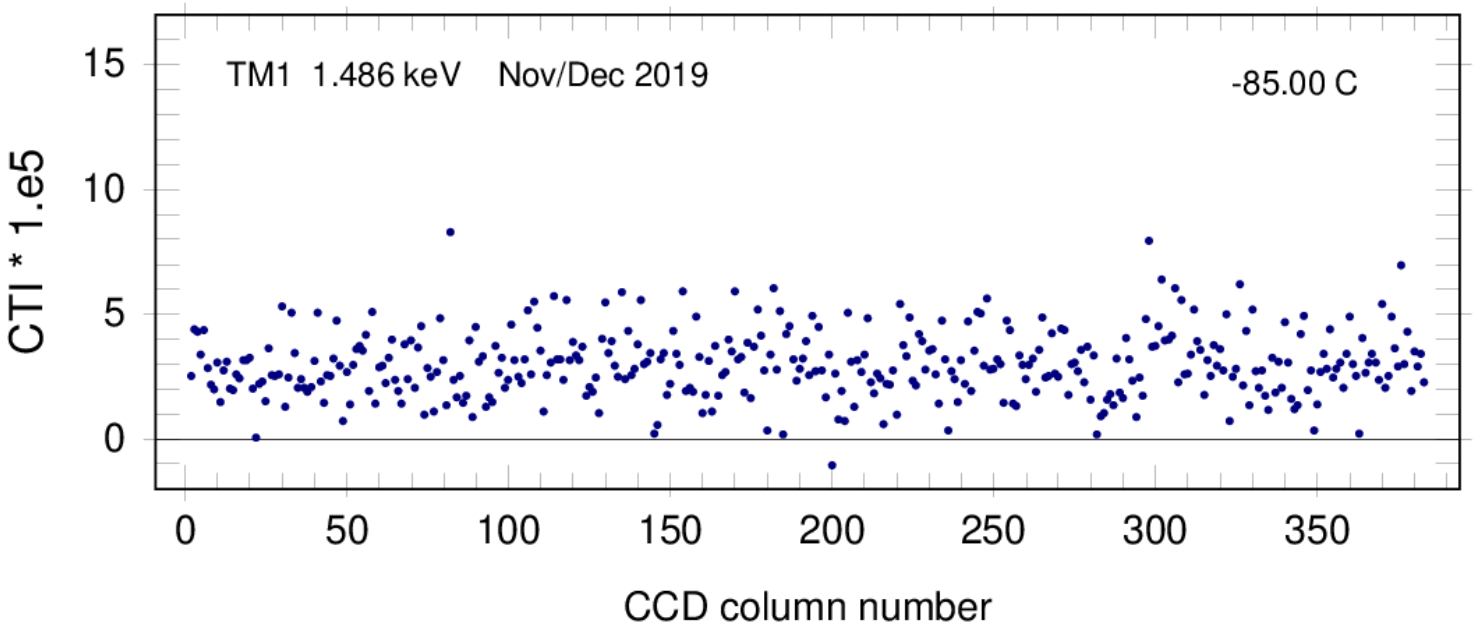

Feb 2022

Aug 2021

Feb 2021

Nov 2020

Nov/Dec 2019

CCD column specific CTI evolution

TM1, Al-K

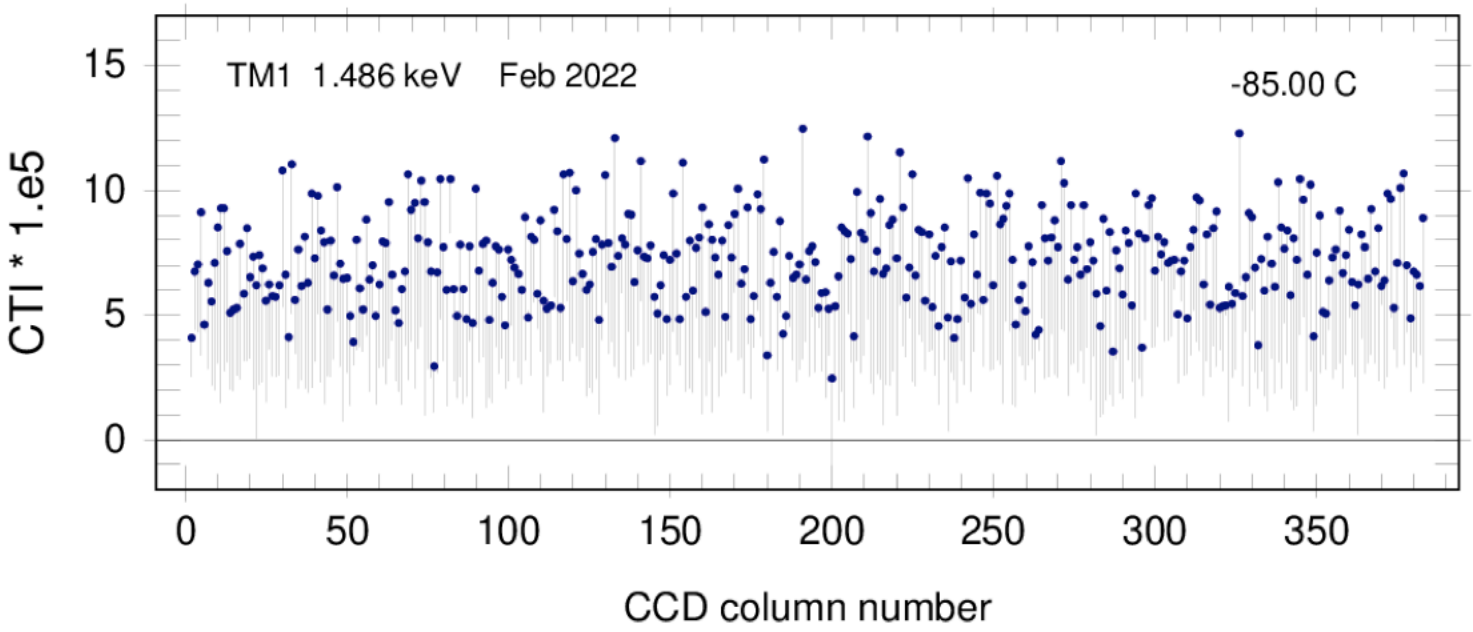

Feb 2022

Aug 2021

Feb 2021

Nov 2020

Nov/Dec 2019

Temporal evolution of the energy resolution (FWHM)

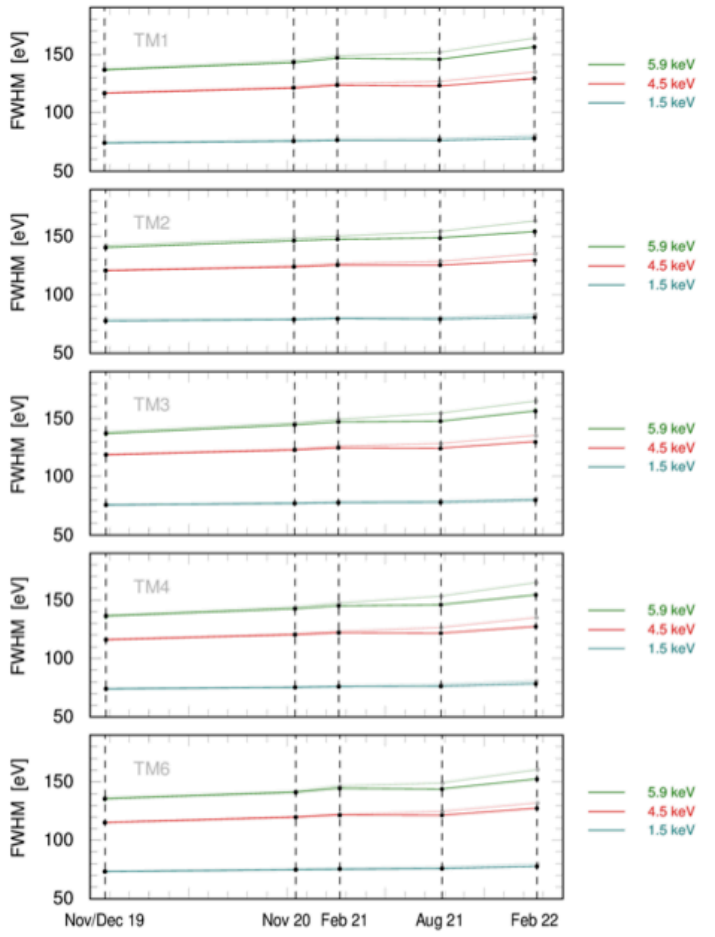

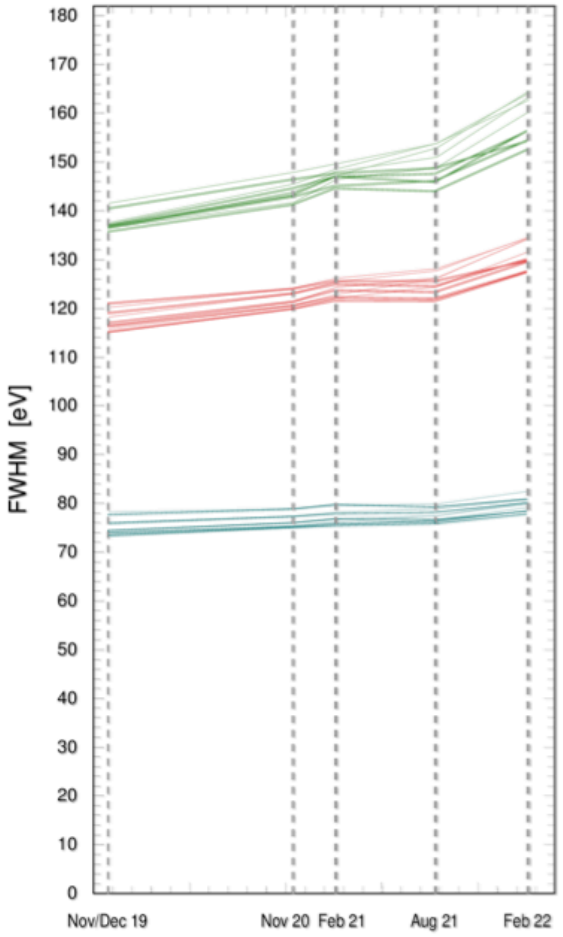

FWHM reduced by ≈8 eV

eROSITA calibration observations of 1E 0102.2-7219

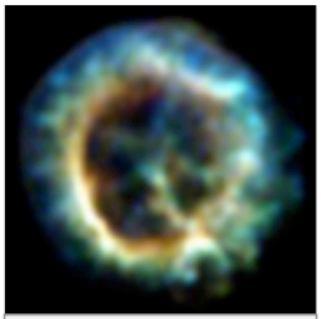

Chandra ACIS

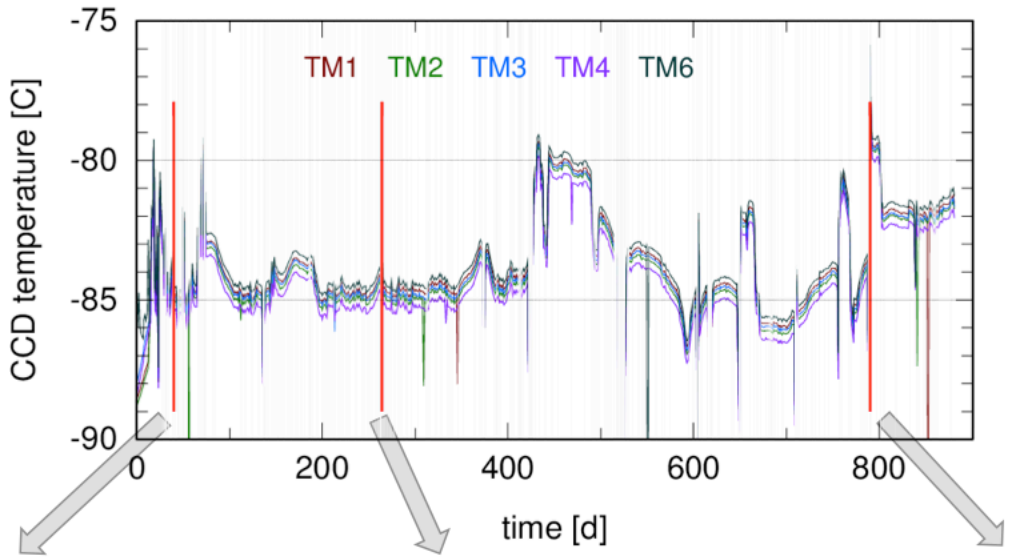

3 long (30-60 ks) pointed eROSITA observations 2019 - 2021

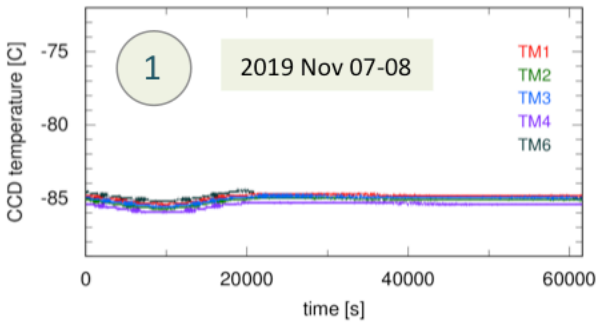

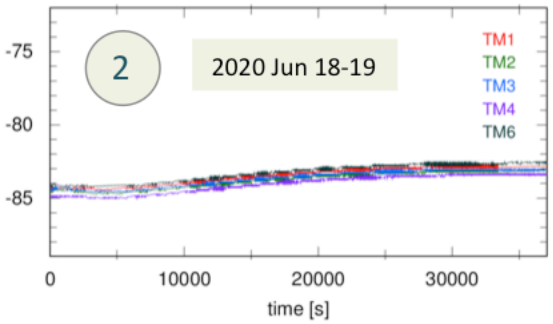

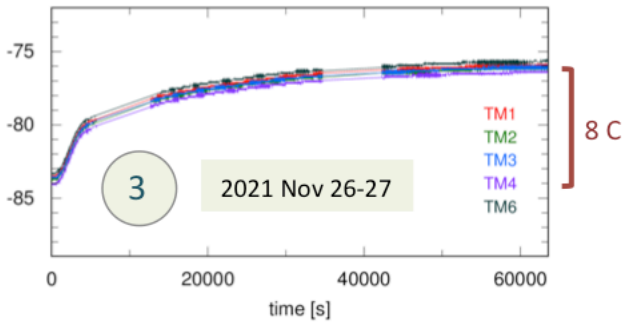

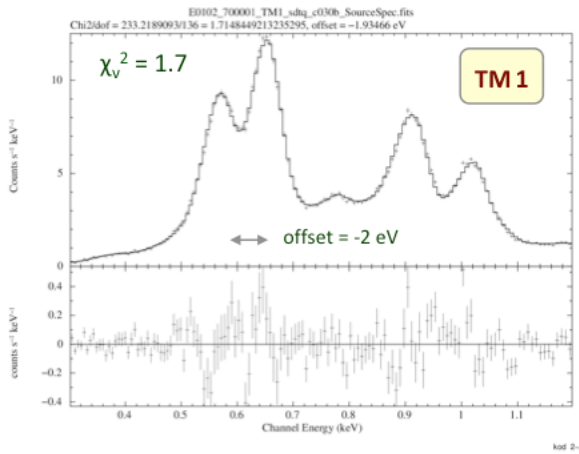

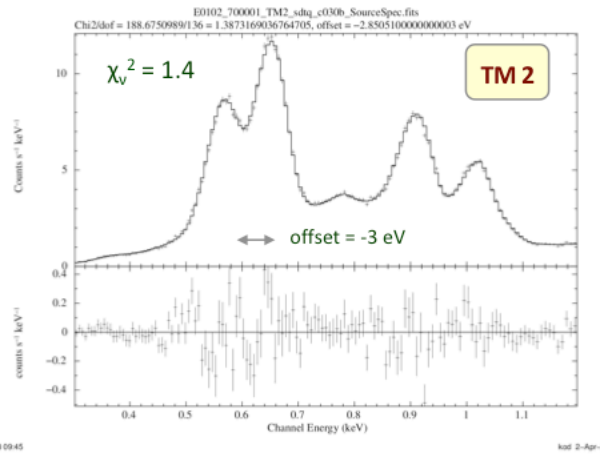

1

1E 0102.2-7219
2019 Nov 07-08
all valid patterns

original IACHEC model used

only 2 free parameters:

offset and normalization

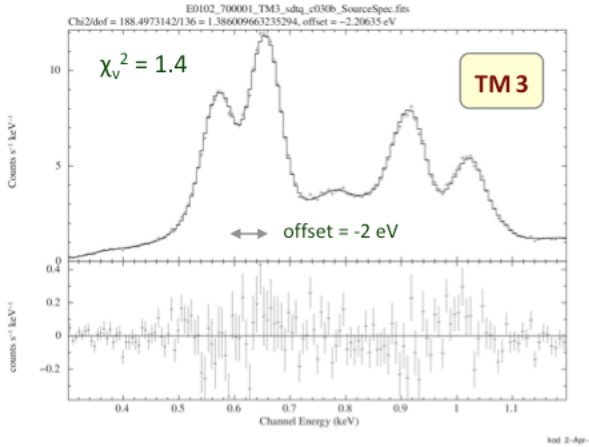

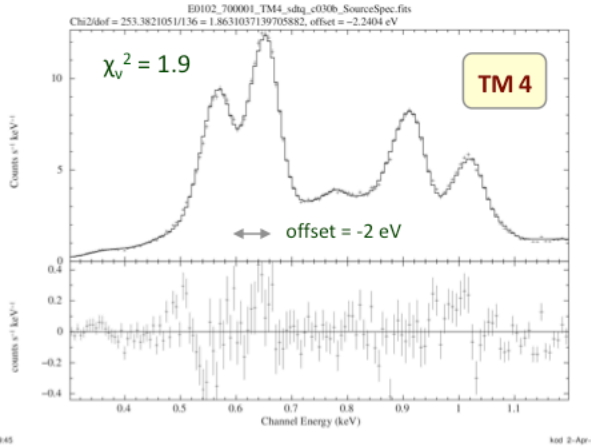

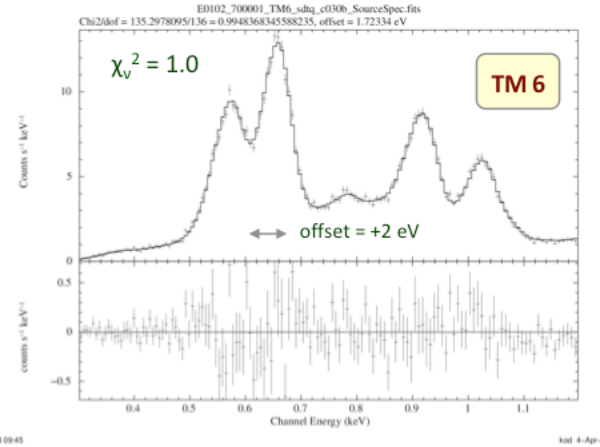

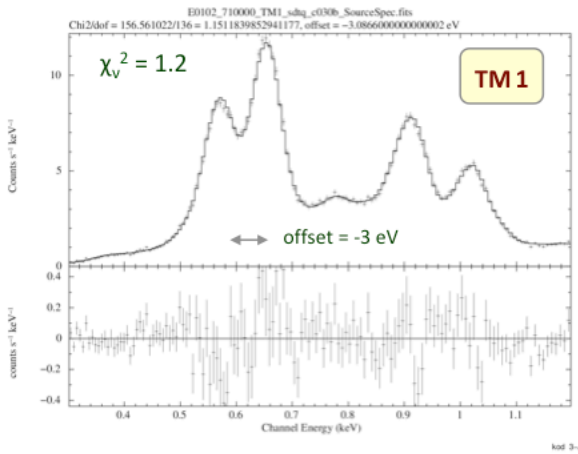

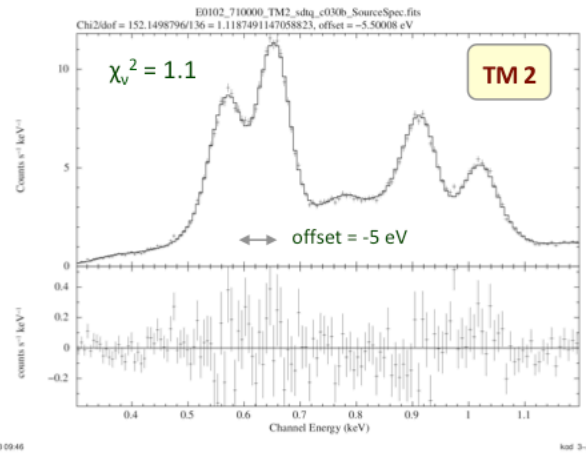

2

1E 0102.2-7219
2020 Jun 18-19
all valid patterns

original IACHEC model used

only 2 free parameters:

offset and normalization

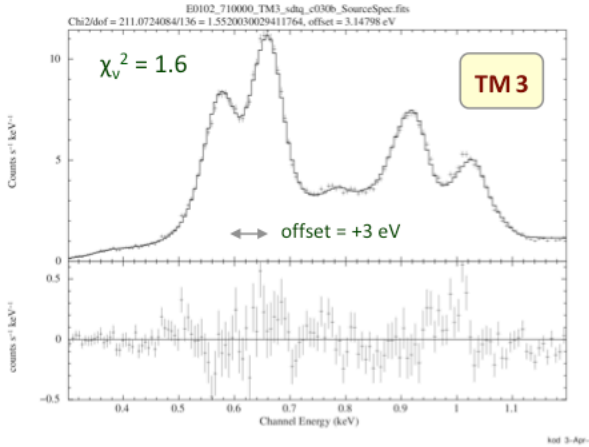

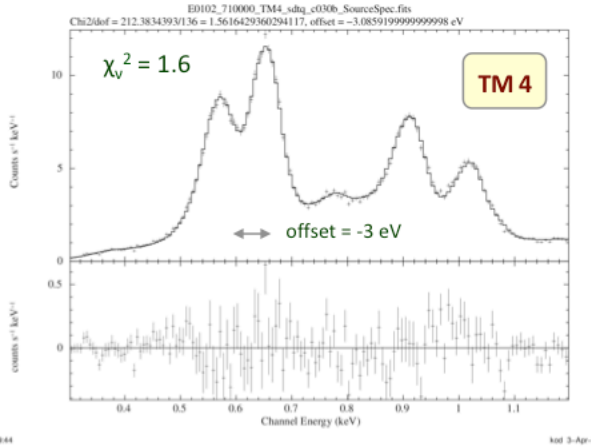

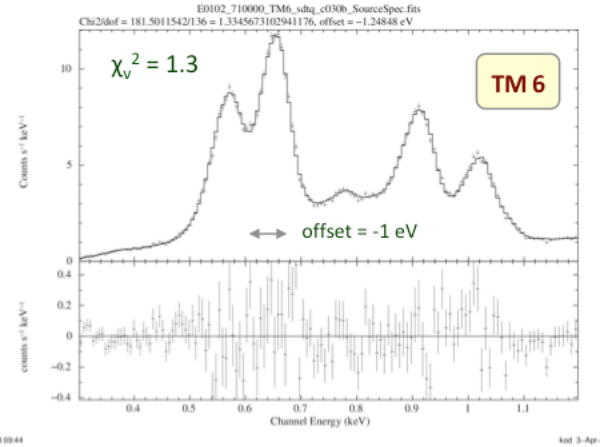

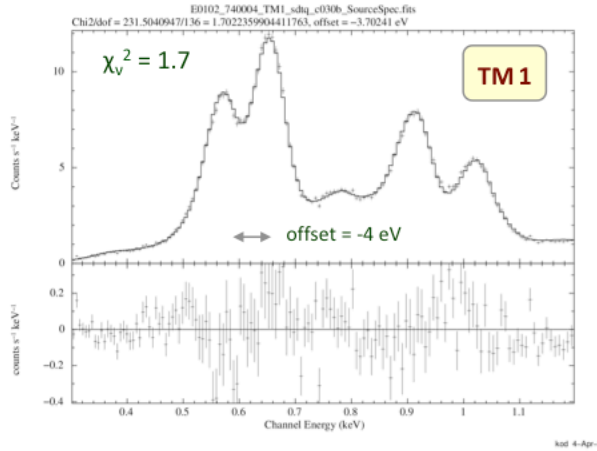

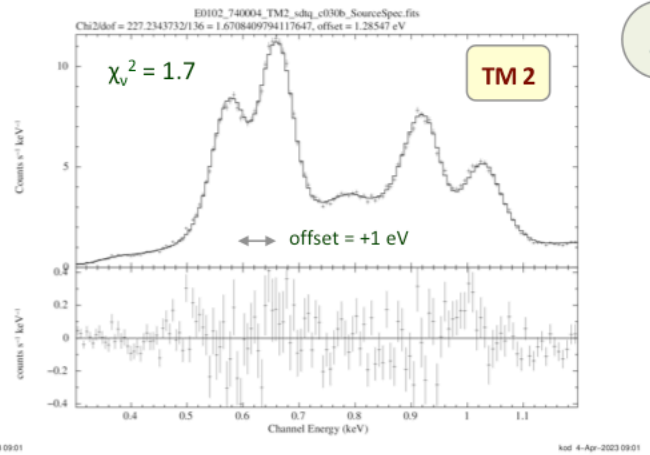

3

1E 0102.2-7219
2021 Nov 26-27
all valid patterns

original IACHEC model used

only 2 free parameters:

offset and normalization

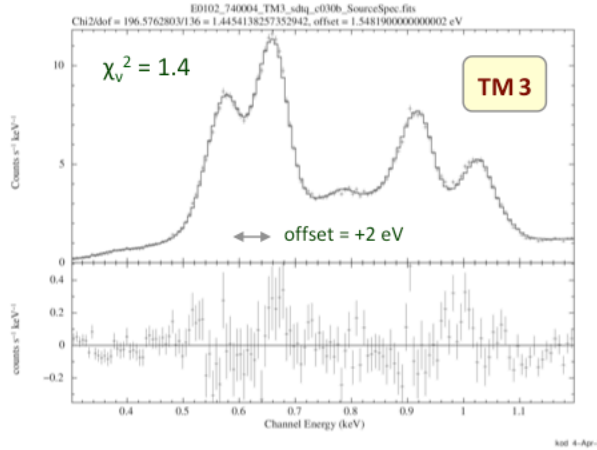

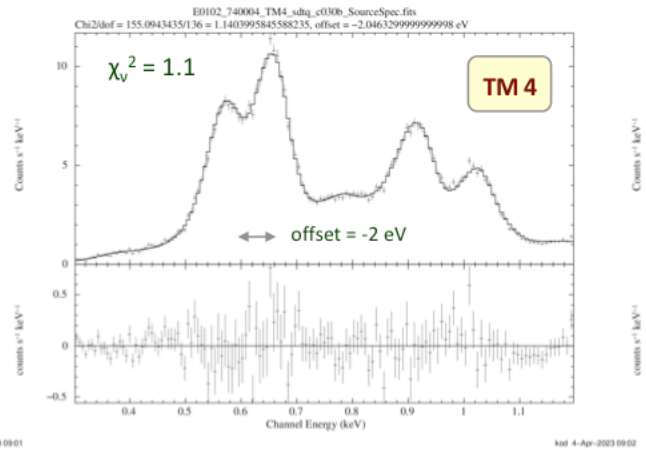

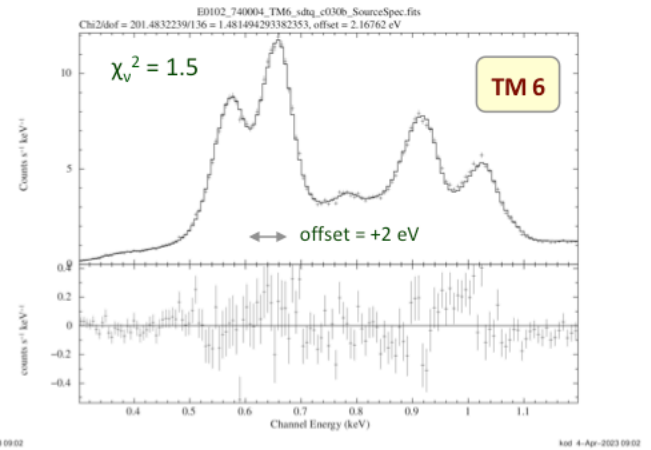

AHEAD 2020

eROSITA - Science and Data Analysis School

2024 November 18 – 22, MPE

eROSITA Calibration

Konrad Dennerl
MPE